2011-07-01

Novel Ion Trap Made Using Lithographically Patterned Plates

Ying Peng
Brigham Young University - Provo

Novel Ion Trap Made Using Lithographically Patterned Plates

Ying Peng

A dissertation submitted to the faculty of
Brigham Young University
in partial fulfillment of the requirements for the degree of

Doctor of Philosophy

Committee Members
Daniel E. Austin, Ph. D., Committee Chair
David V. Dearden, Ph. D., Committee Member
Gregory F. Burton, Ph. D., Committee Member
Matthew R. Linford, Ph. D., Committee Member
Jaron C. Hansen, Ph. D., Committee Member

Department of Chemistry and Biochemistry

Brigham Young University

August 2011

ABSTRACT

Novel Ion Traps Made Using Lithographically Patterned Plates

Ying Peng

Department of Chemistry and Biochemistry

Doctor of Philosophy

A new approach of making ion trap mass analyzers was developed in which trapping fields are created in the space between two ceramic plates. Based on microfabrication technology, a series of independently-adjustable electrode rings is lithographically patterned on the facing surfaces of each ceramic plate. The trapping field can be modified or fine-tuned simply by changing the RF amplitude applied to each electrode ring. By adjusting the potential function applied to the plates, arbitrary trapping fields can be created using the same set of ceramic plates. Unlike conventional ion traps, the electrodes of planar ion traps have a non-equipotential surface, thus the electric field is independent of electrode geometry and can be optimized electronically. The simple geometry and open structure of planar ion traps address obstacles to miniaturization, such as fabrication tolerances, surface smoothness, electrode alignment, limited access for ionization or ion injection, and small trapping volume, thereby offering a great opportunity for a portable mass spectrometer device.

Planar ion traps including the planar quadrupole ion trap and the coaxial ion trap have been designed and tested using this novel method. The planar quadrupole trap has demonstrated a mass range up to 180 Da (Th), with mass resolution typically between 400-700. We have also developed a novel ion trap in which both toroidal and quadrupolar trapping regions are created simultaneously between a set of plates. This "Coaxial Trap" allows trapping and mass analysis of ions in two different regions: ions can be trapped and mass analyzed in either the toroidal or quadrupolar regions, and transferred between these regions. Some simulation work based on the ion motion between two different trapping regions in the coaxial ion trap has been performed. Using a one-dimensional simulation method, ion motion was investigated to transfer ions between these two regions. The effect of the mutipole components in the radial field and axial field, amplitude and frequency of the primary RF and supplementary AC signal were studied to obtain high mass resolution in the axial direction and high transfer efficiency in the radial direction. In all these devices, the independent control of each patterned electrode element allows independent control of higher-order multipole fields. Fields can be optimized and changed electronically instead of physically as is done in conventional traps.

Keywords: Ion trap, Mass spectrometry, Instrumentation, Miniaturization, Planar quadrupole ion trap, Coaxial ion trap.

ACKNOWLEDGEMENTS

First of all, I gratefully acknowledge and thank my advisor, Dr. Daniel E. Austin, for not only allowing me to study and work in his group, but also for providing me a model of what a successful young scientist should be. It has been a pleasant and precious opportunity for me to be advised by him and work with him from the beginning of building his laboratory. I am honored and proud that I can be his first PhD student. His deep knowledge in the field of mass spectrometer instrumentation was a constant source of support to encourage my independent and original thought. Everything I learned from him will be invaluable to my future research and career development.

I would like to sincerely thank my graduate committee members, Dr. David V. Dearden, Dr. Gregory F. Burton, Dr. Matthew R. Linford, and Dr. Jaron C. Hansen for their critical evaluation and constructive suggestions during my research and study. Dr. Milton L. Lee and Dr. Aaron R. Hawkins offered me valuable instruction and problem solving methods during the ion trap building process.

I would like to thank Dr. Stephen A. Lammert for his enlightened instruction to the coaxial ion trap. I also wish to thank Dr. Zhingping Zhang and Dr. Miao Wang for countless discussions and considerable time spending in working with me on my project. Brett J. Hansen and Hannah E. Quist also deserve my appreciation for fabricating ceramic plates for this project.

I wish to acknowledge my colleagues in Dr. Austin's group. Cooperation and friendship from my group always encourage me during my work and I learned a lot from each of them. I would like to thank Junting Wang, Brandon Barney, Sara Nielson, Dr. Nick Taylor, Chongchong Lan, Terik Daly, Cameron Garner, Jonathan Kerby and other

friends in both Dr. Austin's group and other groups. I appreciate their friendships and help at Brigham Young University.

I also would like to give thanks to the staff in the department instrument shop for helping me build electric circuits and accessories for assembly of my ion trap system. I thank the Department of Chemistry & Biochemistry at Brigham Young University for offering me the opportunity and financial support to study here. Financial support from NASA is also gratefully acknowledged.

Finally, I must thank my husband Xin Chen and my parents. The help and love given by my family during my PhD study is indescribable. My deepest gratitude belongs to my husband, Xin, who already achieved his PhD degree in the Department of Chemistry & Biochemistry at BYU. Without his encouragement and support it would have been impossible for me to have had two children and enjoy happiness while pursuing graduate studies during those years. Deep gratitude also belongs to my parents. Bearing great loneliness and inconvenience, they traveled to America to help me take care of my children. Their unselfish love and understanding were the greatest impetus for me to finish this dissertation. This dissertation is dedicated to my parents, my husband, and my two children, Elvin and Kaelyn.

TABLE OF CONTENTS

LIST OF ACRONYMS AND SYMBOLS

RF	radiofrequency
Quistor	quadrupole ion store
3D	three-dimensional
AC	alternating current
A_n	expansion coefficient of the order *n*
A_2	coefficient of quadrupole term
a_u, q_u	Mathieu stability parameters in the radial or axial direction
a_z, q_z	Mathieu stability parameters in the axial direction
CID	collision-induced dissociation
CIT	cylindrical ion trap
LIT	linear ion trap
D	pseudopotential well depth
DC	direct current
e	ion charge
GC-MS	gas chromatograph-mass spectrometer
IT	ion trap
ITMS	ion trap mass spectrometry
M	ion mass
m/*z*	mass-to-charge ratio
MEMS	micro-electro-mechanical system
MS	mass spectrometry
PCB	printed circuit board

$P_n(\cos\ \theta)$	Legendre polynomial
QIT	quadrupole ion trap
r_0	radial dimension of the ion trap
z_0	axial dimension of the ion trap
RIT	rectilinear ion trap
U	DC voltage
V	zero-to-peak amplitude of RF voltage
$\beta_r,\ \beta_z$	parameters for secular frequency in the r or z dimension
ϕ	starting phase angel of drive RF
Φ_0	RF voltage
Ω	angular of RF drive frequency
$\omega_r,\ \omega_z$	secular frequency in the r or z dimension
FWHM	full width at half maximum
LC	liquid chromatography

LIST OF FIGURES

LIST OF TABLES

CHAPTER 1: THEORY, DEVELOPMENT AND MINIATURIZATION OF ION TRAPS

1.1 Quadrupole Ion Traps

Ion traps are a class of devices that use radiofrequency (RF) electric fields to trap, store, and mass-analyze ions or other charged particles. The quadrupole ion trap was invented in 1953 by Wolfgang Paul, for which he jointly shared the 1989 Nobel Prize in Physics with Hans Dehmelt and Norman Ramsey. Initially ion traps were used as ion sources for conventional quadrupole mass filters or drift cells[1] for external analysis of ejected ions. Ion traps have since assumed a prominent role as mass analyzers in the development of mass spectrometry. The discovery in the 1980s of the mass-selective instability mode and collisional cooling using helium were breakthroughs in the development of ion traps, greatly improving their mass resolution and trapping capacity. These two discoveries led to the development of the first commercial ion trap mass spectrometer by Finnigan MAT. Today commercially available ion trap mass spectrometers are characterized by their small size, relatively low cost, high sensitivity and MS^n capability.[2-3]

Todd and March gave a retrospective review of the development and application of the quadrupole ion trap prior to the appearance of commercial instruments.[4] The Quistor, as quadrupole ion traps were previously called, can act as a storage source for ions to be used in the study of ion/molecule reactions[5-8] and function as a low-pressure chemical ionization source.[8-10] Operating an ion source mass selectively can greatly enhance ion signal, in which the source is set to store ions specifically from a trace

component while simultaneously eliminating interference ions from components in excess.[10-11]

1.1.1 Theory of Quadrupole Ion Traps

The quadrupole ion trap is an outstanding device which can serve as both an ion storage source and as a mass spectrometer of considerable mass range and mass resolution. A quadrupole ion trap consists of three hyperboloidal electrodes – one ring electrode and two end-cap electrodes, as shown in Figure 1.1 (a). The cross-section of a typical ion trap is illustrated in Figure 1.1 (b), showing asymptotes and the dimensions r_0 and z_0. Here, r_0 is the radius of the ring electrode and $2z_0$ is the distance between the two end-cap electrodes. In the ideal quadrupole trap, the relationship between r_0 and z_0 is given by:

$$r_0 = 2z_0^2 \qquad (1)$$

In the majority of commercial ion traps, r_0 is 1.00 cm.

When a radiofrequency (RF) signal is applied to the ring electrode of an ion trap, and the two end-cap electrodes are grounded, a time-varying quadratic trapping potential well (a pseudopotential well) is formed in the trap. March[12] compared ion species in the trapping potential well to layers of liquids in a bowl, each with different densities, corresponding to ions of different mass-to-charge ratios (*m/z*). When the bowl is tilted to one side, the layer of least density, corresponding to ions with lowest *m/z* will be poured first from the container as shown in Figure 1.2. The process of titling the bowl corresponds to the ramping of RF potential, while the glass sitting beside the bowl corresponds to the detector.

(a)

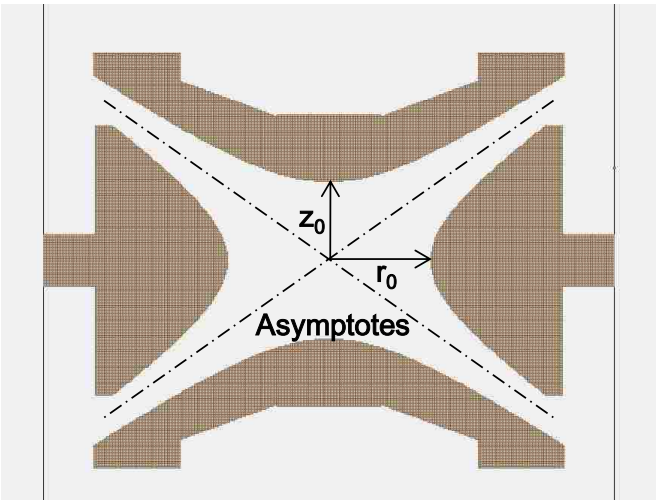

(b)

Figure 1.1. (a) Three hyperboloidal electrodes of the quadupole ion trap in an open array, (b) diagram of a typical three-dimensional (3D) ion trap showing the asymptotes and the dimensions r_0 and z_0.

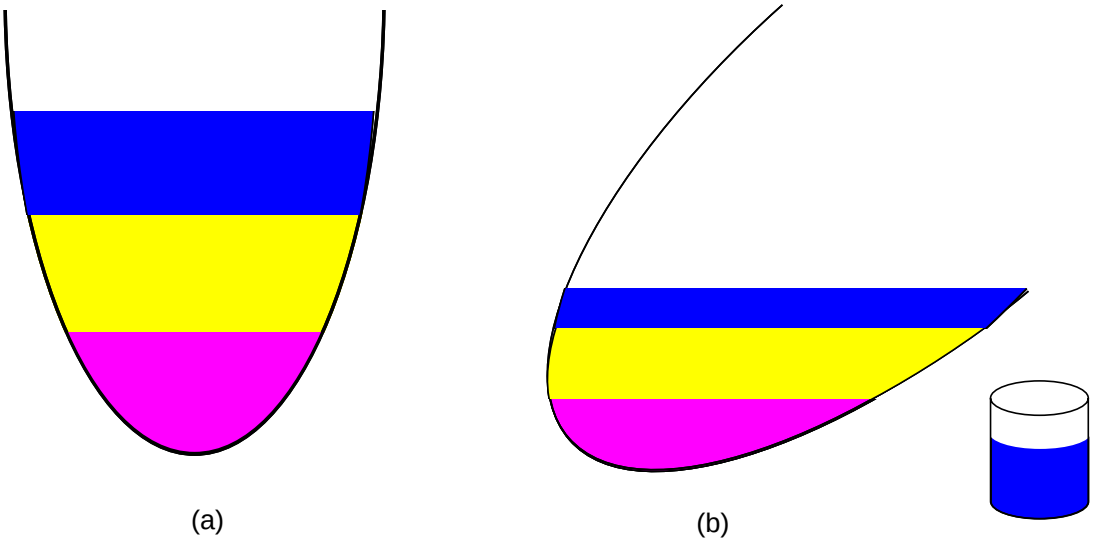

Figure 1.2. Schematic representation of (a) a trapping potential well in which three layers of liquids with different densities represent ions with different *m/z*, (b) ions are mass-selectively ejected from the trapping well to the detector (Adapted from March, R. E., An introduction to quadrupole ion trap mass spectrometry. *J. Mass Spectrom.* **1997,** *32*, 351-369).

The motion of ions in quadrupole devices differs greatly from that of ions in field-free regions and in static fields. Ions in a quadrupole ion trap are affected by a set of time-dependent forces. An ion in a quadrupole field experiences a strong focusing force, and the restoring force increases when the ion deviates from the central region of the device. The motion of ions in a time-varying quadrupole field can be described by the solutions to the Mathieu Equation.[13] Solutions to this equation are either bounded or unbounded, corresponding to parameters in which ions are trapped (the stability region) or not trapped (ejection or instability region), and described using the dimensionless parameters a_u and q_u. In the axial direction (z-direction) where ions are ejected out from the trap, a_z and q_z can be expressed as:

$$a_z = \frac{-8eU}{mr_0^2\Omega^2}; \qquad q_z = \frac{4eV}{mr_0^2\Omega^2} \tag{2}$$

Where e is the charge of an ion in Coulombs, m is the mass of the ion in kg, U is the amplitude of a DC potential applied on the end-cap electrodes, V is the amplitude of an RF potential applied on the ring electrodes, and Ω is the angular frequency of the RF potential. The Mathieu parameters a_z and q_z are plotted in Figure 1.3 as the coordinates of the stability region.

For practical purposes the ring and end-cap electrodes are truncated to a definite length, and holes are drilled in the end-cap electrodes for ion injection and ejection. These modifications introduce higher-order multipole components to the field, i.e., terms in the field that vary with r and/or z faster than quadratic. Many efforts have been applied in order to compensate for these higher order multipole components, including changing the distance or geometry of the electrodes. For example, the distance between the end-cap electrodes of most commercial ion traps has been stretched by 10.6% to

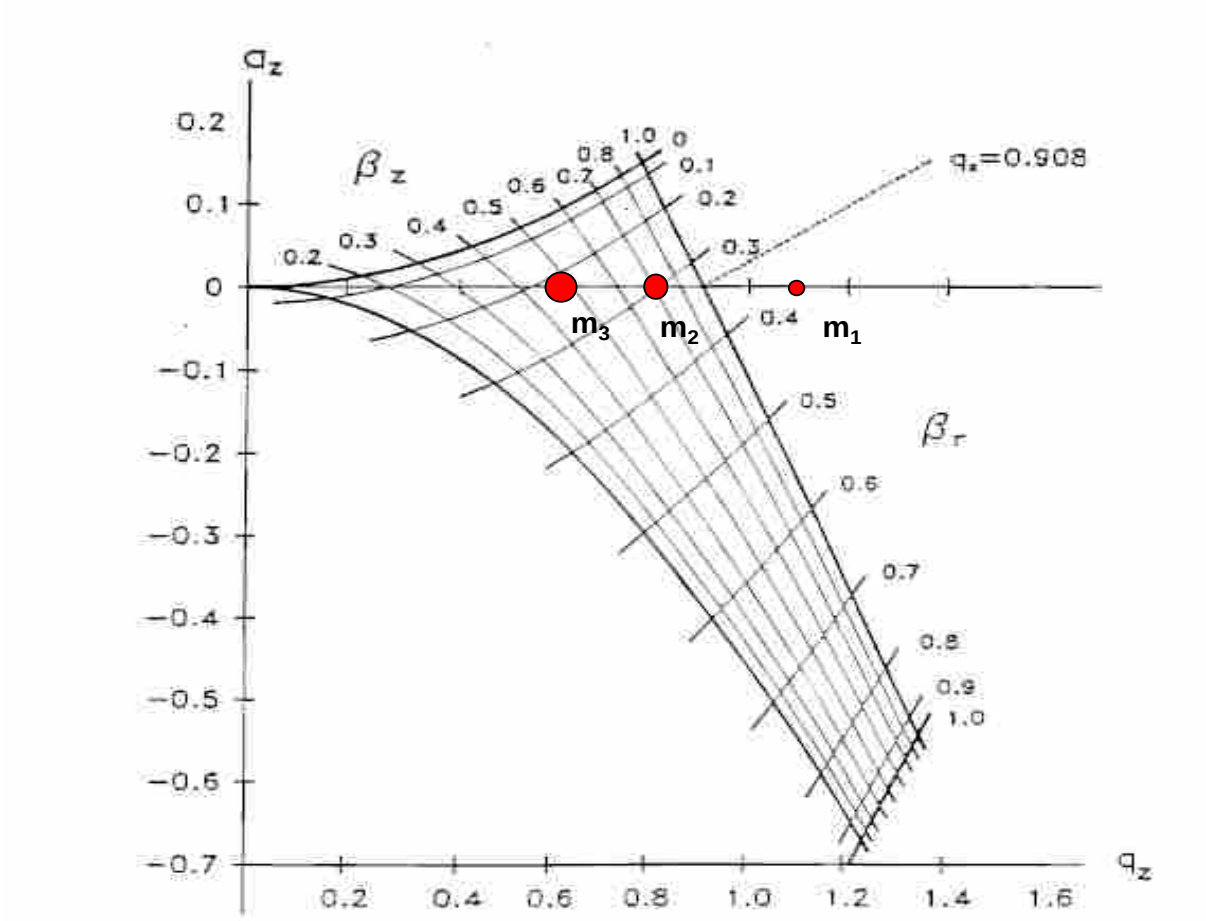

Figure 1.3. Stability diagram in a_z, q_z for simultaneous stability in the z-direction in the three-dimensional quadrupole ion trap. The q_z-axis intersects the β_z=1 boundary at q_z=0.908, which corresponds to q_{max} in the mass-selective instability mode. Red dots correspond to ions with different masses ($m_1<m_2<m_3$). (Adapted from March, R. E., An introduction to quadrupole ion trap mass spectrometry. *J. Mass Spectrom.* **1997,** *32*, 351-369).

achieve better performance. The immediate consequences are the dimension change of the ion trap: $r_0^2 \neq 2z_0^2$, and an expression change for a_z and q_z, as follows:

$$a_z = \frac{-16eU}{m(r_0^2 + 2z_0^2)\Omega^2}; \qquad q_z = \frac{8eV}{m(r_0^2 + 2z_0^2)\Omega^2} \tag{3}$$

For the quadrupole ion trap there are two main methods to eject ions from the trap: the mass-selective instability mode and the mass-selective resonant ejection mode. After ions are trapped they are scanned out of the trap according to their mass-to-charge ratio. In the mass-selective instability method, ions can be ejected out at a fixed q_z value according to their mass-to-charge ratio. With this method, the fundamental RF voltage can be linearly increased to move the ions with an increasing mass-to-charge ratio toward the boundary of the stability region (q_z = 0.908). The ions that reach this fixed q_z point become unstable in the z-direction, and are ejected out of the trap as a function of the applied RF voltage. The mass scale can be expressed as follows:

$$\frac{m}{z} = \frac{8V}{(r_0^2 + 2z_0^2)\Omega^2 q_z} \tag{4}$$

From Equation (4) it can be seen that mass range is limited by the RF frequency (Ω) and RF amplitude (V) and trap size (r_0). However, the mass range can be extended by causing the ions to become unstable at a lower q_z value. This can be accomplished by another detection method: the mass-selective resonant ejection mode. In the mass-selective resonant ejection method, applying a suitable dipolar supplementary AC voltage of appropriate frequency to the end-cap electrodes of a quadrupole ion trap allows ions to be resonantly ejected out of the trap at an arbitrary value of the Mathieu parameter q_z. When a forward resonance ejection scan is performed, the RF amplitude is scanned linearly and the secular frequencies of the ions are increased and approach the frequency

of the applied AC signal from the low-frequency side. As the secular motion of the ions begins to come into resonance with the applied frequency, ions are displaced from the center of the trap and their trajectories grow rapidly until they are ejected from the trap. Williams et al. found that using resonant ejection there is a dramatic anisotropic effect of scan direction on mass spectra acquired with a "stretched" quadrupole ion trap.[14]

1.1.2 Ion Trap Mass Analyzer Types and Their Performance

The original Paul-type quadrupole ion trap, invented by Wolfgang Paul in 1953,[15] has three hyperboloid electrodes (Figure 1.1). Before the quadrupole trap was developed into a mass analyzer this unique device was used for decades for ion storage.[4] When an RF potential is applied between the ring and two end-cap electrodes, ions are trapped in the center region of the three-dimensional (3D) trapping field. Following the work by Todd et al.[9] and March et al.,[16] who applied the device as a mass analyzer, George Stafford et al.[17] discovered the mass-selective instability scan method to eject ions from the trap. Using this analysis method, ions are ejected from the ion trap with increasing mass-to-charge ratio when the RF amplitude is ramped from low to high. Thus the *m/z* versus ion-intensity information is recorded as a mass spectrum. Ions with the same *m/z* trapped in the quadrupole ion trap can be mass-selectively isolated from other ions and subsequently fragmented in the same device, usually by collision-induced dissociation (CID),[18] to acquire tandem mass spectra.

The cylindrical ion trap (CIT), a simplified version of the 3D quadrupole ion trap, has two flat end-cap electrodes and one cylindrical ring electrode. Similar to the development of the quadrupole ion trap, the CIT was first used for ion storage[19-20] and subsequently developed into a mass analyzer. When used as a mass analyzer, it was first

applied with the mass-selective stability scan developed by March[21] and later using the mass-selective instability scan by Cooks and colleagues.[22] Because the simplified geometry of the CIT electrodes lends itself to machining at smaller dimensional scales, the CIT was recognized as a good candidate analyzer for mass spectrometer miniaturization.[23-29]

In a 3D ion trap, when too many ions are trapped and pushed toward the center point of the 3D volume, columbic interactions (i.e., space-charge effects) degrade the ion trap performance including the mass resolution, the efficiency of mass selection (i.e., the ion isolation efficiency) in CID, and mass accuracy. It was reported that good performance of the trap, and thus high-quality mass spectra, can be acquired when only 500 ions or fewer are trapped in a 3D Paul trap with a ring electrode radius (r_0) of 5 mm.[30] While 3D ion traps suffered from the limited trapping capacity, developments in ion trap geometry were focused on the enlargement of the ion storage capacity.[31-34] The Linear ion trap (LIT) was first created in 1996[31] and fully developed and characterized by Thermo Electron (now Thermo FisherTM)[34] as well as by MDS SciexTM[33] in 2002. The LIT allows ions to be trapped along a line instead of at a point, as happens in a 3D ion trap. In a LIT, ions are scanned out through slits in the radial or axial electrodes.

Following the linear ion trap, the rectilinear ion trap (RIT) with flat electrodes, a simplified version of the linear ion trap, was soon developed.[35] The RIT combines the advantages of simpler electrode geometry (as the CIT) and increased ion capacity of the LIT. Comparison between the RIT and the CIT demonstrated that the RIT has a volume 4 times greater and a trapping capacity 40-fold greater than that of a CIT.[35] In addition to

the larger trapping capacity,[36] linear ion traps and rectilinear ion traps are able to trap externally injected ions more efficiently than 3D traps.[37]

At the same time, the toroidal trap, invented by Bier and Syka[31] and developed by Lammert et al.,[32] represents a novel geometric variation on the quadrupole ion trap. A toroidal geometric solid is created by revolving a circle about an axis external to the circle. Analogously, the toroidal ion trap is made conceptually by revolving the cross section of a Paul trap around an axis outside the trap volume. The toroidal ion trap also has enlarged trapping capacities, as it traps the ions on the circumference of a circle. A miniaturized toroidal ion trap[38] has recently been included for the development of Torion Technologies' portable gas chromatography mass spectrometer (GC-MS).[39] The configurations of all these ion traps are demonstrated in Figure 1.4.

1.2 Miniaturized Ion Traps

1.2.1 Significance of Miniaturizing Ion Traps

Mass spectrometers are among the most widely used analytical tools due to their high sensitivity, strong analytical power, and their use in combination with gas or liquid chromatography or capillary electrophoresis.[40-44] In addition, a wealth of new sampling and ionization methods now extend mass spectrometry to many applications including analysis of biomolecules, petroleum, aerosols, explosives, and even intact microorganisms.[45-50] Unfortunately, mass spectrometer systems tend to be both bulky and expensive. There is significant motivation to bring the power and versatility of mass spectrometry into a portable, inexpensive instrument—one that can be taken into the field and to the sample rather than requiring the sample be collected and taken to a lab for

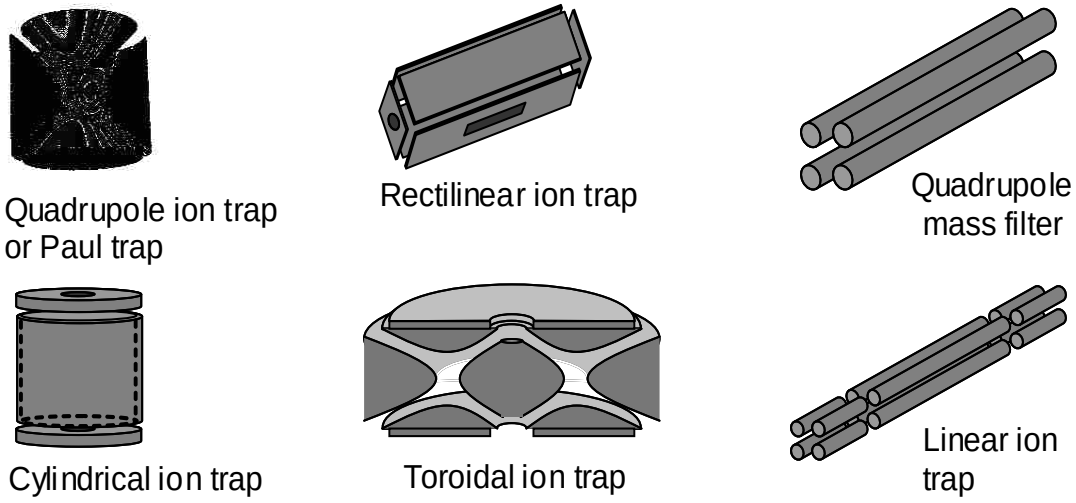

Figure 1.4. Various geometries of radiofrequency quadrupole ion traps.

analysis. Portable mass spectrometry would greatly enhance applications in which laboratory analysis is impractical, too slow or otherwise undesirable, such as emergency response to threats and hazards, sampling in remote locations, and on-line characterization of samples to preserve the native chemical environment or to prevent changes to the sample during transport. In some applications, such as analytical instruments exploring other planets in the solar system, portability is paramount.

Early efforts to miniaturize mass spectrometers can be traced back to the 1960s and 1970s. At that time, small, limited-resolution mass analyzers, such as magnetic sector[51-54] and quadrupole-type mass analyzers,[55-56] were miniaturized for leak detection[51-52] and residual gas analysis.[55] Much of the early work in miniaturizing mass analyzers resulted from the desire to send mass spectrometers to Mars, Venus, and the Moon in the 1970s.

More recently, as applications of mass spectrometry have broadened, advances in other fields have also driven the development of miniaturized mass spectrometers. The need for portable analytical tools covers areas such as national security, emergency response, military, field sciences, environmental on-site monitoring, and illicit drug detection. At the same time, improved techniques used for small-scale fabrication, from computer-controlled machining to microelectromechanical systems (MEMS), have enabled construction of smaller mass analyzers.

Although realization of portable mass spectrometry requires miniaturization of all instrument components—including vacuum system, electronics, sampling, detection, and user interface—the mass analyzer is often seen as the key to overall size reduction. For instance, as the mass analyzer is reduced, the mean free path of ions can also be reduced,

allowing smaller, lower-power vacuum pumps to be used. A given electric field strength can be made using lower voltages when electrodes are spaced more closely, facilitating use of smaller power supplies or batteries.

Recent years have seen miniaturization of all major mass analyzer types, with particular emphasis on quadrupole ion traps (QIT).[12] Ion traps are inherently compact, allow higher operating pressure than other analyzers, are capable of tandem mass analysis (particularly useful for identification of unknowns), and are fast enough to be combined with chromatographic separation devices. Construction techniques used to make small ion traps fall into three categories: 1) conventional machining at reduced size scales, 2) methods based on microfabrication, and 3) novel approaches, often employing unorthodox materials or electrode shapes, that fall between these two extremes.

1.2.2. Conditions to Operate Miniaturized Traps

Ions can be trapped and mass analyzed when their mass-to-charge ratio, *m/z*, falls below a certain limit, given by equation (4) above. For ions and trapping conditions in which q_z<0.908 (Figure 1.3), ions can be trapped. Mass analysis can be accomplished in several ways, but most commonly by applying a supplementary AC signal to resonantly excite the mass-dependent component of ion motion while ramping the RF amplitude.

Full-sized QITs (r_0 = 1 cm) are typically operated with an RF frequency of 1 MHz and an RF amplitude of several kilovolts. In miniaturized traps, there is a tradeoff between higher RF amplitude (greater trapping capacity and resolution) and lower RF frequency(resulting in lower power operation). Equation (4) illustrates the relationship between mass range, operating voltage, and RF frequency as the physical dimensions (r_0) of the trap are reduced. With size reduction of ion traps, the lower driving RF is required

and lower power is required to perform the mass scan. However, a reduction of RF potential decreases the potential well depth, which causes lower trapping efficiency and poorer mass resolution. Because it is desirable to reduce the operating voltage of small ion traps, higher frequency RF is typically used.

1.2.3. Obstacles to Miniaturization

Mass analysis in quadrupole ion traps relies on precisely-shaped electric fields. As traps are miniaturized it becomes increasingly difficult to maintain the relative accuracy of electrode geometry and alignment needed to produce these fields. Miniaturization of mass analyzers has progressively challenged the limits of conventional machining technologies, and has increasingly turned to microfabrication and related techniques to obtain high-precision pieces. However, even with microfabrication, the geometric defects can be quite large relative to the size of the trap. For many fabrication techniques, the field perturbation caused by surface roughness also begins to affect performance.[57]

In addition to the accuracy of field shape, several other issues arise during miniaturization. Ion traps can contain and analyze only a finite number of ions, and this number drops dramatically as traps become smaller. In very small traps the ion-ion repulsion (space-charge) affects the apparent electric field felt by ions, causing broadening of peaks in the mass spectrum. In the extreme case of micrometer-sized ion traps, a trap can contain only a single ion.[23]

There is significant interest in increasing the operating pressure of ion traps so that smaller, lower power vacuum pumps can be used. However, the increased pressure

makes electrical discharge a concern. Additionally, arcing and field emission[58] become greater concerns as the spacing between electrodes is reduced.

1.2.4. Methods for Ion Trap miniaturization

1.2.4.1 Conventional Machining

Ouyang et al.[59] introduced the distinction between top-down vs. bottom-up approaches to mass analyzer miniaturization. The use of conventional machining to make the size of the electrodes as small as possible, while keeping electrode surfaces in the desired shape, is called the top-down method. Efforts that rely on microfabrication techniques to make tiny ion traps are considered bottom-up approaches.

Much of the early ion trap miniaturization efforts in both top-down and bottom-up approaches used cylindrical ion traps (CITs). CITs use cylindrical electrodes to approximate the electrical fields created by hyperboloidal electrodes in QITs.[21-22, 60] Although the electric fields in CITs are not nearly as good for mass analysis, performance is adequate for most potential applications. Importantly, cylindrical surfaces are much easier to create using either conventional machining or microfabrication.

Considerable effort went into top-down miniaturization of CITs in the late 1990s and early 2000s, primarily at Purdue University and at the Oak Ridge National Lab. Many ionization techniques[28, 61-62] were used to demonstrate performance on a single miniaturized CIT, and later on a 2-D array of seven 1-mm (r_0) CITs.[63] The use of an array of traps[26, 64-65] was intended to recover the loss in sensitivity due to the reduced number of ions that could be trapped in a single miniaturized trap.[27, 66-68] At the same time many fundamental studies were performed using sub-mm-sized CITs.[69-71]

Even though the sensitivity loss from trap size reduction can be compensated by arraying traps, the space-charge problem and shallow potential well caused by low operation voltage still exist in three dimensional traps such as the CIT. In contrast, two-dimensional ion traps can provide both improved trapping efficiency and higher trapping capacity. In such devices, which include linear,[72] rectilinear,[35] and toroidal ion traps,[32] the trapping volume is extended in one dimension. Top-down miniaturized rectilinear ion traps (RITs) have been developed and are currently used in a commercial portable mass spectrometer.[73-78] A miniaturized toroidal ion trap[38] has also been developed and is now available in a portable GC-MS system.[39] These instruments demonstrate reasonably high mass resolution and mass range.

1.2.4.2 Microfabrication Approaches to Ion Trap Miniaturization

In the past decade microfabrication techniques have been used to reduce the dimensions of all types of mass analyzers, particularly quadrupole mass filters.[79-81] Because ion traps must constrain ion motion in three dimensions, whereas microfabrication tends to be a 2-dimensional process (i.e., out-of-plane features are limited both in dimensions and in design possibilities), careful consideration has been required to produce working devices. Arrays of CITs on silicon chips and other substrates have been developed by several groups.

Early efforts to produce arrays of CITs at Sandia National Laboratories (Albuquerque, New Mexico) used a layer-by-layer deposition of tungsten and silicon dioxide layers to produce the end caps, ring electrode, spacers, and faraday-style detector[23]. In one of these CIT arrays the individual ion trap had r_0 as small as 1 μm,[23] while later designs used r_0 values of 2, 5 and 10 μm.[82] Operating voltages were on the

order of a few tens of volts. These arrays suffered from large capacitance (and corresponding power and heating), and significant noise due to the close proximity of the detector strip and the RF layer. In addition, it was difficult to introduce ions into the trap or to create ions within the trap due to the small size. Simulations indicated that only one ion could be trapped in the 1 μm traps due to space-charge.[83] Even with up to a million traps in parallel, no noticeable signal could be detected above the noise.

A more recent approach of MEMS-based ion traps by Chaudhary et al. at the University of South Florida involves bonding together two silicon substrates, each containing a single end cap and half of the cylindrical ring electrode for each trap in the array—half of each trap.[84] Bonding the two substrates together makes a set of complete CITs. Electrodes and other features were made in silicon, SiO_2, and Si_3N_4, with conductivity provided by selectively coating electrode surfaces with chromium and gold.

Another MEMS-based device containing an array of 256 CITs (r_0 = 20 μm) was made using p-doped silicon for electrodes and silicon dioxide as insulators reported by Pau et al. at the University of Arizona.[24] The top end cap was left open, with the same diameter as the ring electrode. The trap array was operated with an RF frequency of 100 MHz and amplitude below 90 $V_{0\text{-}p}$. At this trap size, it was estimated that the capacity of each trap was around 10 ions during mass analysis.

MEMS techniques have been applied not only to fabrication of CIT arrays but also to assembly of electron and ion optics to accompany the miniaturized mass analyzers presented by Fox et al. [85] A 1 mm Bradbury-Nielsen gate and a 500 μm Einzel lens have been built in addition to a multi-layer 500 μm CIT. With such an integrated approach it may be possible to build all-in-one mass spectrometer systems.

1.2.5 New Fabrication Approaches

1.2.5.1 New Materials

An emerging area of research in mass analyzer miniaturization makes use of novel fabrication materials, including polymers and ceramics. Techniques used to process these materials allow construction of arbitrary and complex ion trap geometries which cannot be made by conventional machining and are difficult to make using standard microfabrication. For instance, Yu et al. at Purdue University reported polymer-based ion traps made using rapid prototyping techniques with a stereolithography apparatus (SLA).[86] In this fabrication approach, the three-dimensional trap design is realized by rastoring a UV laser over the surface of a photosensitive resin, building up the device one cross-sectional layer at a time. The polymer structure is then selectively metalized to create conducting surfaces. Structures and geometries made using SLA do not face the same physical limitations as are imposed by conventional machining. In addition, complex structures can be made with high precision, so ideal hyperbolic electrode shapes can be used. Surface roughness continues to be an issue with SLA, however. This method was applied to miniaturization and geometry optimization of a polymer-based rectilinear ion trap by Fico et al. at Purdue University.[87] The resolution, mass/charge range (unit mass resolution to mass 300) and tandem capabilities were demonstrated in full-size, half- and 1/3-size devices. SLA demonstrated the ability to fabricate light, small rectilinear ion traps with good performance.

The SLA approach has recently been used to produce circular arrays of polymer-based miniature RITs by Fico et al. (Figure 1.5).[88] Two versions were reported, using

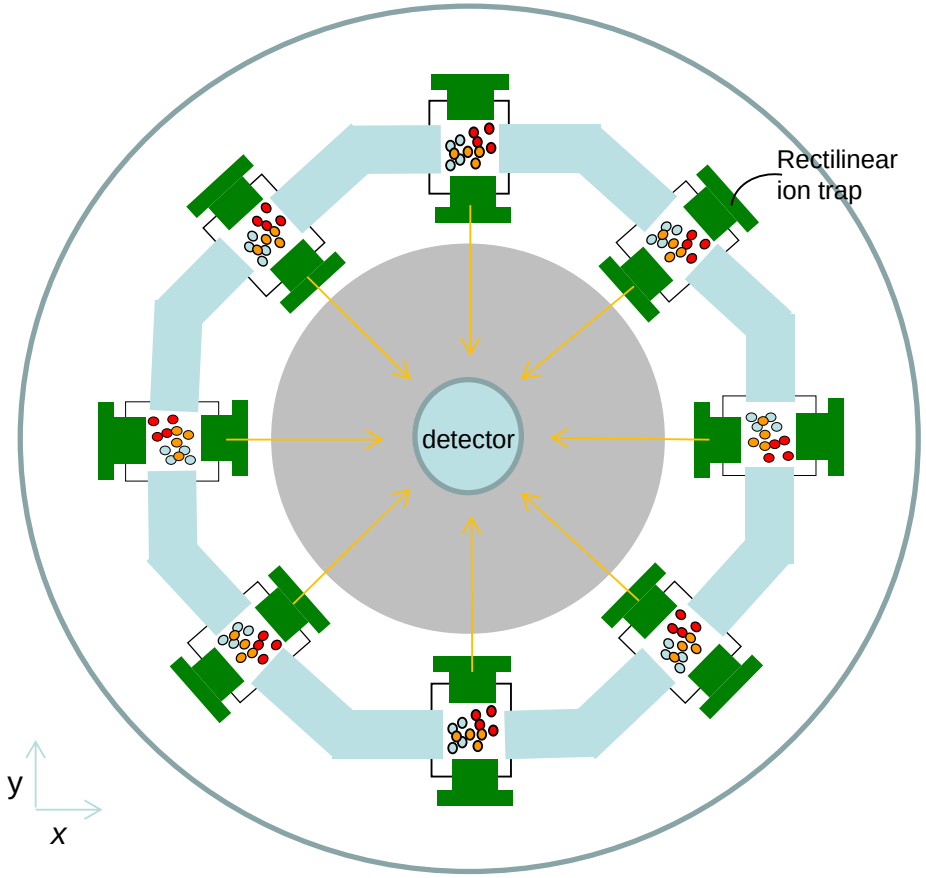

Figure 1.5. Schematics of cross-section of circular arrays of polymer-based miniature rectilinear ion traps. (Adapted from Fico, M.; Maas, J. D.; Smith, S. A.; Costa, A. B.; Ouyang, Z.; Chappell, W. J.; Cooks, R. G., Circular arrays of polymer-based miniature rectilinear ion traps. *Analyst* **2009,** *134*, 1338-1347.)

either six or twelve RITs (x_0 = 1.66mm, y_0 = 1.33mm, z = 16.66 mm). Both arrays of polymer-based mass analyzers and their mounting hardware were constructed with stereolithography apparatus (SLA), involving laser-photopolymerization of a resin, followed by UV curing, thermal baking, and metal plating. The RITs in these two versions were mounted in parallel around the detector positioned in the center of the circle of surrounding traps. All the ions trapped in the array were radially ejected to the centrally located detector. Each trap had its own ion source, or alternatively all the traps in the array can share a single ion source. Thus three distinct modes of operation for a multiplexed system can be performed in the array, which allows single sample analysis with high throughput or parallel spectra analysis for multiple samples.

Miniature monolithic rectilinear ion trap arrays have also been made using stereolithography directly on printed circuit boards (PCB) presented by Maas et al.[89] Integrating stereolithography-fabricated ion traps on planar rigid substrates offers the possibility for more complex monolithic structures and integrated electronics. Assembly of traps and alignment of both individual traps and electrodes is simplified.

An alternative, but conceptually similar technique to producing polymer-based devices relies on digital light processing (DLP). DLP resembles SLA fabrication in many respects, but is capable of better accuracy and improved surface roughness. DLP has been used to produce a linear ion trap made from polymethylmethacrylate (PMMA) reported by Clare et al.[90] Conducting surfaces are made by evaporating gold onto the PMMA. The electrodes conform to the ideal hyperbolic shape, which is not more difficult to make using DLP than the simplified planar shape of the RIT. The trap has been successfully incorporated into a portable mass spectrometer device and measured

resolution (FWHM) of 260 has been achieved for a variety of samples with high mass range (500).

Finally, Chaudhary et al. introduced a small cylindrical ion trap mass spectrometer constructed with low-temperature co-fired ceramic materials.[25] The ring electrode of this CIT (r_0 = 1.375 mm) was fabricated using multiple layers of low temperature co-fired ceramics (LTCC), and endplates were made of stainless steel. Five major steps were processed to fabricate ring electrode, including punching, lamination, firing, metallization and photolithography. A typical peak width of 1.8 Da was achieved with this prototype CIT when operated in the mass-selective instability mode.

In general, new materials allow simpler construction, improved electrode shape and alignment. Demonstrated performance using several different systems shows promise for the use of ion traps based on new materials in portable analytical instruments. On the other hand, much remains to be worked out in terms of the mechanical and thermal properties of these materials. For instance, polymer expansion, softening, and deformation during heating may be an issue for these traps when operated in-field.

1.2.5.2 New Shapes

Simplification of electrode shape has long been pursued in the context of ion trap miniaturization, starting from the original cylindrical ion trap and later with the rectilinear trap. In both cases, cylindrical and planar electrode surfaces are much simpler to machine than the corresponding hyperbolic surfaces. Beyond this, there have been several recent attempts to create ion trap mass analyzers using simplified electrode shapes in new ways and arrangements. Considering that the simplest geometric surface is a plane, and that fewer electrodes result in simpler construction, a novel linear ion trap

mass analyzer was introduced using just four elongated planar electrodes mounted in parallel reported by Song et al. at Purdue University.[91] The performance of this new device was comparable to that of the 6-electrode rectilinear ion trap (RIT) from which it was derived.

A quadrupole ion trap in which all features are patterned on a single planar substrate was built by Pau et al. at the University of Arizona[92] and demonstrated an extremely large mass range for trapping ions and particles with *m/z* from 10^2 to 10^9. For the mass range from 50 to 150, mass resolution of 1.2 amu can be achieved by the device. The basis of this device is a planar ring structure composed of one or several circular ring electrodes on top of a circular ground plane. All the ring electrodes shared the same axis and were fabricated and arrayed by patterning a single layer of conductors. The planar device allowed integration to circuits, easy access to externally injected particles or ions and scalable fabrication to smaller size.

In 2009, an array of linear ion trap mass analyzers designed and constructed using several planar electrodes, including two parallel printed circuit boards (PCB) was reported by Li et al. at Fudan University (Shanghai, China).[93] Four ion trap channels were formed in an enclosed space composed of a pair of printed circuit board plates, a pair of end-cap electrodes, and a pair of boundary electrodes (Figure 1.6). The polarity of RF voltage applied to the adjacent two strips was opposite so the electric potential at the central plane between two adjacent strips is zero. Mass resolution over 1000 has been achieved in one trapping region using this device.

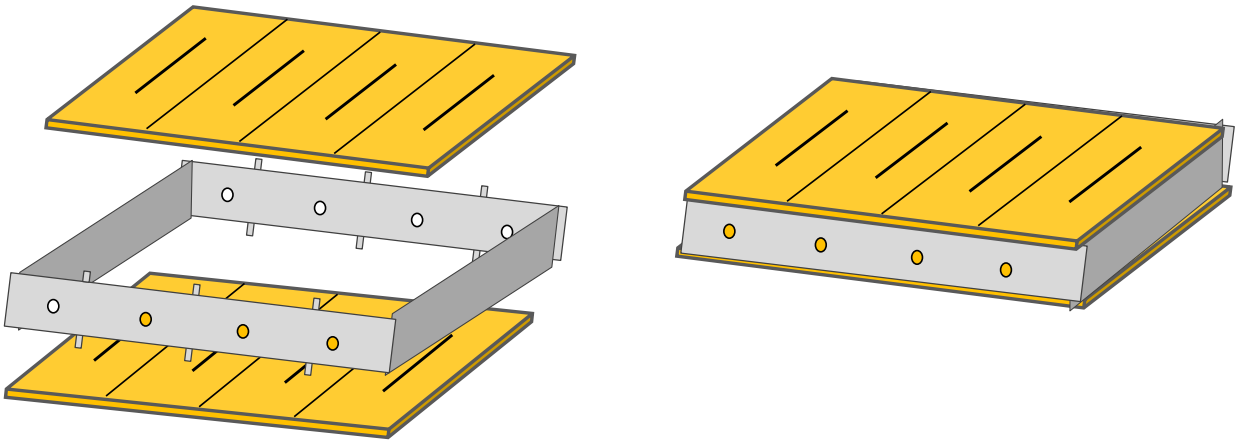

Figure 1.6. Planar linear ion trap array mass analyzer consisted of printed circuit board (PCB). (Adapted from Li, X. X.; Jiang, G. Y.; Luo, C.; Xu, F. X.; Wang, Y. Y.; Ding, L.; Ding, C. F., Ion Trap Array Mass Analyzer: Structure and Performance. *Anal Chem* **2009,** *81*, 4840-4846.)

As a final example of novel designs, a CIT has been developed comprising four disks, each with one 2.05-mm-diameter hole, stacked in parallel with the holes aligned coaxially by Yang et al. at Sam Yang Chemical Company (Korea).[94] The two inner disks with thickness of 0.3 mm function as the ring electrodes and two outer disks function as endcaps. The trap was operated at RF amplitude of up to 1500 Vp-p and frequency of 3.9 MHz, with scanning ion mass of up to *m/z* 300. Sample was introduced to the ion trap with a pulsed inlet system. A palm-portable mass spectrometer using this miniaturized cylindrical ion trap, a getter pump, on-board electronics and software, and a lithium-ion battery has been introduced with a weight of 1.48 kg (3 lbs.) and a size of 1.54 L (8.2 × 7.7 × 24.5 cm^3) that can be operated with an average battery power of 5 W. Trace organic gas in the air up to 6 ppm for toluene and 22 ppm for dimethyl methylphosphonate (DMMP) can be detected with detection time less than 1s.

1.3 Planar Ion Traps with Ceramic Plates

1.3.1 Development of Planar Ion Traps

As mentioned above, several geometrical variations on the original quadrupole ion trap (Paul trap) have been developed, including cylindrical,[82] rectilinear,[35] linear,[72] and toroidal[32] ion trap designs, each with advantages and disadvantages. For instance, rectilinear, linear, and toroidal traps have inherently larger storage volumes compared with quadrupole and cylindrical ion traps. In all ion trap variations, metal electrodes are used to produce the appropriate electric fields. For full-sized ion traps, modern machining equipment easily produces the hyperboloidal electrode surfaces of the quadrupole ion trap. For miniaturized traps, however, machining methods have been pushed to the limit, and simpler electrode geometries such as planar and cylindrical are

required. For this reason, most miniaturized and microfabricated ion traps have utilized the cylindrical trap design.[24, 29, 64, 82, 95-96]

Our research group recently reported[97] a new approach to making ion traps with only two planar ceramic plates. In the planar trap, trapping fields are made using a combination of resistive material and metal electrode rings lithographically imprinted on ceramic disks. A radial potential function can be applied to the resistive material such that the potential between the plates is quadrupolar, and ions are trapped between the plates. The electric field is independent of geometry and can be optimized electronically. Thus potential functions superimposed on the resistive material produce trapping fields that resemble the fields created by shaped metal electrodes. Using this novel design with only two planar ion trap electrodes, obstacles to miniaturization of ion traps, such as fabrication tolerances, surface smoothness, electrode alignment, limited access for ionization or ion injection, and small trapping volume are addressed.

1.3.2 Electric Field Created inside the Planar Ion Trap

Electric fields in ion traps play a key role in the motion of ions, and thus in trap performance. Electric fields in ion traps can be determined by solving the Laplace equation ($\nabla^2\Phi = 0$) for a given set of boundary conditions. These boundary conditions are determined by the electrodes that form the trap. Metal electrodes produce equipotential boundary conditions, so the trapping fields are directly related to, and limited by, the geometry and arrangement of the electrodes.

Other approaches to produce quadrupolar trapping potentials have been explored. Wang and Wanczek proposed a method[98] in which several parallel ring electrodes in the shape of two abutting cones produce the same fields as a quadrupolar ion trap. The RF

amplitude on the rings increases linearly from the smallest to the largest rings. This concept is suggestive of a more general approach, in which the electrode geometry can be independent of the trapping field geometry if the electrodes forming the trap can have an arbitrary potential function.[99]

Consider the quadrupolar potential found in an ideal Paul-type ion trap. The time-independent potential along x, y, or z is quadratic everywhere in the trap:

$$\Phi = A(x^2 + y^2 - 2z^2) + C \qquad (5)$$

in which the rotational axis of the trap lies in the z-direction. A plane parallel to the x-y plane will have a quadratic potential function. Similarly, a cylindrical surface with a constant radius will have a potential that varies quadratically with z. If two such planes and this cylindrical surface form a closed volume, with quadratic potential functions on each surface, the fields within this volume will be identical to those made with hyperboloidal electrodes (Figure 1.7). By applying a radiofrequency signal, the time-dependent fields in this hypothetical volume will match the ideal Paul trap, and ion motion will be identical. Because surfaces with position-varying potential functions can be made using resistive material, any trapping geometry field can be realized in this planar trap by changing the superimposed potential function on the resistive material. With machined metal electrodes, it is impossible to switch trapping field geometry in this manner.

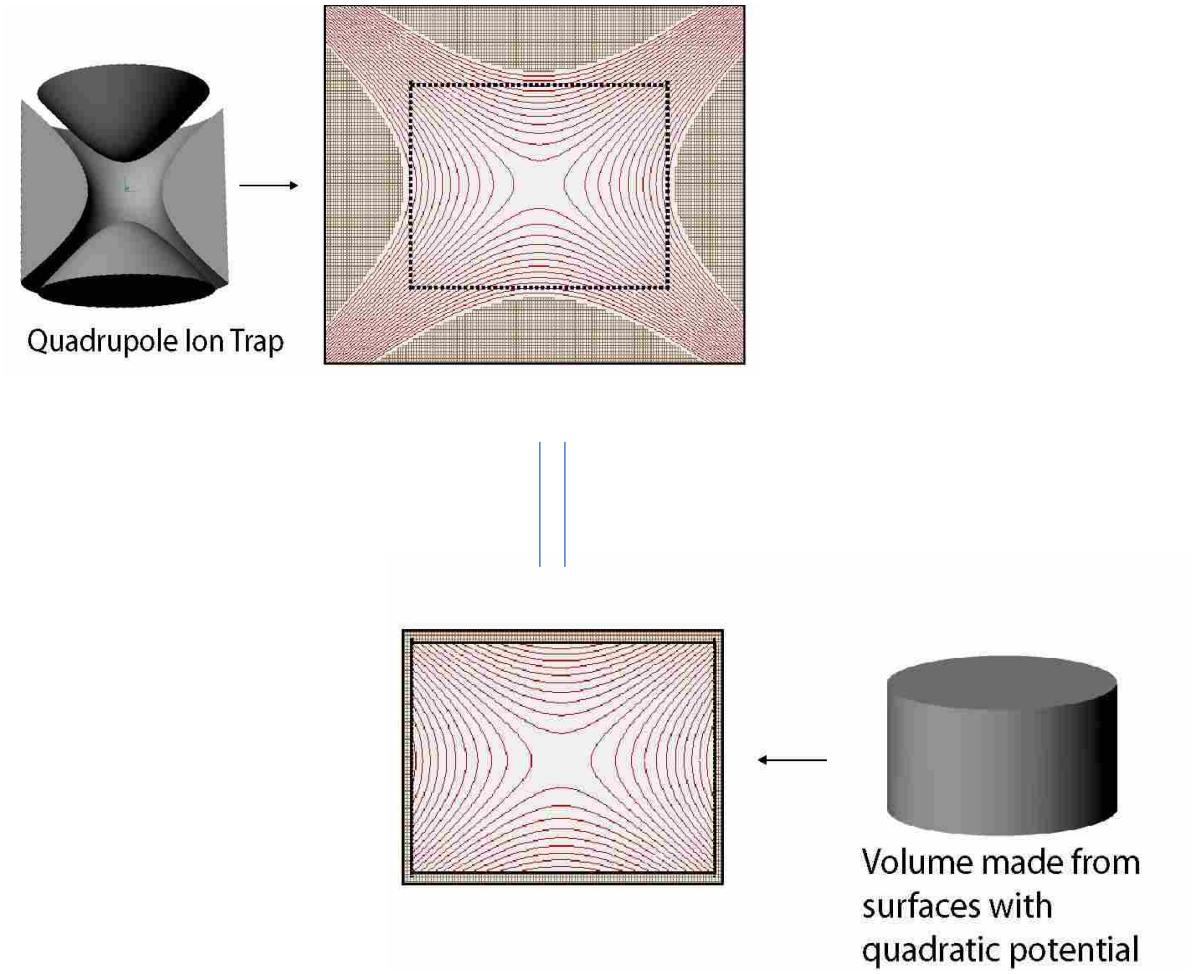

Figure 1.7. Quadratic potential functions on two planes and a cylinder produce a quadrupolar potential distribution identical to that in a trap made using hyperbolic metal electrodes.

1.3.3 Planar Ion Trap with Toroidal Geometry

In an example of a planar trap, called the Halo ion trap (Figure 1.8), resistive material (germanium) and underlying aluminum rings on the facing surfaces of two ceramic plates produce a toroidal trapping field. Trapped ions can be mass analyzed using resonance ejection. Ions are ejected through the center hole of one of the plates, and subsequently detected using an electron multiplier. In this reported Halo ion trap,[97] experiments using toluene, dichloromethane, and similar compounds showed mass resolution in the range of 50 to 100 ($m/\Delta m$). Although the trapping fields in the vicinity of the center of the trapping volume agreed very well with the conventional toroidal ion trap, edge effects at the inside and outside of the plates (smaller and larger radial distances from rotational axis) produced significant field distortion that could not be completely eliminated by varying the ring potentials. Experiments in which a copper cylinder with a slit was placed inside this region did not improve resolution or sensitivity. Simulations using SIMION 7[100] and SIMION 8[101] show that the difficulty with this method is in taking ions with primarily radial inward motion and pushing them out along one axis. Another difficulty is that the field drops off significantly near the center of the device—again an edge effect. Simple mass-selective instability scanning, such as a frequency ramp or a voltage ramp, result in ions impacting the electrode plates, rather than ejecting in a radial direction.

Recently a new version of the Halo ion trap was presented, in which ions are ejected out from annular slits in the ceramic plates.[102] Both of these designs use a larger trapping volume—a ring—increasing the number of ions that can be analyzed and improving sensitivity. These two-plate devices combine both new materials and new

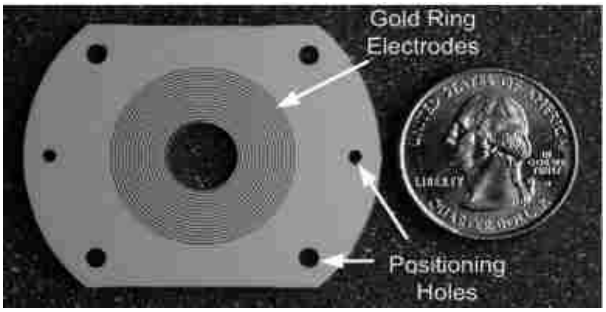

(a)

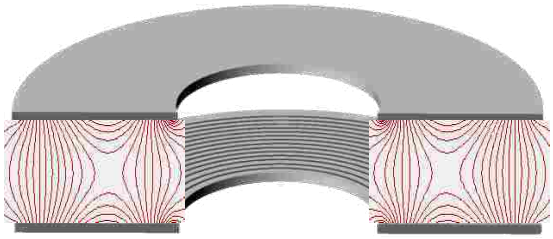

(b)

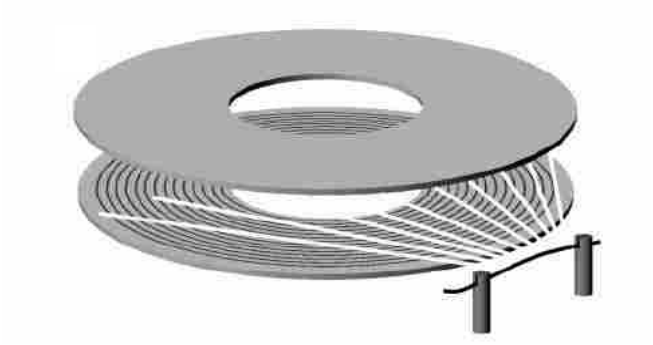

(c)

Figure 1.8. (a) Planar ceramic plates used in the Halo ion trap, (b) electric field in the Halo ion trap, and (c) illustration of electron beam irradiation of neutrals in the Halo ion trap.

designs for ion trap construction. In ion traps made using patterned planar surfaces, the accuracy and shape of the electric fields are not limited by electrode geometry nor machining precision, as is the case in traps made with metal electrodes.

1.3.4 Performance and Advantages of the Planar Trap

A planar trap with toroidal trapping field has been successfully developed and efforts are currently underway to explore other trapping geometries. In the Halo ion trap, the potential was applied to each ring electrode and the resulting field was determined by the potential function on the ceramic plates. Therefore not only arbitrary trapping geometries can be achieved by this method, but also multipole field components can be independently controlled by adjusting the potentials on the ring electrodes. In conventional traps it is not possible to change trapping fields using the same set of metal electrodes. This planar geometry offers a great advantage to miniaturized ion traps since it is not necessary to make trap electrodes smaller and smaller. In addition, the planar geometry can address the issues raised from mechanical tolerances, surface roughness, alignment of electrodes, shallower pseudopotential depth, limited applied voltage range, limited access to the trapping region, reduced ion trapping capacity, and difficulty of trap fabrication.

1.4 Conclusions and Summary

Now ion traps are among the most widely used mass analyzers, used in applications ranging from proteomics to chemical warfare agent detection[67, 103-105] and used for tandem mass analysis and other ion dissociation techniques.[106-107] Because ions can be accumulated and stored, ion molecule reactions can be carried out and studied within the trap.[108-110] Ion traps are frequently combined with gas chromatographs and other separation instruments,[111-112] enhancing

their capabilities. The simple design and relatively high operating pressure make ion traps attractive choices for instrument miniaturization.

The need for a portable mass spectrometer has largely driven efforts to produce miniaturized ion traps.[113] Although the mass analyzer is just one of several components of a complete mass spectrometer system, miniaturization of the mass analyzer can often reduce the size and weight of other components. Many efforts have been made on miniaturization of ion traps including conventional fabrication and microfabrication (MEMS) to make trap size smaller. Because of the limitations of those technologies, new geometry and new material of trap electrodes have been applied to the miniaturization of ion traps. Planar ion traps using only two ceramic plates, the facing surfaces of which are imprinted with concentric metal ring electrodes have raised increasing interest for trap miniaturization.

Although still in early development, ion traps made using planar electrodes have several inherent advantages, many of which apply to miniaturization. Planar traps provide a simpler solution to mechanical tolerance, surface quality, fabrication, and alignment issues. Trap access is also improved. Trapping capacity can be increased by using a toroidal, linear, or rectilinear geometry. Further experiments are now being carried out to examine other opportunities and limitations of planar resistive electrode ion traps.

1.5 Dissertation Overview

The planar ion trap family now includes the Halo ion trap, the planar Paul ion trap, the coaxial ion trap and other traps under exploration. The simple geometry and open design of the planar traps offer great opportunity for miniaturized systems.

In this dissertation, Chapter 2 describes the method to created trapping fields in planar traps, microfabrication technology to make ceramic plates, configuration, instrumentation and

performance of the planar quadruople ion trap. Much of this chapter is adapted from "Novel Ion Traps Using Planar Resistive Electrodes: Implications for Miniaturized Mass Analyzers" (Austin, D. E.; Peng, Y.; Hansen, B. J.; Miller, I. W.; Rockwood, A. L.; Hawkins, A. R.; Tolley, S. E., *J. Am. Soc. Mass Spectr.* **2008**, *19*, 1435-1441.) and "Paul Trap Mass Analyzer Consisting of Opposing Microfabricated Electrode Plates (Zhang, Z. P.; Peng, Y.; Hansen, B. J.; Miller, I. W.; Wang, M.; Lee, M. L.; Hawkins, A. R.; Austin, D. E., *Anal. Chem.* **2009,** *81*, 5241-5248). A designed RF function is applied to each ring, such that the trapping field produced is similar to that of the conventional Paul trap. Experiments demonstrate the effects of ion ejection mode and scan rate on mass resolution for several small organic compounds. The current instrument has a mass range up to ~180 Thomsons (Th), with better than unit mass resolution over the entire range.

Chapter 3 presents the design and results for another new radiofrequency ion trap mass analyzer, the coaxial ion trap, in which both toroidal and quadrupolar trapping regions are created simultaneously. Much of this chapter is adapted from "Coaxial Ion Trap Mass Spectrometer: Concentric Toroidal and Quadrupole Trapping Regions" (Peng, Y.; Hansen, B. J.; Quist, H.; Zhang, Z. P.; Wang, M.; Hawkins, A. R.; Austin, D. E., *Anal. Chem.* in press). Experiments demonstrate that ions can be trapped in either region, transferred from the toroidal to the quadrupolar region, and mass-selectively ejected from the quadrupolar region to a detector. Ions trapped in the toroidal region can be transferred to the quadrupole region using an applied AC signal in the radial direction with amplitude of 25 $V_{p\text{-}p}$ and frequency of 1100 kHz, although it appears that the mechanism of this transfer does not involve resonance with the ion secular frequency, and the process is not mass selective. Ions in the quadrupole trapping region are mass analyzed using dipole resonant ejection. Multiple transfer steps and mass analysis scans on a

single population of ions illustrate the larger ion capacity of the toroidal ion trap compared to the quadrupole trap, and possible applications in analyzing transient or dynamic events.

Chapter 4 describes some simulation work focused on exploring the fields to realize resonant ejection of ions from the toroidal trapping region to the quadrupople trapping region. A one-dimensional calculation method was applied to simulate the movement of ions along the radial direction. The effect of radial field superimposed with high-order components was investigated on the oscillation of ions. Variables like amplitude and frequency of driving RF and supplementary AC (ejecting β values) were investigated, and are presented in this chapter. The material from Chapter 4 has not yet been submitted for publication.

Finally the summary for the whole work during the period of my PhD study and future work are presented in Chapter 5.

1.6 References

1. Benyezzar, M.; Creaser, C. S.; Stygall, J. W. Proceedings of the 46th ASMS Conference on Mass Spectrometry and Allied Topics, Orlando, FL, Orlando, FL, 1998; p 1246.

2. Henry, C., Building a better trap. *Anal. Chem.* **1998,** *70*, 533A-536A.

3. Ziegler, Z., Ion traps come of age - Software control helps these versatile mass spectrometers mature. *Anal. Chem.* **2002,** *74*, 489a-492a.

4. Todd, J. F. J.; March, R. E., A retrospective review of the development and application of the quadrupole ion trap prior to the appearance of commercial instruments. *Int. J. Mass. Spectrom.* **1999,** *191*, 9-35.

5. Bonner, R. F.; Lawson, G.; Todd, J. F. J., *Int. J. Mass Spectrom. Ion Phys.* **1972,** *10*, 197-203.

6. Lawson, G.; Bonner, R. F.; Mather, R. E.; Todd, J. F. J.; March, R. E., Quadrupole Ion Store (Quistor) .1. Ion Molecule Reactions in Methane, Water and Ammonia. *J. Chem. Soc. Farady Trans. 1* **1976,** *72*, 545-557.

7. Bonner, R. F.; Lawson, G.; Todd, J. F. J.; March, R. E., in *Advances in Mass Spectrometry*, A.R. West ed.; Applied Science: London, 1974; Vol. 6.

8. Bonner, R. F.; Lawson, G.; Todd, J. F. J., A low-pressure chemical ionisation source: an application of a novel type of ion storage mass spectrometer. *J. Chem. Soc. Chem. Commun.* **1972**, 1179-1180.

9. Mather, R. E.; Lawson, G.; Todd, J. F. J.; Bakker, J. M. B., Quadrupole Ion Storage Trap (Quistor) as a Low-Pressure Chemical Ionization Source for a Magnetic-Sector Mass-Spectrometer. *Int. J. Mass Spectrom.* **1978,** *28*, 347-364.

10. Lawson, G.; Todd, J. F. J., Weak Peak Enhancement by Selective Ion Trapping in a Quadrupole Ion Storage Source. *Anal. Chem.* **1977,** *49*, 1619-1622.

11. Buttrill Jr., S. E.; Shaffer, B.; Karnicky, J.; Arnold, J. T. Proceedings of the 40th ASMS Conference on Mass Spectrometry and Allied Topics, Washington DC, May/June 1992; p 1015.

12. March, R. E., An introduction to quadrupole ion trap mass spectrometry. *J. Mass Spectrom.* **1997,** *32*, 351-369.

13. Mathieu, E., *J. Math. Pure Appl . (J. Liouville)* **1868,** *13*, 137-203.

14. Williams, J. D.; Cox, K. A.; Cooks, R. G.; McLuckey, S. A.; Hart, K. J.; Goeringer, D. E., Resonance Ejection Ion Trap Mass Spectrometry and Nonlinear Field Contributions - The Effect of Scan Direction on Mass Resolution. *Anal. Chem.* **1994,** *66*, 725-729.

15. Paul, W.; Steinwedel, H., A new mass spectrometer without a magnetic field. *Z. Naturforsch. Sect. A* **1953,** *8*, 448-450.

16. Fulford, J. E.; Hoa, D. N.; Hughes, R. J.; March, R. E.; Bonner, R. F.; Wong, G. J., Radio-Frequency Mass Selective Excitation and Resonant Ejection of Ions in a 3-Dimensional Quadrupole Ion Trap. *J. Vac. Sci. Technol.* **1980,** *17*, 829-835.

17. Stafford, G. C.; Kelley, P. E.; Syka, J. E. P.; Reynolds, W. E.; Todd, J. F. J., Recent Improvements in and Analytical Applications of Advanced Ion Trap Technology. *Int. J. Mass Spectrom.* **1984,** *60*, 85-98.

18. Louris, J. N.; Cooks, R. G.; Syka, J. E. P.; Kelley, P. E.; Stafford, G. C.; Todd, J. F. J., Instrumentation, Applications, and Energy Deposition in Quadrupole Ion-Trap Tandem Mass-Spectrometry. *Anal. Chem.* **1987,** *59*, 1677-1685.

19. Grebner, T. L.; Neusser, H. J., Laser-Produced Ions Stored in a Cylindrical Ion-Trap and Detected in a Reflectron Time-of-Flight Mass-Spectrometer. *Int. J. Mass Spectrom.* **1994,** *137*, L1-L6.

20. Mikami, N.; Miyata, Y.; Sato, S.; Sasaki, T., Ion Trap Method Combined with 2-Color Laser Spectroscopy of Supersonic Molecular-Beams - Photodissociation of Trapped $C_6H_5Cl^+$. *Chem. Phys. Lett.* **1990,** *166*, 470-474.

21. Fulford, J. E.; March, R. E.; Mather, R. E.; Todd, J. F. J.; Waldren, R. M., The Cylindrical Ion Trap - a Theoretical and Experimental-Study. *Can. J. Spectrosc.* **1980,** *25*, 85-97.

22. Wells, J. M.; Badman, E. R.; Cooks, R. G., A quadrupole ion trap with cylindrical geometry operated in the mass selective instability mode. *Anal. Chem.* **1998,** *70*, 438-444.

23. Blain, M. G.; Riter, L. S.; Cruz, D.; Austin, D. E.; Wu, G. X.; Plass, W. R.; Cooks, R. G., Towards the hand-held mass spectrometer: design considerations, simulation, and fabrication of micrometer-scaled cylindrical ion traps. *Int. J. Mass Spectrom.* **2004,** *236*, 91-104.

24. Pau, S.; Pai, C. S.; Low, Y. L.; Moxom, J.; Reilly, P. T. A.; Whitten, W. B.; Ramsey, J. M., Microfabricated quadrupole ion trap for mass spectrometer applications. *Phys. Rev. Lett.* **2006,** *96*, 120801.

25. Chaudhary, A.; van Amerom, F. H. W.; Short, R. T.; Bhansali, S., Fabrication and testing of a miniature cylindrical ion trap mass spectrometer constructed from low temperature co-fired ceramics. *Int. J. Mass Spectrom.* **2006,** *251*, 32-39.

26. Ouyang, Z.; Badman, E. R.; Cooks, R. G., Characterization of a serial array of miniature cylindrical ion trap mass analyzers. *Rapid Commun. Mass Spctrom.* **1999,** *13*, 2444-2449.

27. Badman, E. R.; Johnson, R. C.; Plass, W. R.; Cooks, R. G., A miniature cylindrical quadrupole ion trap: Simulation and experiment. *Anal. Chem.* **1998,** *70*, 4896-4901.

28. Kornienko, O.; Reilly, P. T. A.; Whitten, W. B.; Ramsey, J. M., Micro ion trap mass spectrometry. *Rapid Commun. Mass Spectrom.* **1999,** *13*, 50-53.

29. Van Amerom, F. H. W.; Chaudhary, A.; Cardenas, M.; Bumgarner, J.; Short, R. T., Microfabrication of cylindrical ion trap mass spectrometer arrays for handheld chemical analyzers. *Chem. Eng. Commun.* **2008,** *195*, 98-114.

30. Schwartz, J. C. In *Do space charge effects limit LC quadrupole ion trap performance?*, Sanibel Conf. Mass Spectrom., Quadrupole Ion Traps, 9th, Sanibel Island, FL, Sanibel Island, FL, 1997.

31. Bier, M. E.; Syka, J. E. P. U.S. Patent No. 5, 1995.

32. Lammert, S. A.; Plass, W. R.; Thompson, C. V.; Wise, M. B., Design, optimization and initial performance of a toroidal rf ion trap mass spectrometer. *Int. J. Mass Spectrom.* **2001,** *212*, 25-40.

33. Hager, J. W., A new linear ion trap mass spectrometer. *Rapid Commun. Mass Spectrom.* **2002,** *16*, 512-526.

34. Schwartz, J. C.; Senko, M. W.; Syka, J. E. P., A two-dimensional quadrupole ion trap mass spectrometer. *J. Am. Soc. Mass Spectr.* **2002,** *13*, 659-669.

35. Ouyang, Z.; Wu, G. X.; Song, Y. S.; Li, H. Y.; Plass, W. R.; Cooks, R. G., Rectilinear ion trap: Concepts, calculations, and analytical performance of a new mass analyzer. *Anal. Chem.* **2004,** *76*, 4595-4605.

36. Dolnikowski, G. G.; Kristo, M. J.; Enke, C. G.; Watson, J. T., Ion-Trapping Technique for Ion Molecule Reaction Studies in the Center Quadrupole of a Triple Quadrupole Mass-Spectrometer. *Int. J. Mass Spectrom.* **1988,** *82*, 1-15.

37. Quarmby, S. T.; Yost, R. A., Fundamental studies of ion injection and trapping of electrosprayed ions on a quadrupole ion trap. *Int. J. Mass Spectrom.* **1999,** *191*, 81-102.

38. Lammert, S. A.; Rockwood, A. A.; Wang, M.; Lee, M. L.; Lee, E. D.; Tolley, S. E.; Oliphant, J. R.; Jones, J. L.; Waite, R. W., Miniature toroidal radio frequency ion trap mass analyzer. *J. Am. Soc. Mass Spectr.* **2006,** *17*, 916-922.

39. Contreras, J. A.; Murray, J. A.; Tolley, S. E.; Oliphant, J. L.; Tolley, H. D.; Lammert, S. A.; Lee, E. D.; Later, D. W.; Lee, M. L., Hand-Portable Gas Chromatograph-Toroidal Ion Trap Mass Spectrometer (GC-TMS) for Detection of Hazardous Compounds. *J. Am. Soc. Mass Spectr.* **2008,** *19*, 1425-1434.

40. Geromanos, S. J.; Vissers, J. P. C.; Silva, J. C.; Dorschel, C. A.; Li, G. Z.; Gorenstein, M. V.; Bateman, R. H.; Langridge, J. I., The detection, correlation, and comparison of peptide

precursor and product ions from data independent LC-MS with data dependant LC-MS/MS. *Proteomics* **2009,** *9*, 1683-1695.

41. Yu, L. R.; Zhu, Z. Y.; Chan, K. C.; Issaq, H. J.; Dimitrov, D. S.; Veenstra, T. D., Improved titanium dioxide enrichment of phosphopeptides from HeLa cells and high confident phosphopeptide identification by cross-validation of MS/MS and MS/MS/MS spectra. *J. Proteome. Res.* **2007,** *6*, 4150-4162.

42. Hao, C. Y.; Zhao, X. M.; Yang, P., GC-MS and HPLC-MS analysis of bioactive pharmaceuticals and personal-care products in environmental matrices. *Trends Anal. Chem.* **2007,** *26*, 569-580.

43. Bosco, G. L., The development of LC-MS - the marriage of the bird and the fish. *Trends Anal. Chem.* **2010,** *29*, 781-794.

44. Timerbaev, A. R., Capillary electrophoresis coupled to mass spectrometry for biospeciation analysis: critical evaluation. *Trends Anal. Chem.* **2009,** *28*, 416-425.

45. Haddrell, A. E.; van Eeden, S.; Agnes, G. R., MALDI-MS monitoring of differential biomolecule secretion from human lung cells in vitro following incubation with < 150 particles. *J. Proteome. Res.* **2008,** *7*, 2539-2545.

46. Soin, A. V.; Maryutina, T. A.; Arbuzova, T. V.; Spivakov, B. Y., Sample preparation in the determination of metals in oil and petroleum products by ICP-MS. *J. Anal. Chem.* **2010,** *65*, 571-576.

47. Holzinger, R.; Williams, J.; Herrmann, F.; Lelieveld, J.; Donahue, N. M.; Rockmann, T., Aerosol analysis using a Thermal-Desorption Proton-Transfer-Reaction Mass Spectrometer (TD-PTR-MS): a new approach to study processing of organic aerosols. *Atmos. Chem. Phys.* **2010,** *10*, 2257-2267.

48. Chen, H. W.; Hu, B.; Hu, Y.; Huan, Y. F.; Zhou, Z. Q.; Qiao, X. F., Neutral Desorption Using a Sealed Enclosure to Sample Explosives on Human Skin for Rapid Detection by EESI-MS. *J. Am. Soc. Mass Spectr.* **2009,** *20*, 719-722.

49. Giebel, R.; Worden, C.; Rust, S. M.; Kleinheinz, G. T.; Robbins, M.; Sandrin, T. R., Microbial Fingerprinting using Matrix-Assisted Laser Desorption Ionization Time-Of-Flight Mass Spectrometry (MALDI-TOF MS): Applications and Challenges. *Adv. Appl. Microbiol.* **2010,** *71*, 149-184.

50. Peng, W. P.; Yang, Y. C.; Kang, M. W.; Lee, Y. T.; Chang, H. C., Measuring masses of single bacterial whole cells with a quadrupole ion trap. *J. Am. Chem. Soc.* **2004,** *126*, 11766-11767.

51. Allenden, D.; Craig, R. D.; Johnson, R. G. 16th ASMS Conference on Mass Spectrometry and Allied Topics, Pittsburgh, PA, Pittsburgh, PA, May, 1968.

52. Swingler, D. L., Compact Helium Monitor. *Int. J. Mass Spectrom.* **1975,** *17*, 321-327.

53. Baril, M., Application des miroirs électrostatiques à 1'élimination de l'effet chromatique dans les spectrométres magnètiques. Deuxième partie les aberrations. *Can. J. Phys.* **1970,** *48*, 2487-2498.

54. Swingler, D. L., A small magnetic analyzer mass spectrometer with a velocity filter for residual gas analysis. *Vacuum* **1971,** *21*, 121-125.

55. von Zahn, U., *Rev. Sci. Instr.* **1963,** *34*, 1-4.

56. Dawson, P. H.; Hedman, J. W.; Whetten, N. R., Miniature Mass Spectrometer. *Anal. Chem* **1970,** *42*, 103A-108A.

57. Xu, W.; Chappell, W. J.; Cooks, R. G.; Ouyang, Z., Characterization of electrode surface roughness and its impact on ion trap mass analysis. *J. Mass Spectrom.* **2009,** *44*, 353-360.

58. Cruz, D.; Chang, J. P.; Blain, M. G., Field emission characteristics of a tungsten microelectromechanical system device. *Appl. Phys. Lett.* **2005,** *86*, 153502.

59. Ouyang, Z.; Gao, L.; Fico, M.; Chappell, W. J.; Noll, R. J.; Cooks, R. G., Quadrupole ion traps and trap arrays: geometry, material, scale, performance. *Eur. J. Mass Spectrom.* **2007,** *13*, 13-18.

60. Langmuir, D. B.; Langmuir, R. V.; Shelton, H.; Wuerker, R. F. US Patent No.3, 1962.

61. Kornienko, O.; Reilly, P. T. A.; Whitten, W. B.; Ramsey, J. M., Electron impact ionization in a microion trap mass spectrometer. *Rev. Sci. Instrum.* **1999,** *70*, 3907-3909.

62. Kornienko, O.; Reilly, P. T. A.; Whitten, W. B.; Ramsey, J. M., Field-emission cold-cathode El source for a microscale ion trap mass spectrometer. *Anal. Chem.* **2000,** *72*, 559-562.

63. Reilly, P. T. A.; Kornienko, O.; Whitten, W. B.; Ramsey, J. M. 48th ASMS Conference on Mass Spectrometry and Allied Topics, Long Beach, CA, Long Beach, CA, June 2000.

64. Badman, E. R.; Cooks, R. G., A parallel miniature cylindrical ion trap array. *Anal. Chem.* **2000,** *72*, 3291-3297.

65. Tabert, A. M.; Griep-Raming, J.; Guymon, A. J.; Cooks, R. G., High-throughput miniature cylindrical ion trap array mass spectrometer. *Anal. Chem.* **2003,** *75*, 5656-5664.

66. Patterson, G. E.; Guymon, A. J.; Riter, L. S.; Everly, M.; Griep-Raming, J.; Laughlin, B. C.; Zheng, O. Y.; Cooks, R. G., Miniature cylindrical ion trap mass spectrometer. *Anal. Chem.* **2002,** *74*, 6145-6153.

67. Riter, L. S.; Peng, Y. A.; Noll, R. J.; Patterson, G. E.; Aggerholm, T.; Cooks, R. G., Analytical performance of a miniature cylindrical ion trap mass spectrometer. *Anal. Chem.* **2002,** *74*, 6154-6162.

68. Wu, G. X.; Cooks, R. G.; Ouyang, Z., Geometry optimization for the cylindrical ion trap: field calculations, simulations and experiments. *Int. J. Mass Spectrom.* **2005,** *241*, 119-132.

69. Moxom, J.; Reilly, P. T. A.; Whitten, W. B.; Ramsey, J. M., Sample pressure effects in a micro ion trap mass spectrometer. *Rapid Commun. Mass Sp.* **2004,** *18*, 721-723.

70. Moxom, J.; Reilly, P. T. A.; Whitten, W. B.; Ramsey, J. M., Double resonance ejection in a micro ion trap mass spectrometer. *Rapid Commun. Mass Sp.* **2002,** *16*, 755-760.

71. Moxom, J.; Reilly, P. T. A.; Whitten, W. B.; Ramsey, M., Analysis of volatile organic compounds in air with a micro ion trap mass analyzer. *Anal. Chem.* **2003,** *75*, 3739-3743.

72. Douglas, D. J.; Frank, A. J.; Mao, D. M., Linear ion traps in mass spectrometry. *Mass Spectrom. Rev.* **2005,** *24*, 1-29.

73. Xu, W.; Manicke, N. E.; Cooks, G. R.; Ouyang, Z., Miniaturization of Mass Spectrometry Analysis Systems. *Jala* **2010,** *15*, 433-439.

74. Tadjimukhamedov, F. K.; Jackson, A. U.; Nazarov, E. G.; Ouyang, Z.; Cooks, R. G., Evaluation of a Differential Mobility Spectrometer/Miniature Mass Spectrometer System. *J. Am. Soc. Mass. Spectr.* **2010,** *21*, 1477-1481.

75. Keil, A.; Hernandez-Soto, H.; Noll, R. J.; Fico, M.; Gao, L.; Ouyang, Z.; Cooks, R. G., Monitoring of toxic compounds in air using a handheld rectilinear ion trap mass spectrometer. *Anal. Chem.* **2008,** *80*, 734-741.

76. Keil, A.; Talaty, N.; Janfelt, C.; Noll, R. J.; Gao, L.; Ouyang, Z.; Cooks, R. G., Ambient mass spectrometry with a handheld mass spectrometer at high pressure. *Anal. Chem.* **2007,** *79*, 7734-7739.

77. Gao, L.; Song, Q. Y.; Patterson, G. E.; Cooks, R. G.; Ouyang, Z., Handheld rectilinear ion trap mass spectrometer. *Anal. Chem.* **2006,** *78*, 5994-6002.

78. Chen, H. W.; Xu, R. F.; Chen, H.; Cooks, R. G.; Ouyang, Z., Ion/molecule reactions in a miniature RIT mass spectrometer. *J. Mass Spectrom.* **2005,** *40*, 1403-1411.

79. Cheung, K.; Velasquez-Garcia, L. F.; Akinwande, A. I., Chip-Scale Quadrupole Mass Filters for Portable Mass Spectrometry. *J. Microelectromech. S.* **2010,** *19*, 469-483.

80. Wright, S.; O'Prey, S.; Syms, R. R. A.; Hong, G. D.; Holmes, A. S., Microfabricated Quadrupole Mass Spectrometer With a Brubaker Prefilter. *J. Microelectromech. S.* **2010,** *19*, 325-337.

81. Hogan, T. J.; Taylor, S.; Cheung, K.; Velasquez-Garcia, L. F.; Akinwande, A. I.; Pedder, R. E., Performance Characteristics of a MEMS Quadrupole Mass Filter With Square Electrodes: Experimental and Simulated Results. *IEEE T. Instrum. Meas.* **2010,** *59*, 2458-2467.

82. Cruz, D.; Chang, J. P.; Fico, M.; Guymon, A. J.; Austin, D. E.; Blain, M. G., Design, microfabrication, and analysis of micrometer-sized cylindrical ion trap arrays. *Rev. Sci. Instrum.* **2007,** *78*, 015107.

83. Austin, D. E.; Cruz, D.; Blain, M. G., Simulations of ion trapping in a micrometer-sized cylindrical ion trap. *J. Am. Soc. Mass Spectr.* **2006,** *17*, 430-441.

84. Chaudhary, A.; van Amerom, F. H. W.; Short, R. T., Development of Microfabricated Cylindrical Ion Trap Mass Spectrometer Arrays. *J. Microelectromech. S.* **2009,** *18*, 442-448.

85. Fox, J.; Saini, R.; Tsui, K.; Verbeck, G., Microelectromechanical system assembled ion optics: An advance to miniaturization and assembly of electron and ion optics. *Rev. Sci. Instrum.* **2009,** *80* (9), 093302.

86. Yu, M.; Fico, M.; Kothari, S.; Ouyang, Z.; Chappell, W. J., Polymer-based ion trap chemical sensor. *IEEE Sens. J.* **2006,** *6*, 1429-1434.

87. Fico, M.; Yu, M.; Ouyang, Z.; Cooks, R. G.; Chappell, W. J., Miniaturization and geometry optimization of a polymer-based rectilinear ion trap. *Anal. Chem.* **2007,** *79*, 8076-8082.

88. Fico, M.; Maas, J. D.; Smith, S. A.; Costa, A. B.; Ouyang, Z.; Chappell, W. J.; Cooks, R. G., Circular arrays of polymer-based miniature rectilinear ion traps. *Analyst* **2009,** *134*, 1338-1347.

89. Maas, J. D.; Hendricks, P. I.; Ouyang, Z.; Cooks, R. G.; Chappell, W. J., Miniature Monolithic Rectilinear Ion Trap Arrays by Stereolithography on Printed Circuit Board. *J. Microelectromech. S.* **2010,** *19*, 951-960.

90. Clare, A. T.; Gao, L.; Brkic, B.; Chalker, P. R.; Taylor, S., Linear Ion Trap Fabricated Using Rapid Manufacturing Technology. *J. Am. Soc. Mass Spectr.* **2010,** *21* (2), 317-322.

91. Song, Y. S.; Wu, G. X.; Song, Q. Y.; Cooks, R. G.; Ouyang, Z.; Plass, W. R., Novel linear ion trap mass analyzer composed of four planar electrodes. *J. Am. Soc. Mass Spectr.* **2006,** *17*, 631-639.

92. Pau, S.; Whitten, W. B.; Ramsey, J. M., Planar geometry for trapping and separating ions and charged particles. *Anal. Chem.* **2007,** *79*, 6857-6861.

93. Li, X. X.; Jiang, G. Y.; Luo, C.; Xu, F. X.; Wang, Y. Y.; Ding, L.; Ding, C. F., Ion Trap Array Mass Analyzer: Structure and Performance. *Anal. Chem.* **2009,** *81*, 4840-4846.

94. Yang, M.; Kim, T. Y.; Hwang, H. C.; Yi, S. K.; Kim, D. H., Development of a Palm Portable Mass Spectrometer. *J. Am. Soc. Mass Spectr.* **2008,** *19*, 1442-1448.

95. Badman, E. R.; Cooks, R. G., Cylindrical ion trap array with mass selection by variation in trap dimensions. *Anal. Chem.* **2000,** *72*, 5079-5086.

96. Riter, L. S.; Meurer, E. C.; Handberg, E. S.; Laughlin, B. C.; Chen, H.; Patterson, G. E.; Eberlin, M. N.; Cooks, R. G., Ion/molecule reactions performed in a miniature cylindrical ion trap mass spectrometer. *Analyst* **2003,** *128*, 1112-1118.

97. Austin, D. E.; Wang, M.; Tolley, S. E.; Maas, J. D.; Hawkins, A. R.; Rockwood, A. L.; Tolley, H. D.; Lee, E. D.; Lee, M. L., Halo ion trap mass spectrometer. *Anal. Chem.* **2007,** *79*, 2927-2932.

98. Wang, Y.; Wanczek, K. P., Generation of an Exact 3-Dimensional Quadrupole Electric-Field and Superposition of a Homogeneous Electric-Field within a Common Closed Boundary with Application to Mass-Spectrometry. *J. Chem. Phys.* **1993,** *98*, 2647-2652.

99. Franzen, J.; Gabling, R.-H.; Schubert, M.; Wang, Y., In *In Practical Aspects of Ion Trap Mass Spectrometry, Vol. I. Fundamentals.*, March, R. E.; Todd, J. F. J., Eds. CRC Press: Boca Raton, FL, 1995; pp 68-69.

100. Dahl, D. A. *SIMION Version 7.0*, Idaho National Engineering and Environmental Laboratory: Idaho Falls, ID, 2000.

101. Manura, D.; Dahl, D. A. *SIMION Version 8.04*, Scientific Instrument Services, Inc.: Ringoes, NJ, 2006.

102. Wang, M. A.; Quist, H. E.; Hansen, B. J.; Peng, Y.; Zhang, Z. P.; Hawkins, A. R.; Rockwood, A. L.; Austin, D. E.; Lee, M. L., Performance of a Halo Ion Trap Mass Analyzer with Exit Slits for Axial Ejection. *J. Am. Soc. Mass Spectr.* **2011,** *22*, 369-378.

103. Le Blanc, J. C. Y.; Hager, J. W.; Ilisiu, A. M. P.; Hunter, C.; Zhong, F.; Chu, I., Unique scanning capabilities of a new hybrid linear ion trap mass spectrometer (Q TRAP) used for high sensitivity proteomics applications. *Proteomics* **2003,** *3*, 859-869.

104. Xie, H. W.; Griffin, T. J., Trade-off between high sensitivity and increased potential for false positive peptide sequence matches using a two-dimensional linear ion trap for tandem mass spectrometry-based proteomics. *J. Proteome. Res.* **2006,** *5*, 1003-1009.

105. Laughlin, B. C.; Mulligan, C. C.; Cooks, R. G., Atmospheric pressure ionization in a miniature mass spectrometer. *Anal. Chem.* **2005,** *77*, 2928-2939.

106. Venable, J. D.; Wohlschlegel, J.; McClatchy, D. B.; Park, S. K.; Yates, J. R., Relative quantification of stable isotope labeled peptides using a linear ion trap-orbitrap hybrid mass spectrometer. *Anal. Chem.* **2007,** *79*, 3056-3064.

107. Kosanam, H.; Prakash, P. K. S.; Yates, C. R.; Miller, D. D.; Ramagiri, S., Rapid screening of doping agents in human urine by vacuum MALDI-linear ion trap mass spectrometry. *Anal. Chem.* **2007,** *79*, 6020-6026.

108. Xia, Y.; Thomson, B. A.; McLuckey, S. A., Bidirectional ion transfer between quadrupole arrays: MSn ion/ion reaction experiments on a quadrupole/time-of-flight tandem mass spectrometer. *Anal. Chem.* **2007,** *79*, 8199-8206.

109. Liang, X. R.; McLuckey, S. A., Transmission mode ion/ion proton transfer reactions in a linear ion trap. *J. Am. Soc. Mass Spectr.* **2007,** *18*, 882-890.

110. Sharifi, M.; Einhorn, J., Isomeric differentiation of conjugated diene epoxides by polar [4+2(+)] Diels-Alder cycloaddition of acylium ions in an ion trap mass spectrometer. *Int. J. Mass Spectrom.* **1999,** *191*, 253-264.

111. Wang, Y. H.; Wu, S. L.; Hancock, W. S., Monitoring of glycoprotein products in cell culture lysates using lectin affinity chromatography and capillary HPLC coupled to electrospray linear ion trap-Fourier transform mass spectrometry (LTQ/FTMS). *Biotechnol. Progr.* **2006,** *22*, 873-880.

112. Jin, W. H.; Dai, J.; Li, S. J.; Xia, Q. C.; Zou, H. F.; Zeng, R., Human plasma proteome analysis by multidimensional chromatography prefractionation and linear ion trap mass spectrometry identification. *J. Proteome Res.* **2005,** *4*, 613-619.

113. Badman, E. R.; Cooks, R. G., Special feature: Perspective - Miniature mass analyzers. *J. Mass Spectrom.* **2000,** *35*, 659-671.

CHAPTER 2: PLANAR QUADRUPOLE ION TRAP INSTRUMENTATION AND ITS PERFORMANCE

2.1 Introduction

Since the invention of the radio-frequency (RF) quadrupole ion trap by Wolfgang Paul et al. in 1953,[1] quadrupole ion-trap mass analyzers have played an increasingly important role in chemical and biological analyses. In addition to high sensitivity and specificity, ion traps combine reasonable simplicity of operation with complex functions such as multistage tandem mass analysis using a single analyzer. However, the hyperboloidal electrode shape of the original Paul trap is difficult to machine, especially on the miniaturized scale. As a result, significant effort has been spent on the development of alternative ion-trap structures.

In 1998, Wells et al.[2] demonstrated a mass-selective instability scan on an ion trap with cylindrical geometry. The cylindrical ion trap, which had been introduced previously,[3-4] simplified the hyperbolic ring electrode and end-cap electrodes with a cylindrical electrode and planar end-caps. This simplified trap geometry has facilitated and been the basis for most miniaturized ion trap systems.[5-10] Unfortunately, the cylindrical trap, similar to the Paul trap, has a limited ion storage capacity because the three-dimensional RF field confines trapped ions to a point at the center of the device.

Several ion trap mass analyzers have been developed with the aim of increasing trapping capacity. For instance, an ion trap with a toroidal trapping volume was developed by Lammert et al.[11-12] Linear ion traps, in which the trapping volume is extended in one linear dimension, have been developed.[13-19] In linear ion traps, the ions are focused to a line rather than a point, as in Paul-type or cylindrical traps. As a result, both ion-trapping capacity and efficiency are improved. Ouyang et al. introduced the rectilinear ion trap,[20] which combines the advantages of

both simplified electrode geometry and extended trapping volume. The rectilinear ion trap has recently been incorporated into a hand-held mass spectrometer system designed for air monitoring and other applications.[21-23] Another ion trap design, in which a single microfabricated plate creates a trapping field, has been reported by Pau et al.[24]

In all ion trap variations, metal electrodes are used to produce the appropriate electric fields. For full-sized ion traps, modern machining equipment easily produces the hyperboloidal electrode surfaces of the quadrupole ion trap. For miniaturized traps, however, machining methods have been pushed to the limit, and simpler electrode geometries such as planar and cylindrical are required. For this reason, most miniaturized and microfabricated ion traps have utilized the cylindrical trap design.[25-30]

Recently, a novel ion trap mass analyzer was presented by Austin el al.,[31] which was based on a toroidal (circular) trapping geometry and microfabrication technology. The device, called the Halo ion trap, consisted of a pair of planar ceramic plates mounted in parallel, in which the facing surfaces were lithographically imprinted with a series of concentric ring electrodes, covered with a layer of resistive germanium. The electric fields, established by applying different RF potentials to each ring, produced the same field shape as that in the toroidal ion trap. Although this type of mass analyzer is promising, because of its high ion-storage capacity, sensitivity, and ease of fabrication and miniaturization, its performance (e.g., resolution and mass range) as presented was not optimal.

2.2 Planar Ion Trap Composed of Ceramic Plates

2.2.1 Method to Create Trapping Field in Planar Traps

To create a useful electric field with the ability to control and optimize field shape, it is necessary to superimpose an arbitrary potential function on the resistive material. This can be

accomplished using narrow electrode "wires" beneath the resistive material. For cylindrically-symmetric trapping fields, concentric electrode rings are used (Figure 2.1). The voltage on each ring is independently variable using a capacitive voltage divider or through other control electronics. Although the capacitive voltage divider and the resistive material both modify the voltage between each ring, the majority of the voltage dividing occurs as a result of the capacitors, not the resistive material. In other words, the resistive material is not the voltage divider. Similarly, very little current flows through the resistive material as the voltage across the capacitors oscillates. Thus, minimal heating of the resistive material occurs.

With a superimposed potential function, the resistive material performs several roles. The resistive material establishes a continuous boundary condition with a well-defined potential function, thereby creating the trapping fields. The resistive material prevents charge build-up from occurring, which would otherwise interfere with the fields of the trap. The superimposed potential function on the resistive material allows creation of electrical fields independent of the material geometry. As a result, the resistive material and electrode can be the simplest possible geometry—planar.

The potential function on the germanium surface was modeled in SIMION using the following approach (Figure 2.1). First, ring electrodes were created as concentric cylindrical surfaces, and the potentials solved for the space between the cylindrical surfaces. Next, the points representing the space between the cylinders were converted to electrode points with the same potential they had as points in free space. After this, a radial plane of points was selected near the middle of the array, and all other points were converted to non-electrode points. At this

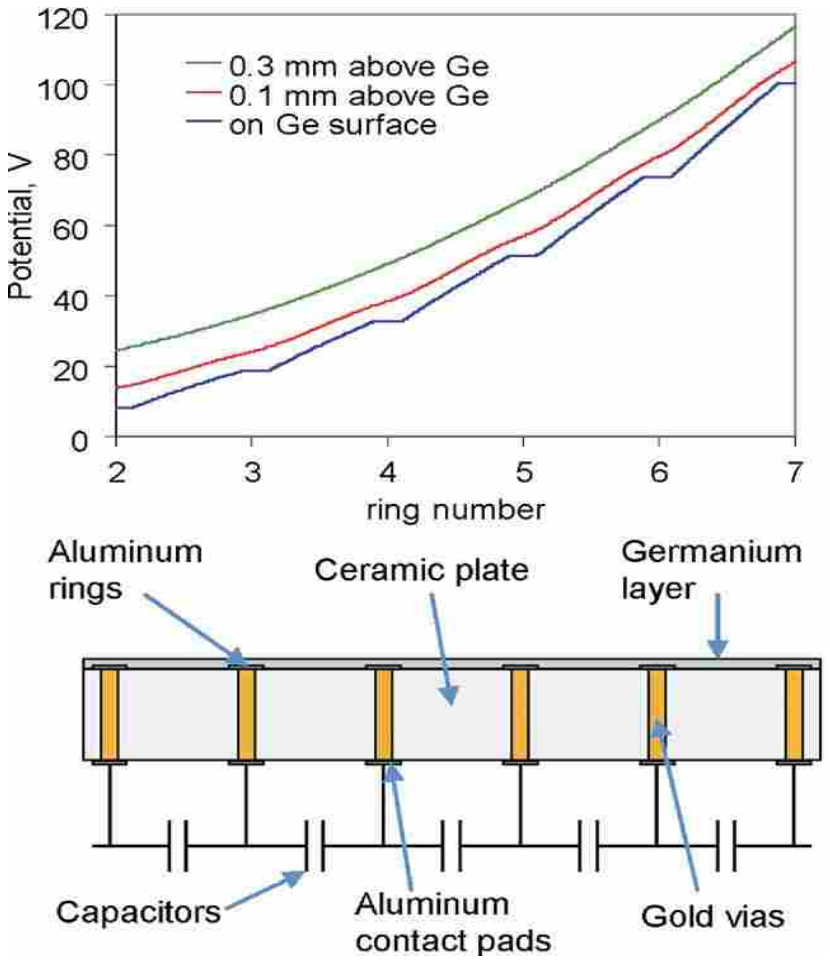

Figure 2.1. Electrode wires impose an arbitrary potential function on the overlaying resistive material. Plot shows the variation of the potential along the germanium surface and also 100 and 300 μm above the germanium surface (within the trap).

point, the potential along this plane of points resembled the potential that would exist on a planar sheet of resistive material. Two such planes of points were used to determine the potentials within the trap. This method relies on the fact that the potential varies as 1/r in both a planar resistive material and in the space between cylindrical electrodes, and that the latter can be calculated quite well using the approximations of SIMION. Finally, the thickness of the underlying rings can be taken into account as the thickness of the cylindrical electrodes used in this approach.

2.2.2 Configuration of the Planar Quadrupole Ion Trap

In the present work, the electrode approach of the Halo ion trap has been used to produce a mass analyzer of the Paul trap geometry. Whereas the electric fields of the Halo ion trap mimicked those of the toroidal trap, including a toroidal trapping volume, the electric fields in the planar Paul trap follow the design of the conventional quadrupole or Paul trap. Instead of the toroidal trapping volume of the Halo trap, ions in the present traps – the planar Paul traps – are confined to a small spherical volume at the device center. Although the larger trapping volume of the toroidal geometry is lost, the equations of ion motion are better understood in the Paul geometry. In particular, ion ejection is more straightforward.

Construction of an ion-trap mass analyzer using two microfabricated plates provides several important advantages. For instance, two pieces can be mechanically aligned more easily than a larger number of electrode pieces. Polished flat plates have a smoother surface than traps made using other methods. Hence, surface roughness, which has been identified as an issue for miniaturized traps,[32] is less of a problem. Microfabricated plates can be produced in quantity less expensively and more accurately

than machined electrodes. The space between the plates provides convenient access for ionization sources, optics, pressure measurement, or other peripheral components. Finally, the use of an array of microfabricated electrode rings underneath a resistive layer allows the electric fields within the trap to be modified in a way that is not possible using machined electrodes.[33] Although the microfabricated plates themselves are fairly complex in both design and fabrication, other advantages make this approach potentially valuable.

2.3 Experimental Section

2.3.1 Microfabriation of Ceramic Plates

Electrode plates were made using high-purity alumina (Al_2O_3) wafers, 0.635 mm thick (Micro Substrate, Tempe, AZ). Holes were laser drilled for mounting, ion ejection, and electrical connections (vias, with a diameter of 127 μm) between the front and back sides of the plates. The vias were filled with gold, after which the plates were polished. Using standard photomask-photoresist techniques, aluminum electrodes were deposited on both sides of the plate: ring electrodes on the trapping side, leading to connection pads on the back side. Finally, a 50-nm layer of germanium was evaporated onto the trapping side of the plates. Because of constraints in via hole drilling near an edge in the ceramic plates, the width of the first ring was 1.30 mm. From the 2nd ring to the 24th ring, the width was 0.10 mm. The resulting electrode plates are shown in Figure 2.2. Two plates are mounted together using a metal spacer.

The electric field between the plates is determined by the potentials put on each aluminum ring electrode. A capacitive voltage divider was used to produce the potentials

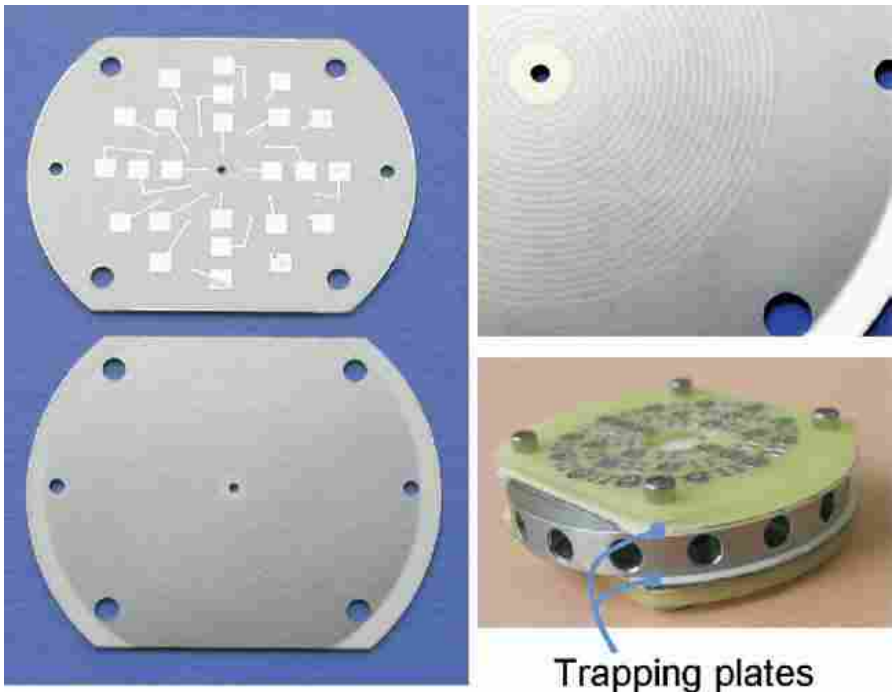

Figure 2.2. Electrode plates used to produce a quadrupole ion trap. At left are shown top and back sides. Electrode rings are under the germanium and, therefore, cannot be seen easily, but can be seen in enlargement at upper right. Lower right shows trap assembly without voltage divider or connectors.

for each ring. The resistance of the germanium layer contributes only a small amount to the voltage division.

2.3.2 Instrumentation - Ionization Source, Trapping Regions, RF signal, AC signal, pumping system and detector

Figure 2.3 shows the instrument setup for the experiments, including the electron gun assembly, trapping region, and the detector assembly. Behind each of the two ceramic plates comprising the trapping region was a printed circuit board (PCB) with a capacitor network. The capacitor network was used to establish the voltages on each of the ring electrodes under RF excitation. Spring-loaded pins were soldered to the PCB boards to make electrical contact with the back sides of the trapping plates. A 6-mm stainless steel spacer was mounted between the trapping plates. Holes in the spacer admitted the electron beam, sample vapor, helium gas, and a Teflon tube leading to a pirani gauge (Kurt J. Lesker, Clairton, CA). An RF signal with a frequency of 1.26 MHz and variable amplitude up to 738 $V_{0\text{-}p}$ (PSRF-100, Ardara Technologies, North Huntingdon, PA) was applied to the capacitor network on the PCB boards, and the spacer was grounded during ion ejection. In addition, a supplementary low-voltage AC signal, generated using two 30 MHz synthesized function generators (DS345, Stanford Research Systems, Sunnyvale, CA) with a 180° phase difference, and amplified to 3.5 $V_{0\text{-}p}$ by a custom-made amplifier, was applied between the trapping plates to provide a dipole field for resonant ion ejection during the RF scan. The amplified supplementary AC signals were applied to the innermost ring on each plate, using a simple filter circuit to isolate the supplementary AC from the main RF signals. The applied frequency of the AC signal

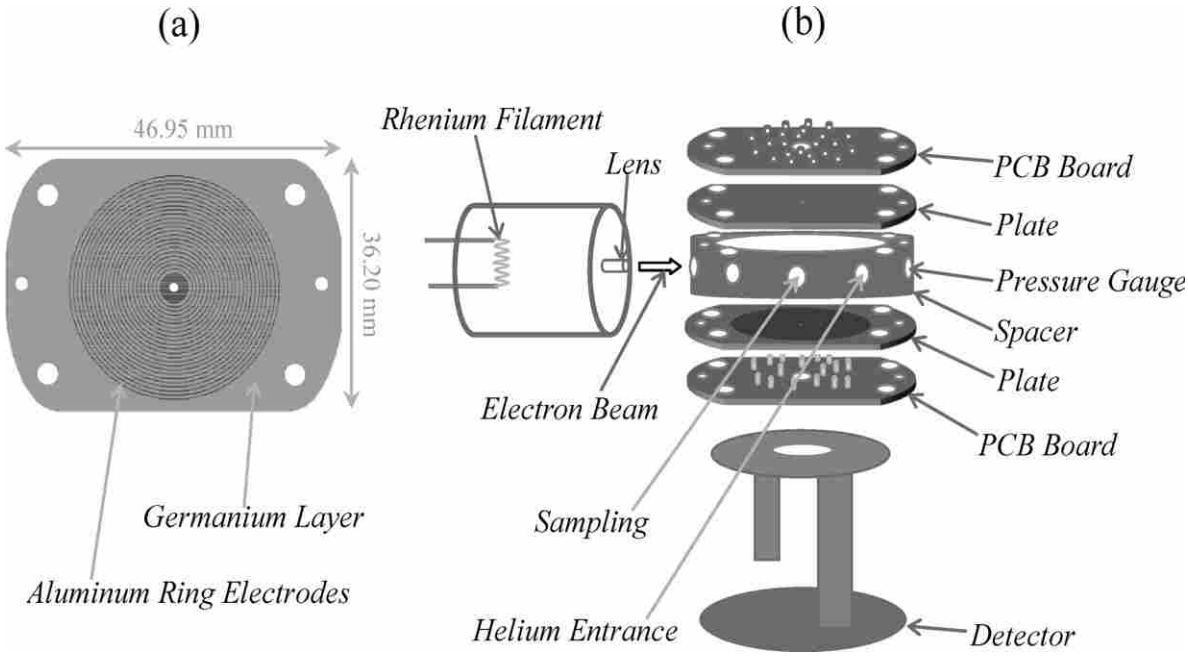

Figure 2.3. (a) Top-view diagram of electrode plate and (b) the instrument setup for the experiments (Figure by Zhang et al.).

was 290 kHz, and β_z was ~ 0.46. Other values of β_z up to ~ 1 were also tested, with comparable mass resolution but reduced peak intensity.

Operational details of the planar Paul ion trap are given in Figure 2.4, which shows the time intervals and sequence for ionization, RF trapping, and ejection. First, the RF voltage was turned off to clear previously trapped ions out of the trap. The RF then was turned back on, along with the electron gun, allowing sample to be ionized in the trapping volume. The electron gun was then turned off, allowing the ionized and trapped sample to collisionally cool. The ejection AC was then turned on, and a voltage sweep of the drive RF was initiated. As the RF amplitude reached a level at which the secular frequency of any ion matched the applied supplementary AC frequency, that ion was resonantly ejected from the trap. Because ejection voltage was ramped from lower to higher voltages, ions were ejected in order of increasing *m/z* out of the trap. After an ion was ejected through the hole in the trapping plates, it continued toward the detector. Ejected ions were detected using an ETP electron multiplier detector (SGE Analytical Science, Austin, TX), with a conversion dynode operated at -4000 V. The signal was amplified using a current amplifier (Model 427, Keithley Instruments, Cleveland, OH) and recorded using a digital oscilloscope (WaveRunner 6000A, LeCroy, Chestnut Ridge, NY).

2.3.3 Samples

In the experiments reported herein, helium was used as the buffer gas at an indicated pressure of 5.34×10^{-3} Torr (uncorrected, 1 Torr = 133 Pa), as read from a Pirani gauge (Kurt J. Lesker, Clairton, CA). Headspace vapor of the organic compounds of interest, without further purification, was leaked into the vacuum through two leak

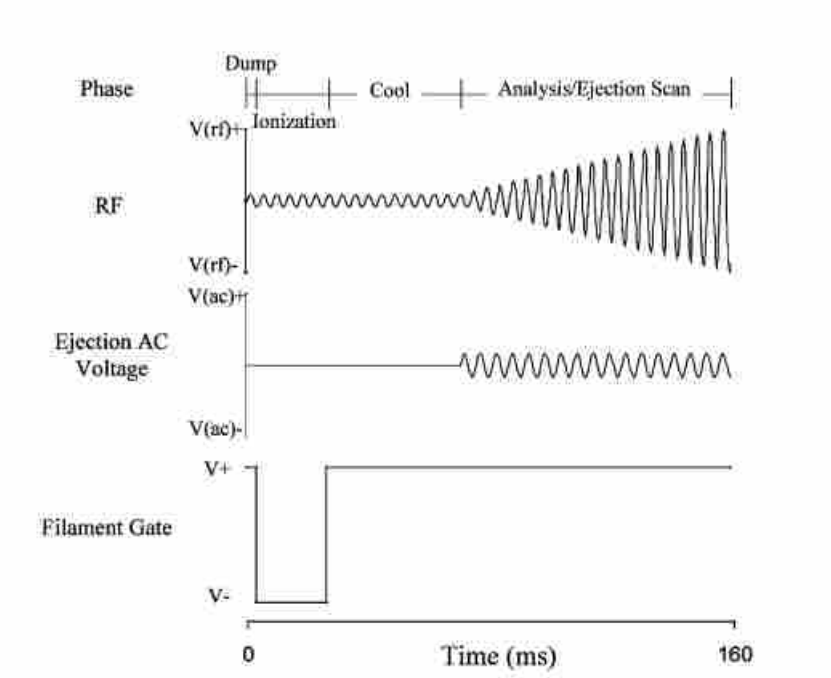

Figure 2.4. Timing diagram for the planar Paul ion trap, including ionization, cooling, mass analysis and dumping of ions in a complete cycle (Figure by Zhang et al.).

valves (Swagelok, Solon, OH) to maintain a nominal pressure of (1.0-8.0) × 10^{-5} Torr. In situ electron ionization was achieved using a custom-built electron gun comprising a rhenium-tungsten filament, a lens, a gate, and a 1.6 A and -70 V power supply.

2.3.4 Ejection Methods

The performance of the planar Paul trap mass analyzer was tested using three modes of ion ejection: boundary ejection, quadrupole resonant ejection, and dipole resonant ejection. Boundary ejection, in which the RF amplitude is ramped and ions eject spontaneously at q_z = 0.908, was used historically in Paul traps; however, it is not currently in common use.[34] Quadrupole[35] and dipole[36-37] resonant ejection rely on applying a small supplementary AC signal to the trap. Ions are ejected when the supplementary signal resonantly excites the secular motion of ions. Ions can be ejected either just before the q_z = 0.908 boundary or at significantly lower q_z values.

2.4 Results and Discussion

2.4.1 Optimization of Electric Field

As shown in Figure 2.5 (a), the planar Paul ion trap consists of two parallel ceramic plates with facing surfaces imprinted with concentric metal rings, overlaid with germanium. The metal rings superimpose a potential function on the germanium layer, which, in turn, establishes the 3-dimensional potential distribution of the trapping region. This method of producing the trapping field is distinctive from the method used in

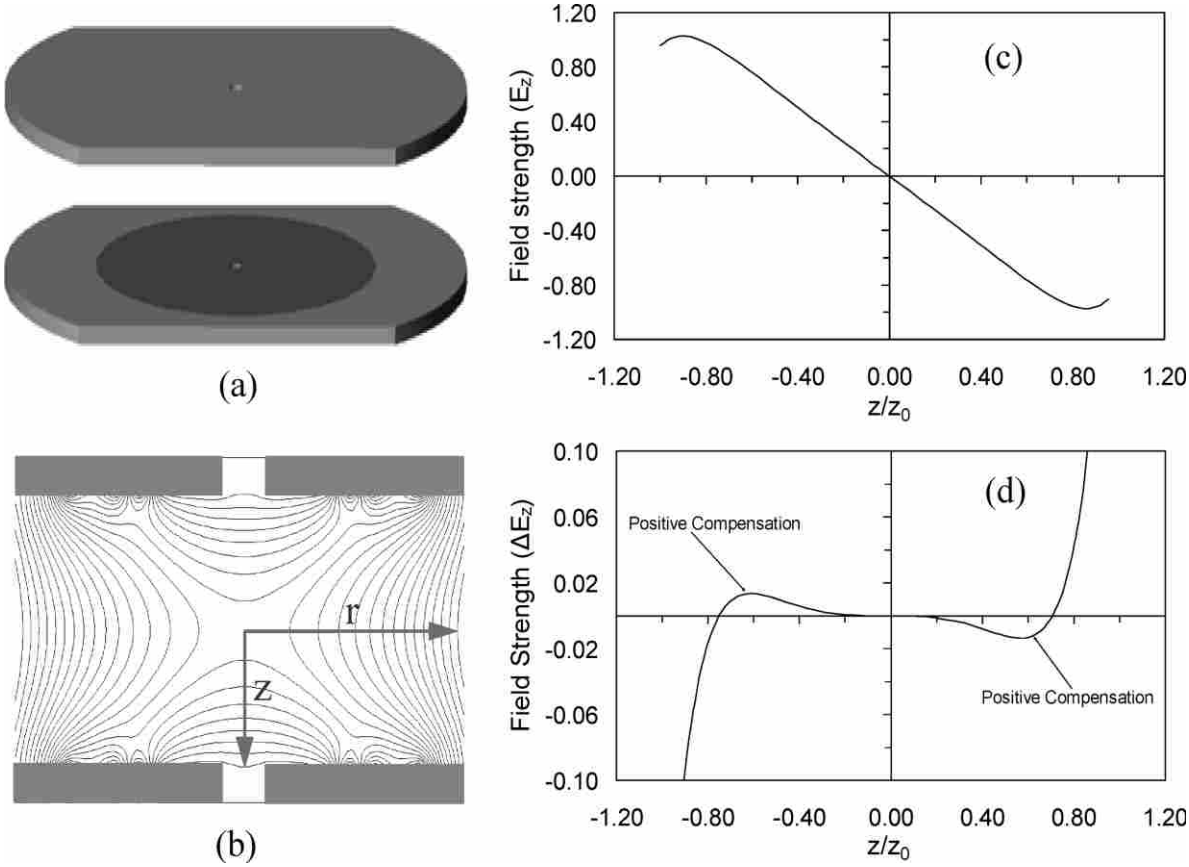

Figure 2.5. Schematics of (a) the trapping plates, (b) electric field distribution, (c) axial electric field (E_z), and (d) nonlinear high-order distribution to the axial electric field (ΔE_z) along the z-axis in the planar Paul trap (Figure by Zhang et al.).

conventional ion traps, both those made using hyperboloidal or curved electrodes (e.g., Paul trap, quadrupole mass filter and linear ion trap) and from traps made using planar metal electrodes (e.g., cylindrical trap, rectilinear trap). The electric field within the planar Paul trap is a function of the potentials applied to each ring, as well as the spatial arrangement of the rings and plates. Because the RF potential on each ring is independently adjustable, there is a great deal of flexibility in constraining and optimizing the trapping field. As with any other ion trap, the shape of the electric field inside the trap plays an important role in determining the performance of the ion trap as a mass analyzer.

The ion motion for the present trap is governed by the RF electric field and by the auxiliary AC signal applied to the plates. Optimal electric fields for several trapping geometries have been reported by Ouyang el al.[20] Generally, the performance of any ion trap is influenced by components of the electric field higher than quadrupolar (i.e., octopolar). After investigation of the electric field for the cylindrical ion trap with different dimensions, Wu et al.[38] concluded that the increase of spectral resolution can be realized by appropriate compensation for high-order, nonlinear field components, particularly octopolar and dodecapolar fields. This approach was also used in the original Finnigan ion trap detector and was accomplished by increasing the spacing between electrodes.[39] Lammert et al.[11] reported that a certain amount of positive octopole contributed to the increase of resolution of the toroidal ion trap.

For the planar Paul trap, the electric fields within the trapping volume were calculated, and voltages on individual rings optimized, using SIMION 7.[40] The nonlinear components of the axial electric field (along r = 0) in the planar Paul trap were selected to

be similar to those used in the asymmetric toroidal trap[11] and cylindrical ion trap.[38] During the course of optimization of electric fields, several sets of potentials were identified as feasible. The one chosen for this study gave the greatest linear axial field of those examined. Surprisingly, the potentials on rings 1, 3, and 5 are all zero, resulting in an unusual feature in the electric field near the plate surfaces at these radii (observable in Figure 2.5 b). It is not clear at this point why these values produced the best field among those examined, or whether there might be better sets of potentials possible. The permutation of possible values is large, and as yet no algorithm for complete optimization exists.

Figures 2.5(c) and 2.5(d) show the axial electric field (E_z) and nonlinear contribution to the axial electric field (ΔE_z) along the z-axis by subtracting a linear extrapolation of a narrow region of the derived electric field near the center of the trap, respectively. Similar to the electric fields in the traps previously mentioned, the potential distribution used in the planar Paul trap included a small positive compensation of higher-order components and is expected to improve the mass resolution of this novel trap. In contrast to methods used with other ion traps, however, the higher-order components were not added into the planar Paul trap by modifying the shape or arrangement of the electrodes, but rather by choosing the appropriate potential function that was applied to the set of rings. Changing the electric fields within the planar Paul trap is done by changing the values of the capacitors on the PCBs.

With the current plate spacing, only the first 11 rings had a noticeable effect on the electric fields in the trapping region. To save on cost, the plates were fabricated with

additional rings, with the intent of using them in other experiments. In the present work, rings beyond ring 11 were shorted to ring 11.

During the development of the planar Paul ion trap, changes in the ion ejection mode were observed to affect mass resolution. Figure 2.6 shows three arrangements (boundary ejection, quadrupole ejection, and dipole ejection) for the applications of an auxiliary AC potential to the planar Paul trap. Supplemental AC signals were connected to the innermost ring in each case. Comparisons of spectra obtained with these three arrangements were made using toluene as the sample, as illustrated in Figure 2.6. When boundary ejection was performed without application of a supplementary AC voltage to the trapping plates, the mass resolution was far too low to resolve peaks *m/z* 91 and 92, and peak intensity was poor (Figure 2.6(a)). After the supplementary AC voltage was applied to the trapping plates, the resolution for spectra of toluene was greatly improved. As the in-phase potentials were applied to both of trapping plates (quadrupole ejection), the resolution ($m/\Delta m$, full width at half maximum (FWHM) definition) for peak *m/z* 91 from toluene was ~370 (Figure 2.6(b)). The resolution was increased to ca. 700, as given in Figure 2.6(c), when out-of-phase potentials were applied to both trapping plates (dipole ejection), which is due to the kinetic excitation of ions when the frequency of the supplementary AC voltage coincides with one of their secular oscillation frequencies.[41] Therefore, dipole ejection was used for subsequent experiments.

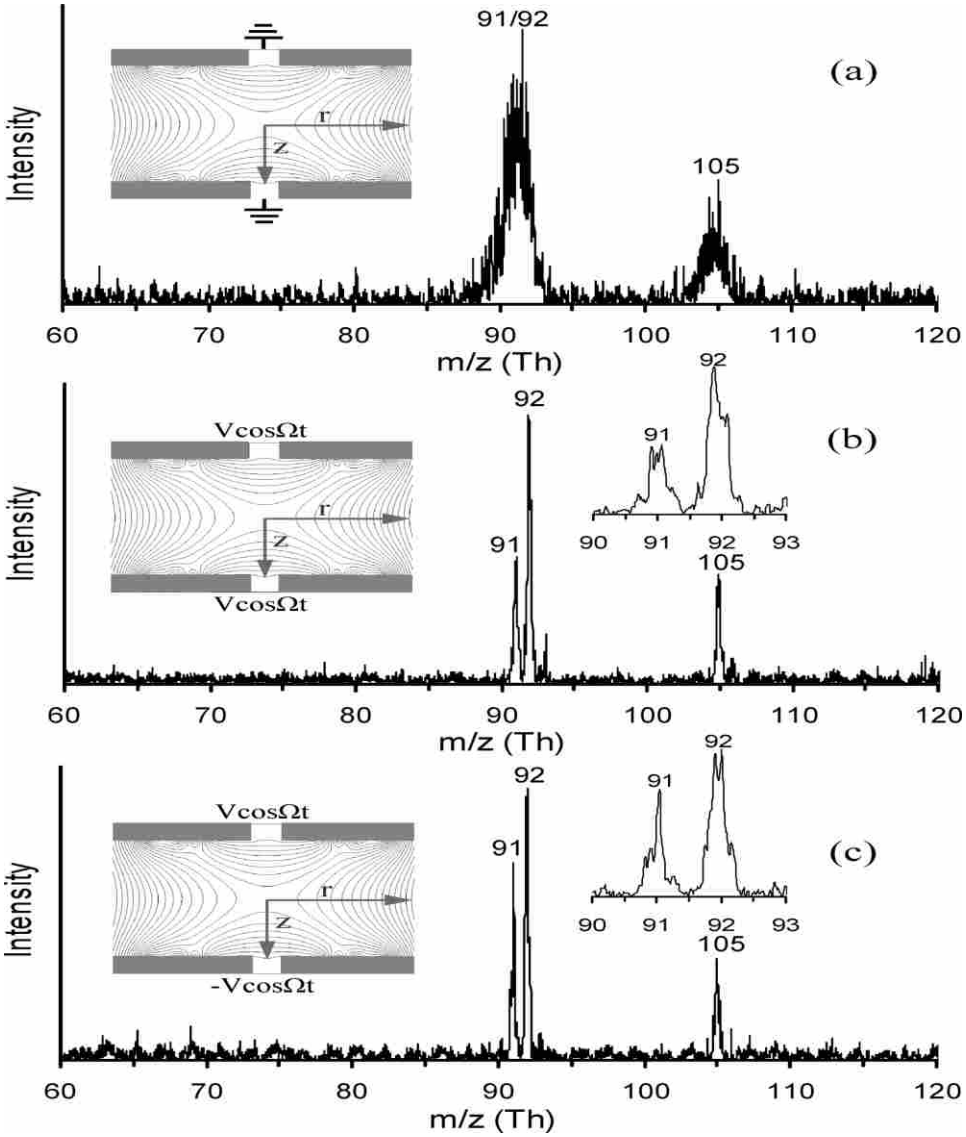

Figure 2.6. Mass spectra of toluene recorded at different ejection modes: (a) boundary ejection; (b) quadrupole ejection; and (c) dipole ejection with an applied supplementary AC signal of 290 kHz; 3.5 $V_{0\text{-}p}$; a partial pressure of toluene, $P_{toluene} = 1.0 \times 10^{-5}$ Torr, $P_{helium} = 5.34 \times 10^{-3}$ Torr, ionization time = 4 ms (Figure from Zhang et al.).

2.4.2 Effect of Scan Rate

It is well-known[42-45] that decreasing the RF scan rate can improve mass resolution in ion traps. Figure 2.7 shows mass spectra of the molecular-ion region of toluene and demonstrates the improvement in resolution obtained by varying the RF scan rate. The peaks of *m/z* 91 and 92 were partially resolved at a scan rate of 7074 Th/s, as shown in Figure 2.7(a). With the decrease of scan rate to 3583 Th/s, the peaks are almost resolved from each other (Figure 2.7(b)). The mass spectrum that shows baseline separation of peaks 91 and 92 was recorded by further decreasing the scan rate to 1792 and 862 Th/s, and mass resolution at FWHM of 0.26 and 0.12 for *m/z* 91, as shown in Figure 2.7(c) and 2.7(d), was obtained. From the aforementioned results, the resolution is enhanced ca. 4.5-fold by reduction of the mass scan rate by a factor of ~ 8.2, which can be attributed to the increased number of increments of the RF voltage in a given mass range and the increased time allowed for ions with adjacent *m/z* values to be ejected at the threshold of their instability.[16, 42, 46-48] With increasing the scan rate from 862 Th/s to 7074 Th/s, the mass shift increases with an exception at a scan rate of 7074 Th/s for peak *m/z* 91. The mass shift in this case could be due to ripple or inconsistencies in the power supplies or frequencies used to operate the trap, or could result from space-charge effects.

2.4.3 Spectra for Target Samples

To better understand the performance of this novel mass analyzer, the planar Paul ion trap was used to record mass spectra for several compounds, including dichloromethane, isobutylbenzene, and others, with the aforementioned experimental conditions. Figure 2.8 shows the mass spectra of dichloromethane and isobutylbenzene.

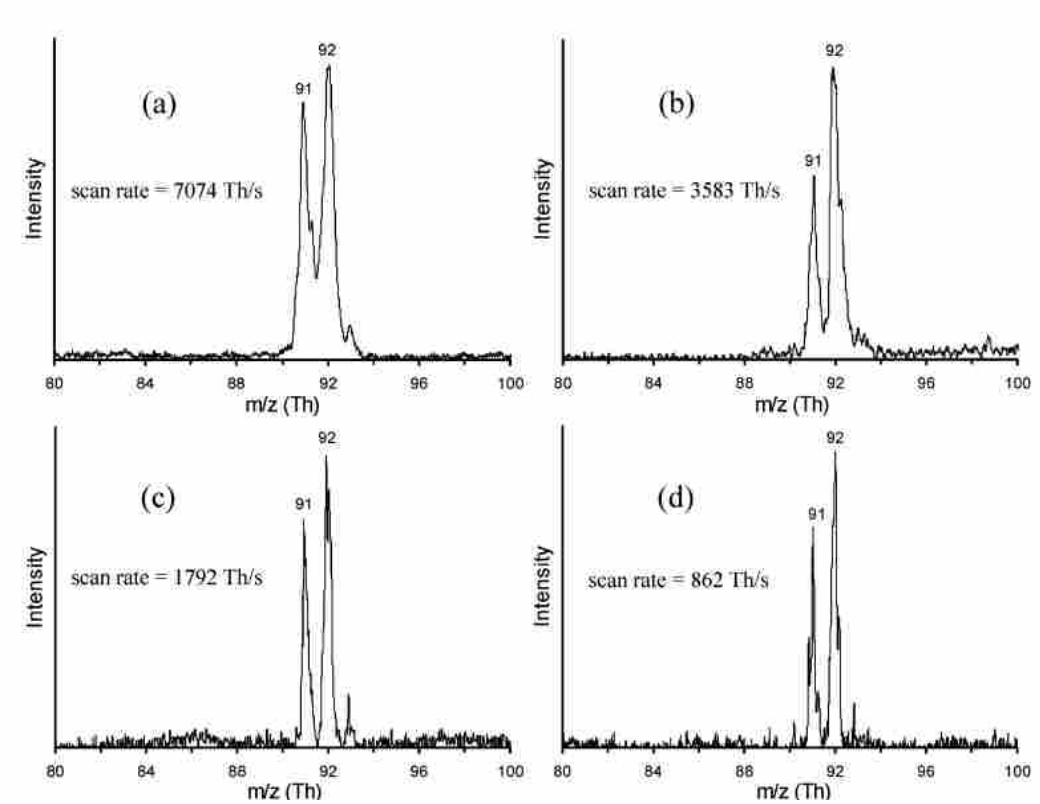

Figure 2.7. Mass spectra of toluene recorded at different RF scan rates using dipole ejection mode (supplementary AC: 290 kHz, 3.5 $V_{0\text{-}p}$, $P_{toluene} = 1.0 \times 10^{-5}$ Torr, $P_{helium} = 5.34 \times 10^{-3}$ Torr, ionization time = 4 ms (Figure from Zhang et al.)).

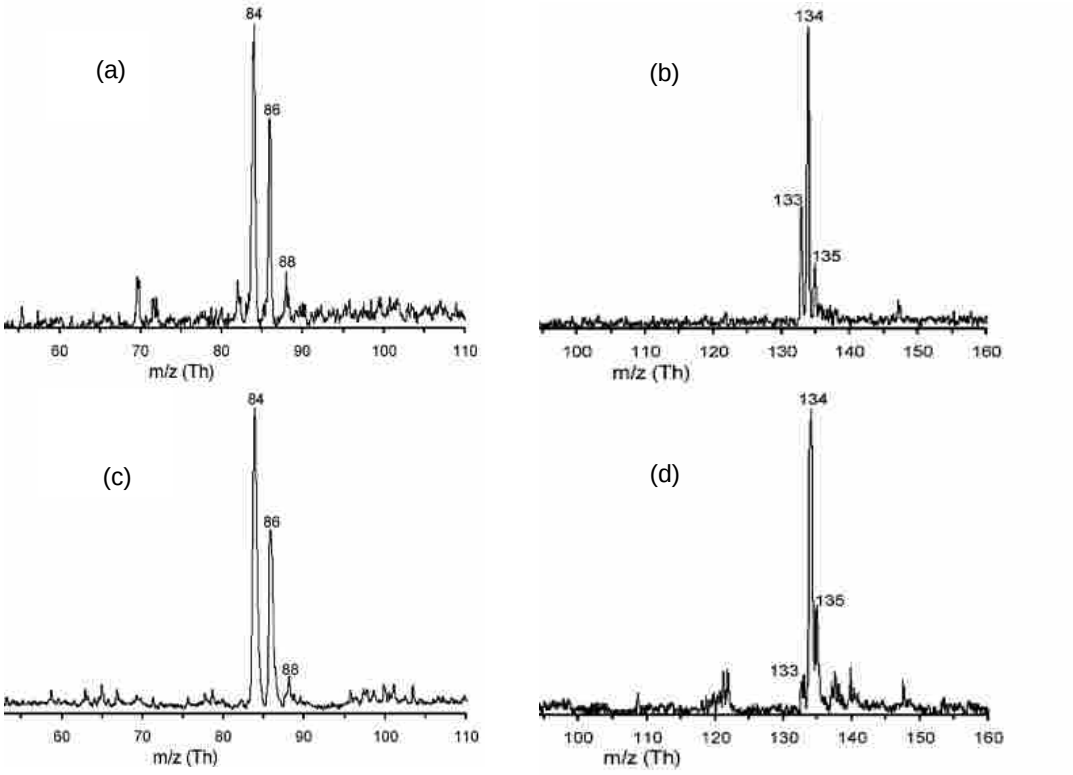

Figure 2.8. Mass spectra of several compounds recorded at RF scan rates of (a, b) 862 Th/s and (c, d) 7074 Th/s, using dipole ejection mode with an applied supplementary AC of 290 kHz, 3.5 $V_{0\text{-}p}$: (a) dichloromethane; (b) isobutylbenzene; (c) dichloromethane (d) isobutylbenzene (Figure from Zhang et al.).

From this figure, it is apparent that the peaks at *m/z* 84, 86, and 88 (Figure 2.8(a)), and at *m/z* 133, 134, and 135 (Figure 2.8(b)), are fully resolved, and the full widths at half-maximum for peaks *m/z* 86 and *m/z* 133 are 0.38 and 0.31 Th, respectively. There is one extra peak for toluene (at *m/z* 105) at a mass higher than the molecular ion. The origin of this peak, as explained by Katritzky,[49] and based on work by Ausloos[50] and Shen,[51] is the exchange of a methyl group for a hydrogen in a reaction between ionized and neutral toluene molecules. Figures 2.8(c) and 2.8(d) show the typical mass spectra of dichloromethane and isobutylbenzene obtained by increasing the RF scan rate from 862 Th/s to 7074 Th/s. The mass resolution for the triplet peaks at *m/z* 84, 86 and 88, and at *m/z* 133, 134 and 135, becomes poorer due to the high scan rate. These results further demonstrate that increasing the trapping potential can improve the trapping efficiency of both lower and higher *m/z* ions (mass range is 37-183 with the existing power supply).

Experiments were performed over a range of sample pressures from 10^{-5} Torr to 10^{-3} Torr. The number of ions detected at each pressure was adequate for quantitation. Dynamic range is an issue in all ion trap devices, because ion density in the trapping region must be small enough that the perturbation to the electric field is minimal. In Paul-type traps, methods such as automatic gain control (AGC) are used to improve experimental dynamic range. Linear, rectilinear, and toroidal ion traps have a larger storage volume, and therefore an inherently higher dynamic range. Trap arrays can also be used to improve performance in this regard. The planar Paul trap is expected to have a dynamic range that is limited by the small trapping volume (typical of other Paul-type traps) and by the low operating voltage used.

Although mass resolution observed in these experiments is reasonably high, the present system is not optimized in several ways. Limitations to resolution may be due to electronic jitter or noise, electric field shape, space-charge, or other effects.

2.5 Conclusion

A novel mass analyzer, the planar Paul ion trap, has been designed and constructed. SIMION 7 was used to determine the potential function on a planar resistive material, such that the electric field within the trapping region would be primarily quadrupolar, with a small positive octopolar contribution. Both dipolar and quadrupolar resonant ejection improved mass resolution over a simple boundary scan. Mass resolution is enhanced by reduction of the scan rate. The data reported here show that the electric field produced by the trapping plates, rather than by conventionally shaped electrodes, is applicable to perform mass spectra of various compounds, and high resolution can be obtained.

The present study also demonstrates the use of microfabricated plates to create and modify quadrupolar trapping fields. Desirable electric fields can be created without the issues that arise from machining precision or complex electrode shapes. That this approach has also been used to produce a toroidal trapping geometry illustrates the versatility of such plates in producing various electric field configurations. Future work on the planar Paul trap is aimed at improving mass resolution, performing tandem MS experiments, and a better understanding the electric fields within the trap.

2.6 References

1. Paul, W.; Steinwedel, H. Z., *Naturfrosch.* **1953**, *8A*, 448-450.

2. Wells, J. M.; Badman, E. R.; Cooks, R. G., A quadrupole ion trap with cylindrical geometry operated in the mass selective instability mode. *Anal. Chem.* **1998**, *70*, 438-444.

3. Dawson, P. H.; Hedman, J.; Whetten, N. R., *Rev. Sci. Instrum.* **1969**, *40*, 1444-1450.

4. Lawson, G.; Bonner, R. F.; Todd, J. F. J., The quadrupole ion store (quistor) as a novel source for a mass spectrometer. *J. Phys. E* **1973**, *6*, 357-362.

5. Badman, E. R.; Johnson, R. C.; Plass, W. R.; Cooks, R. G., A miniature cylindrical quadrupole ion trap: Simulation and experiment. *Anal. Chem.* **1998**, *70*, 4896-4901.

6. Dobson, G. S.; Enke, C. G., Axial ion focusing in a miniature linear ion trap. *Anal. Chem.* **2007**, *79*, 3779-3785.

7. Tabert, A. M.; Griep-Raming, J.; Guymon, A. J.; Cooks, R. G., High-throughput miniature cylindrical ion trap array mass spectrometer. *Anal. Chem.* **2003**, *75*, 5656-5664.

8. Patterson, G. E.; Guymon, A. J.; Riter, L. S.; Everly, M.; Griep-Raming, J.; Laughlin, B. C.; Zheng, O. Y.; Cooks, R. G., Miniature cylindrical ion trap mass spectrometer. *Anal. Chem.* **2002**, *74*, 6145-6153.

9. Erickson, B. E., Miniaturized rectilinear ion trap. *Anal. Chem.* **2004**, *76*, 305a-305a.

10. Janfelt, C.; Graesboll, R.; Lauritsen, F. R., Characterization and optimization of membrane inlets for a miniature ion trap mass spectrometer operating at a high background pressure of humid air. *Int. J. Mass Spectrom.* **2008**, *276*, 17-23.

11. Lammert, S. A.; Plass, W. R.; Thompson, C. V.; Wise, M. B., Design, optimization and initial performance of a toroidal rf ion trap mass spectrometer. *Int. J. Mass Spectrom.* **2001**, *212*, 25-40.

12. Lammert, S. A.; Rockwood, A. A.; Wang, M.; Lee, M. L.; Lee, E. D.; Tolley, S. E.; Oliphant, J. R.; Jones, J. L.; Waite, R. W., Miniature toroidal radio frequency ion trap mass analyzer. *J. Am. Soc. Mass Spectr.* **2006**, *17*, 916-922.

13. Fisk, P. T. H.; Lawn, M. A.; Coles, C., Laser Cooling of Yb-171(+) Ions in a Linear Paul Trap. *Appl. Phys. B-Photo* **1993**, *57*, 287-291.

14. Campbell, J. M.; Collings, B. A.; Douglas, D. J., A new linear ion trap time-of-flight system with tandem mass spectrometry capabilities. *Rapid Commun. Mass Sp.* **1998**, *12*, 1463-1474.

15. Schultz-Johanning, M.; Schnabel, R.; Kock, M., A linear Paul trap for radiative lifetime measurements on ions. *Eur. Phys. J. D* **1999**, *5*, 341-344.

16. Schwartz, J. C.; Senko, M. W.; Syka, J. E. P., A two-dimensional quadrupole ion trap mass spectrometer. *J. Am. Soc. Mass Spectrom.* **2002**, *13*, 659-669.

17. Syka, J. E. P.; Marto, J. A.; Bai, D. L.; Horning, S.; Senko, M. W.; Schwartz, J. C.; Ueberheide, B.; Garcia, B.; Busby, S.; Muratore, T.; Shabanowitz, J.; Hunt, D. F., Novel linear quadrupole ion trap/FT mass spectrometer: Performance characterization and use in the comparative analysis of histone H3 post-translational modifications. *J. Proteome Res.* **2004**, *3*, 621-626.

18. Hager, J. W., A new linear ion trap mass spectrometer. *Rapid Commun. Mass Sp.* **2002**, *16*, 512-526.

19. Hager, J. W.; Le Blanc, J. C. Y., Product ion scanning using a Q-q-Q (linear ion trap) (Q TRAP (TM)) mass spectrometer. *Rapid Commun. Mass Spectrom.* **2003**, *17*, 1056-1064.

20. Ouyang, Z.; Wu, G. X.; Song, Y. S.; Li, H. Y.; Plass, W. R.; Cooks, R. G., Rectilinear ion trap: Concepts, calculations, and analytical performance of a new mass analyzer. *Anal. Chem.* **2004**, *76*, 4595-4605.

21. Gao, L.; Song, Q. Y.; Patterson, G. E.; Cooks, R. G.; Ouyang, Z., Handheld rectilinear ion trap mass spectrometer. *Anal. Chem.* **2006**, *78*, 5994-6002.

22. Keil, A.; Hernandez-Soto, H.; Noll, R. J.; Fico, M.; Gao, L.; Ouyang, Z.; Cooks, R. G., Monitoring of toxic compounds in air using a handheld rectilinear ion trap mass spectrometer. *Anal. Chem.* **2008**, *80*, 734-741.

23. Liang, G.; Sugiarto, A.; Harper, J. D.; Cooks, R. G.; Zheng, O. Y., Design and characterization of a multisource hand-held tandem mass spectrometer. *Anal. Chem.* **2008**, *80*, 7198-7205.

24. Pau, S.; Whitten, W. B.; Ramsey, J. M., Planar geometry for trapping and separating ions and charged particles. *Anal. Chem.* **2007**, *79*, 6857-6861.

25. Cruz, D.; Chang, J. P.; Fico, M.; Guymon, A. J.; Austin, D. E.; Blain, M. G., Design, microfabrication, and analysis of micrometer-sized cylindrical ion trap arrays. *Rev. Sci. Instrum.* **2007**, *78*, 015107.

26. Van Amerom, F. H. W.; Chaudhary, A.; Cardenas, M.; Bumgarner, J.; Short, R. T., Microfabrication of cylindrical ion trap mass spectrometer arrays for handheld chemical analyzers. *Chem. Eng. Commun.* **2008**, *195*, 98-114.

27. Pau, S.; Pai, C. S.; Low, Y. L.; Moxom, J.; Reilly, P. T. A.; Whitten, W. B.; Ramsey, J. M., Microfabricated quadrupole ion trap for mass spectrometer applications. *Phys. Rev. Lett.* **2006**, *96* 120801.

28. Badman, E. R.; Cooks, R. G., A parallel miniature cylindrical ion trap array. *Anal. Chem.* **2000**, *72* , 3291-3297.

29. Badman, E. R.; Cooks, R. G., Cylindrical ion trap array with mass selection by variation in trap dimensions. *Anal. Chem.* **2000**, *72*, 5079-5086.

30. Riter, L. S.; Meurer, E. C.; Handberg, E. S.; Laughlin, B. C.; Chen, H.; Patterson, G. E.; Eberlin, M. N.; Cooks, R. G., Ion/molecule reactions performed in a miniature cylindrical ion trap mass spectrometer. *Analyst* **2003,** *128*, 1112-1118.

31. Austin, D. E.; Wang, M.; Tolley, S. E.; Maas, J. D.; Hawkins, A. R.; Rockwood, A. L.; Tolley, H. D.; Lee, E. D.; Lee, M. L., Halo ion trap mass spectrometer. *Anal. Chem.* **2007**, *79*, 2927-2932.

32. Xu, W.; Chappell, W. J.; Cooks, R. G.; Ouyang, Z., Characterization of electrode surface roughness and its impact on ion trap mass analysis. *J. Mass Spectrom.* **2009**, *44*, 353-360.

33. Austin, D. E.; Peng, Y.; Hansen, B. J.; Miller, I. W.; Rockwood, A. L.; Hawkins, A. R.; Tolley, S. E., Novel Ion Traps Using Planar Resistive Electrodes: Implications for Miniaturized Mass Analyzers. *J. Am. Soc. Mass Spectr.* **2008**, *19*, 1435-1441.

34. Traldi, P.; Catinella, S.; March, R. E.; Creaser, C. S., In *In Practical Aspects of Ion Trap Mass Spectrometry*, March, R. E.; Todd, J. F. J., Eds. CRC Press: New York, **1995**; Vol. 1, pp 229-341.

35. March, R. E.; McMahon, A. W.; Londry, F. A.; Alfred, R. L.; Todd, J. F. J.; Vedel, F., Resonance Excitation of Ions Stored in a Quadrupole Ion Trap. 1. A Simulation Study. *Int. J. Mass Spectrom. Ion Process.* **1989**, *95*, 119-156.

36. Zhao, X. Z.; Douglas, D. J., Dipole excitation of ions in linear radio frequency quadrupole ion traps with added multipole fields. *Int. J. Mass Spectrom.* **2008**, *275*, 91-103.

37. Ioanoviciu, D.; Ioanoviciu, A. S., Paul trap: axial ejection by auxiliary radio frequency voltage connection to the end-caps or by pure dipole field. *Nucl. Instrum. Methods Phys. Res. Sect. A-Accel. Spectrom. Dect. Assoc. Equip.* **1999**, *427*, 161-165.

38. Wu, G. X.; Cooks, R. G.; Ouyang, Z., Geometry optimization for the cylindrical ion trap: field calculations, simulations and experiments. *Int. J. Mass Spectrom.* **2005**, *241*, 119-132.

39. Franzen, J.; Gabling, R.-H.; Schubert, M.; Wang, Y., In *Practical Aspects of Ion Trap Mass Spectrometry*, March, R. E.; Todd, J. F. J., Eds. CRC Press: New York, **1995**; Vol. 1, pp 66-69.

40. Dahl, D. A. *SIMION Version 7.0*, Idaho National Engineering and Environmental Laboratory: Idaho Falls, ID, **2000**.

41. Goeringer, D. E.; Whitten, W. B.; Ramsey, J. M.; McLuckey, S. A.; Glish, G. L., Theory of High Resolution Mass-Spectrometry Achieved via Resonance Ejection in the Quadrupole Ion Trap. *Anal. Chem.* **1992**, *64*, 1434-1439.

42. Schwartz, J. C.; Syka, J. E. P.; Jardine, I., High-Resolution on a quadrupole Ion Trap Mass-Spectrometer. *J. Am. Soc. Mass Spectr.* **1991**, *2*, 198-204.

43. Goeringer, D. E.; McLuckey, S. A.; Glish, G. L. In Proceedings of the 39th Annual Conference of Mass Spectrometry and Allied Topics, Nashville, TN, Nashville, TN, 1991; p 532.

44. Williams, J. D.; Cox, K.; Morand, K. L.; Cooks, R. G.; Julian, R. K., Jr.; Kaiser, R. E. In Proceedings of the 39th Annual Conference of Mass Spectrometry and Allied Topics, Nashville, TN, Nashville, TN, 1991; p 1481.

45. Kaiser, R. E.; Cooks, R. G.; Stafford, G. C.; Syka, J. E. P.; Hemberger, P. H., Operation of a Quadrupole Ion Trap Mass-Spectrometer to Achieve High Mass Charge Ratios. *Int. J. Mass Spectrom. Ion Process.* **1991**, *106*, 79-115.

46. Williams, J. D.; Cox, K. A.; Cooks, R. G.; Kaiser, R. E.; Schwartz, J. C., High Mass-Resolution Using a Quadrupole Ion-Trap Mass-Spectromter. *Rapid Commun. Mass Sp.* **1991**, *5*, 327-329.

47. Makarov, A. A., Resonance ejection from the Paul trap: A theoretical treatment incorporating a weak octapole field. *Anal. Chem.* **1996**, *68*, 4257-4263.

48. Song, Q. Y.; Kothari, S.; Senko, M. A.; Schwartz, J. C.; Amy, J. W.; Stafford, G. C.; Cooks, R. G.; Ouyang, Z., Rectilinear ion trap mass spectrometer with atmospheric pressure interface and electrospray ionization source. *Anal. Chem.* **2006**, *78*, 718-725.

49. Katritzky, A. R.; Degaszafran, Z.; Ramanathan, R.; Eyler, J. R., Ion-cyclotron resonance mass-spectromtric study of ion-molecule reactions in toluene-pyridine mixtures. *Org. Mass Spectrom.* **1994**, *29*, 96-101.

50. Ausloos, P., Structure and isomerization of $C_7H_7^+$ ions formed in the charge-transfer-induced fragmentation of ethylbenzene, toluene, and norbornadiene. *J. Am. Chem. Soc.* **1982**, *104*, 5259-5265.

51. Shen, J.; Dunbar, R. C.; Olah, G. A., Gas-phase benzyl cations from toluene precursors. *J. Am. Chem. Soc.* **1974**, *96*, 6227-6229.

CHAPTER 3: COAXIAL ION TRAP MASS SPECTROMETER: CONCENTRIC TOROIDAL AND QUADRUPOLE TRAPPING REGIONS

3.1 Introduction

Radio-frequency (RF) ion traps are among the most widely-used mass analyzers, combining several advantages including high sensitivity, reasonable mass resolution, high duty cycle, compact size, tandem capability, and reasonable cost.[1-5] Besides the original Paul-type quadrupole ion trap, several geometrical variants, such as linear,[6-8] rectilinear,[9-10] cylindrical,[11-12] and toroidal ion traps[13-14] have been developed, each with unique attributes resulting from the trapping geometry. For instance, the ion trapping capacity is larger in the linear, rectilinear and toroidal ion traps compared with the quadrupole trap due to the extended axial dimension of the trapping volume.

The toroidal ion trap, developed by Lammert et al.,[13] represents a geometric variation on the quadrupole ion trap. The toroidal trapping region provides a larger ion capacity than in quadrupole traps. A toroidal ion trap has recently been included in a commercial, portable GC-MS system[15]—an application in which ion capacity and corresponding sensitivity are important considerations.

Austin et al.[16] described a device called the Halo ion trap, in which a toroidal trapping field was made using two planar electrode substrates. A set of 15 concentric ring electrodes was lithographically deposited on each substrate, which were then covered with a thin film of germanium. The two plates were mounted facing each other to form the trap. RF voltages were applied to each ring using a capacitive voltage divider, with the amplitude on each ring chosen to establish the desired fields within the trap. Ions were resonantly ejected toward the center of the device, then pushed out toward a detector. A more recent version of the Halo ion trap included

annular slits in the ceramic plates.[17] Ions were ejected axially, that is, parallel to the axis of geometric rotation—the same ejection direction as was employed in the toroidal ion trap described by Lammert. Because of the improved ejection, mass resolution was better relative to the original Halo ion trap. Both versions of the Halo ion trap retained the large storage volume of the toroidal ion trap.

Zhang et al.[18] used this same two-plate approach to create and demonstrate a quadrupole ion trap, called the planar quadrupole trap mass analyzer. In the planar quadrupole trap, a capacitive voltage divider provided different RF amplitudes to each of 24 lithographically patterned rings on each plate, resulting in a quadrupolar potential distribution. Higher-order multipoles could be individually controlled and adjusted to optimize performance.[19-20] Although the large trapping volume of the toroidal geometry was lost, the equations of ion motion are better understood in the quadrupole geometry. As a result, the planar quadrupole trap demonstrated significantly higher mass resolution than either design of the Halo ion trap.

These two-plate ion traps demonstrate a novel, general method for producing electric fields for ion traps or other devices.[21] The use of microlithography allows devices and fields to be relatively free of the physical limitations imposed by machining tolerances, surface roughness, electrode alignment and placement, and similar obstacles. In addition, using a number of independent electrodes allows substantial variability and opportunity for creating electric fields. In essence, field geometry using this approach is not constrained or limited by substrate geometry, in contrast to conventional ion traps. Within limits, any potential distribution can be created by using the correct combination of electrode patterns and applied voltages.

This chapter describes a surprising twist to this approach: the ability to produce multiple, linked trapping regions simultaneously between two such plates. A toroidal region is formed using the outer rings, and a quadrupolar trapping region is formed in the center. The two trapping regions share a common axis of symmetry—hence the name coaxial ion trap—and can be operated more or less independently of one another due to the independent nature of the rings. In addition to trapping and mass analysis, ions can be transferred between the two trapping regions. After ions are ejected from the toroidal trapping region into the quadrupole trapping region, they can be collisionally cooled down in the center region and mass-selectively ejected out. The arrangement of the two trapping regions and the electric fields in the coaxial ion trap are shown in Figure 3.1. An ion trap with two or more trapping regions may combine the advantages of both trapping geometries and demonstrate unique opportunities for experiments in tandem mass analysis, quantum computing, and ion-ion reactions.

3.2 Methods

3.2.1 Fabrication and Assembly of Device

The coaxial trap is made using plates identical to those used in the previously-described planar quadrupole trap mass analyzer.[18] .Each of the two trapping plates began as a 99.6% pure alumina substrate, 47×36×0.635 mm (Micro Substrate, Tempe, AZ). Holes for mounting, electrical vias, and ion ejection were laser cut (Questech Services, Garland, TX) through the alumina. Holes for the vias, which provide electrical connection between the front and back of the plates, were filled with gold, and each side of the substrate was polished to a surface

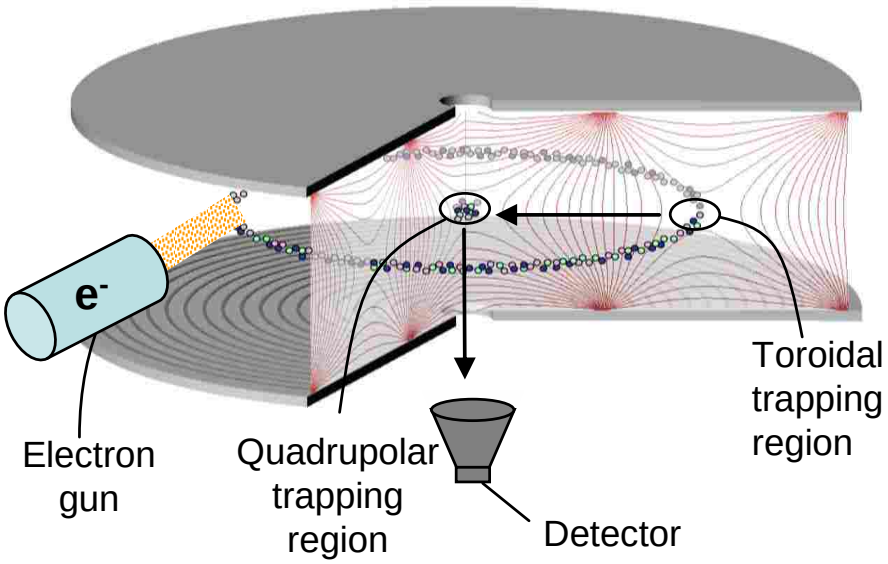

Figure 3.1. Arrangement of patterned electrode plates and electric fields in the coaxial ion trap. Ions are created in situ with an electron gun and trapped initially in both trapping regions. Direction of subsequent ion transfer is indicated.

roughness of better than 50nm (HybridTek, NJ). The prepared substrates were evaporatively coated with 400 nm of either aluminum or gold metal, then spin-coated with a layer of photoresist. The photoresist was then photolithographically patterned using a chrome mask (Advanced Reproductions, North Andover, MA), and the substrates were wet-etched to leave behind the desired pattern of aluminum or gold rings. Finally, a thin film (100 nm) of germanium was evaporatively deposited over the active area on the trapping side of each substrate. The trap consists of two ceramic plates mounted 6 mm apart, the facing surfaces of which are imprinted with concentric metal rings (Figure 3.2). Appropriate RF potentials are applied to each ring, producing trapping fields in the space between the plates.

Each trapping plate was patterned with 24 aluminum rings, ranging in radius from 0.5 mm to 13.2 mm in increments of 0.5 mm. All but the innermost ring were 0.1 mm wide. Due to processing constraints, the innermost ring extended from the center hole to a radius of 1.8 mm, and was therefore much wider than any other ring. The center hole in each plate, through which ions are ejected, was 1 mm in diameter. The deposited aluminum layer extended throughout the inside of the central hole in order to maintain a well-defined electric potential as ions eject from the trap. The holes for vias, 0.127 mm in diameter were positioned to fall immediately beneath the corresponding rings. Aluminum patterning on the backside of each plate consisted of connections from each via to a contact pad. Each ring had its own contact pad for independent control. Backside connections between vias and contact pads were 0.25 mm wide. Each trapping plate was controlled using a printed circuit board (PCB). The contact pads on the backsides of the substrates were connected to the PCBs using spring-loaded (pogo-style) pin connectors as shown in Figure 3.2. A voltage divider consisting of a series of capacitors was

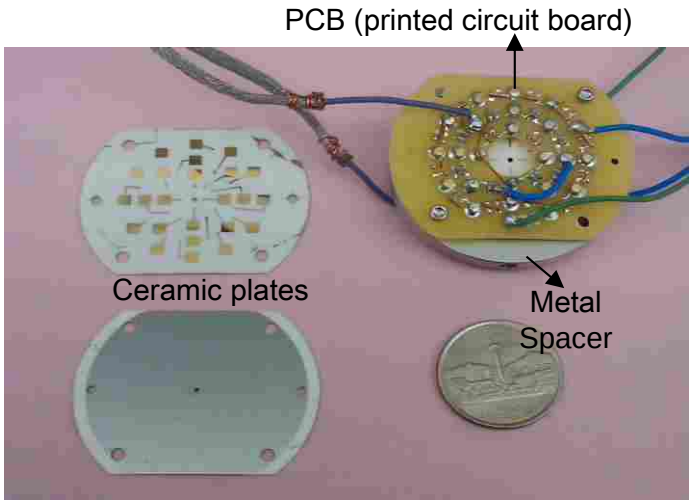

(a)

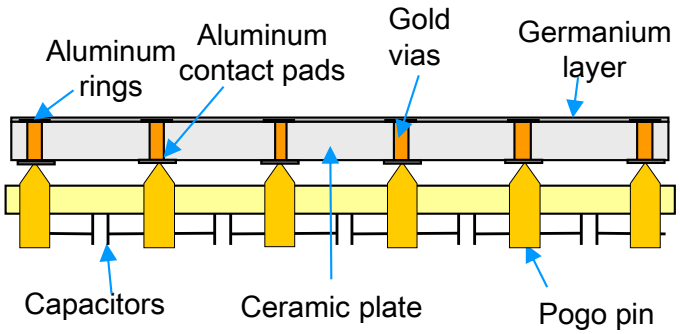

(b)

Figure 3.2. (a) Photograph showing front and back side of the patterned ceramic plates and the assembled device, (b) design cross section and electrical connections between the piece of ceramic plate and PCB.

soldered onto each PCB. The value of the capacitors between each ring was determined by the potential intended for each ring, while maintaining a constant overall capacitance for each plate (25 pF).

3.2.2 Calculating and Optimizing Electric Fields

The choice of potential values for each ring was made by modeling the electric fields using SIMION 8.0 (SIS, Ringoes, NJ). The electric field within the trap volume is a result of the potential distribution on the germanium layer, which in turn is determined by the underlying rings. The potential of the germanium immediately above a given ring is the same as the ring itself. The potential between rings can be solved using Ohm's Law and integrating over the radius. This can be done in SIMION using a previously-described method[19].

The trapping field of the radial direction (along z=0) in the coaxial ion trap was simulated to approximate the radial field in the toroidal ion trap[16] and planar quadrupole ion trap[18]. The field in the axial direction was selected to be similar to the axial field of the planar quadrupole ion trap (working within the constraints of the Laplace equation). Several sets of potential functions were identified as feasible during the optimization process. For the potential distribution used for this chapter, the RF amplitudes applied to each ring are given in Table 3.1. A series of capacitors, acting as an RF voltage divider, determined the RF amplitude applied to each ring. Figure 3.3 shows the time-independent electric potential and field distributions within the coaxial trap, as calculated using SIMION. In Figure 3.3(a), equipotential lines indicate the two trapping regions. Figure 3.3(b) shows the axial potential function and electric field, which is the direction in which ions are ejected out from the quadrupolar trapping region. The higher-order component of the axial field is shown Figure 3.4(a) —these components are expected to

Ring Number	Inner -outer radius (mm)	RF potential (V_{p-p})
1	0.5-1.8	8
2	2.2-2.3	81
3	2.7-2.8	0
4	3.2-3.3	81
5	3.7-3.8	0
6	4.2-4.3	118
7	4.7-4.8	318
8	5.2-5.3	379
9	5.7-5.8	500
10	6.2-6.3	460
11	6.7-6.8	500
12	7.2-7.3	467
13	7.7-7.8	491
14	8.2-8.3	500
15	8.7-8.8	491
16	9.2-9.3	500
17	9.7-9.8	479
18	10.2-10.3	472
19	10.7-10.8	472
20	11.2-11.3	362
21	11.7-11.8	264
22	12.2-12.3	138
23	12.7-12.8	0
24	13.2-13.3	0

Table 3.1. Dimension and designed RF potential applied on each ring electrode patterned on the ceramic plates.

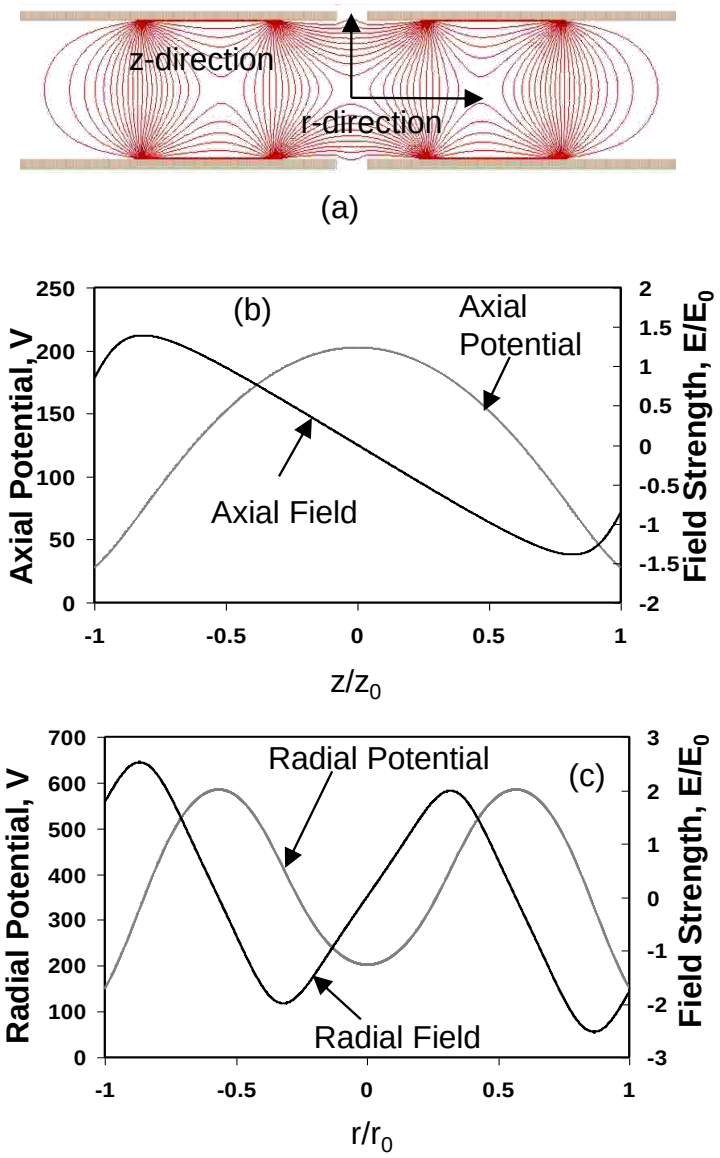

Figure 3.3. (a) Isopotential contours in the coaxial ion trap, (b) potential function and field along axial (z-) direction in quadrupolar region, (c) potential function and field along the radial (r-) direction through both trapping regions.

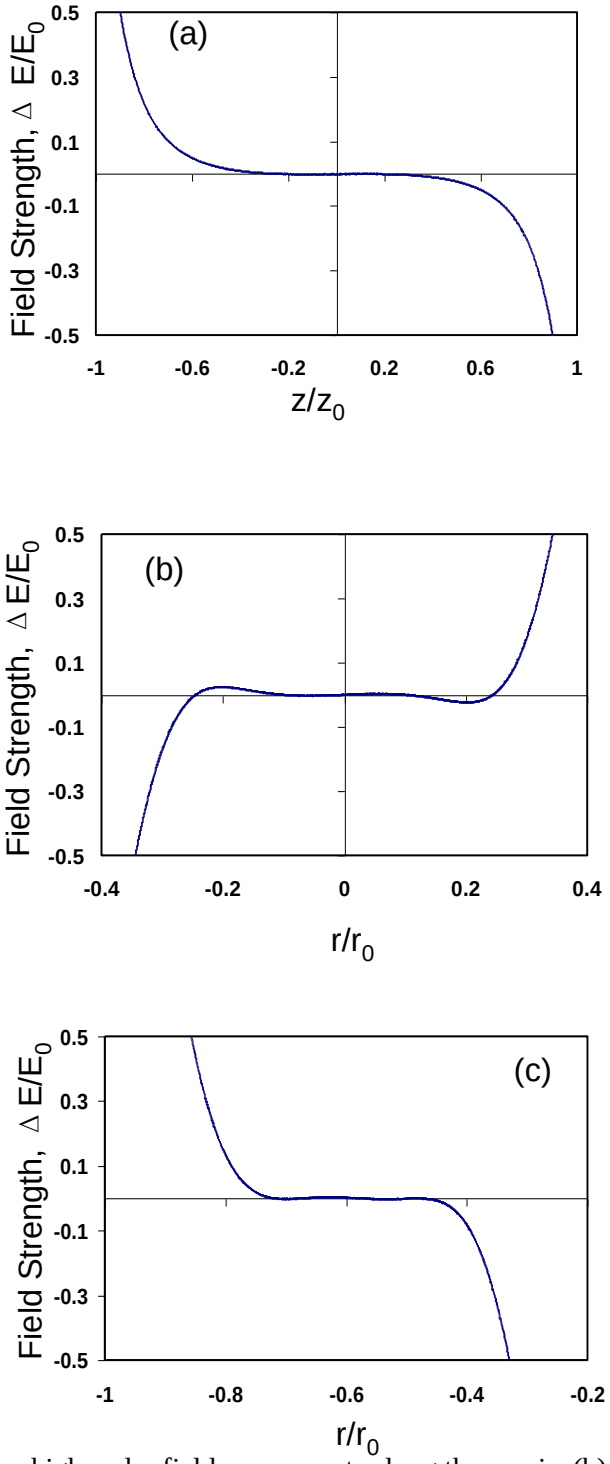

Figure 3.4. (a) Nonlinear high-order field components along the z-axis, (b) nonlinear higher-order field components in the r-direction of the quadrupolar trapping region, (c) nonlinear higher-order field components in the r-direction of the toroidal trapping region.

have a significant effect on the resolving power of the quadrupolar trapping region.[22-23] In Figure 3.3(c), the radial potential function and the resulting electric field are shown. This is the direction in which ions are transferred between the trapping regions. Note that the two trapping regions have opposite polarity. Since the field along the radial direction spans two trapping regions, the high-order components of the field in the toroidal trapping region and quadrupolar trapping region need to be studied separately as shown in Figure 3.4(b) and (c). In both trapping regions the electric fields deviate somewhat from the ideal toroidal and quadrupolar fields. Part of this deviation is a result of the necessity of field continuity between the trapping regions. In addition, the small ratio of plate spacing to ejection hole size increases field imperfections in the quadrupolar trapping region, as is also the case with conventional ion traps.[24-25]

3.2.3 Experimental Setup

An RF power supply (PSRF-100, Ardara, North Huntingdon, PA), operated at 1.43 MHz and 500 V_{p-p}, provided the trapping RF. Supplemental time-varying signals were provided by a function generator (SRS, DS345, Sunnyvale, CA), which controlled the timing of ionization and the ejection AC signals. An AC signal used for axial resonant ejection from the quadrupole trapping region was provided by an arbitrary waveform generator (Agilent, Model 33250A, Santa Clara, CA) and was applied at the central hole. Another AC signal (used to transfer ions from the toroidal region to the quadrupole region) was provided by a function generator (SRS, DS345, Sunnyvale, CA). A custom-made electron gun and the two function generators mentioned above were triggered by two pulse generators (BNC, Models 565 and 575, San Rafael, CA). These two pulse generators and the RF power supply were synchronized by another function generator as demonstrated in Figure 3.5.

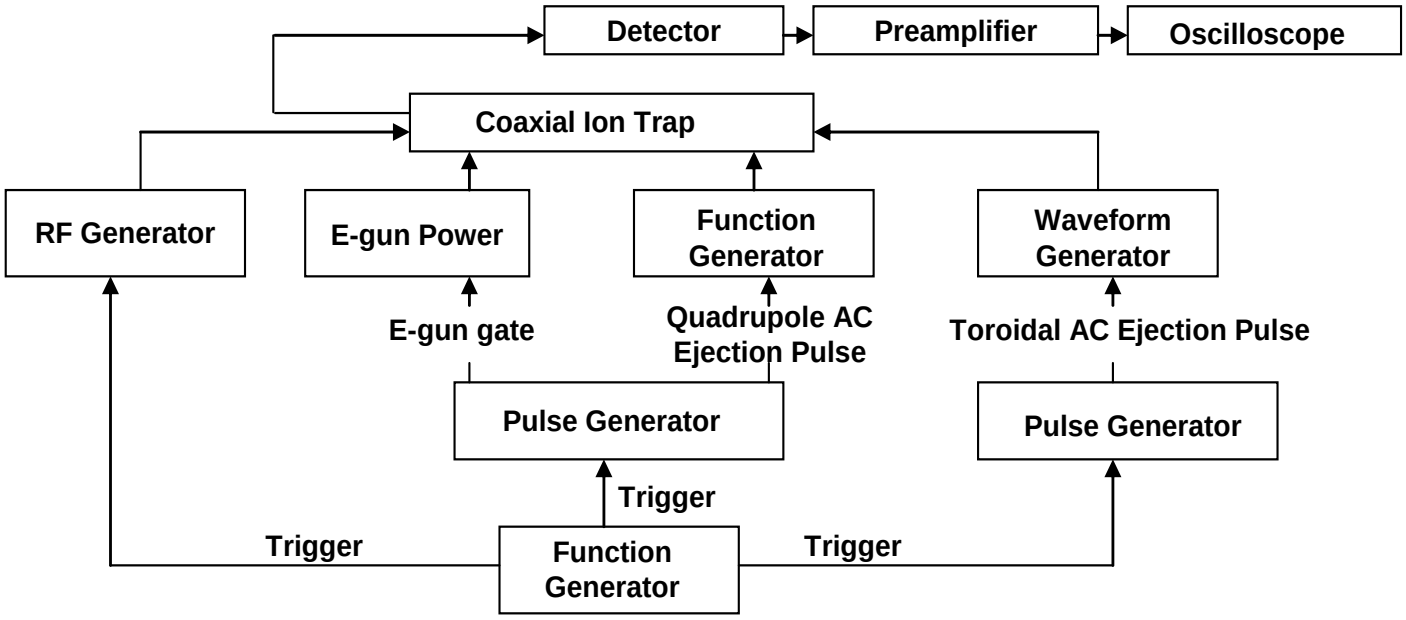

Figure 3.5. Experimental set-up for coaxial ion trap. The electron gun signal, sweeping quadrupole AC signal and toroidal AC signal are controlled by two pulses generators. These two pulse generators and RF generator are triggered by a function generator. The frequency modulation for quadrupole AC and toroidal AC are provided by a function generator and a waveform generator, respectively.

The two plates comprising the ion trap were mounted using a grounded, 6-mm thick metal spacer to maintain accurate plate spacing and alignment. Holes in the spacer allowed introduction of the ionizing electron beam, helium gas, and two Teflon tubes connecting to the sample inlet and to a Pirani gauge (Kurt J. Lesker, Clairton, CA). The entire assembly (Figure 3.2) was contained within a small vacuum chamber, and high vacuum was maintained using a 70 l/s turbomolecular pumping system (Leybold, BMH70 DRY, Export, PA). A continuous-dynode electron multiplier (DeTech, Palmer, MA) was mounted near the ejection hole of one plate. All test samples were HPLC grade or were > 99% pure. The headspace vapors of samples were introduced directly into the trapping region via precision needle leak valves (Nupro/Swagelok, Solon, OH) and heated transfer lines. Sample pressure was normally 2×10^{-5} Torr (uncorrected), and helium buffer gas was admitted into the vacuum chamber to cool the ions via the same precision needle leak valves to a nominal pressure of about 3×10^{-3} Torr.

Basic instrument functionality was demonstrated using the procedure shown in Figure 3.6. Ions were produced in situ within both the toroidal and quadrupolar trapping regions using an electron gun and ionization time of 12 ms. The electron beam was directed tangential to the toroidal region. Following ionization, the ions in the quadrupole trapping region were analyzed using dipole resonant ejection mass analysis. This was followed by a short period in which ions were cooled by collisions with background helium. The quadrupole region was then scanned again to verify that all ions initially trapped in the quadrupole region had been ejected, and that the quadrupole region was empty. This second quadrupole scan was followed by another cooling period. Next, an AC signal (25 V_{p-p}) was applied to the outermost rings of the toroidal trapping region to transfer ions into the quadrupole region. These ions were then trapped and

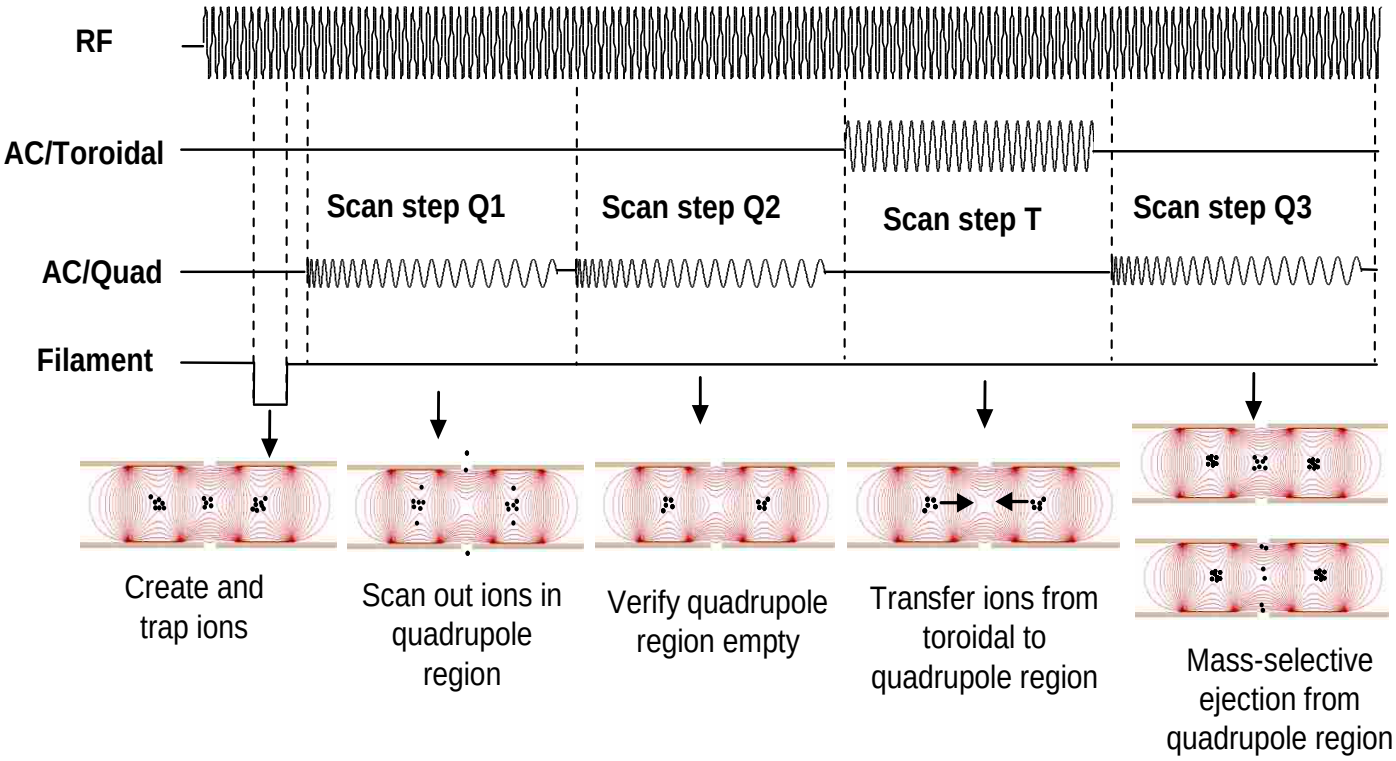

Figure 3.6. Coaxial ion trap scan function. Ions are created in situ in both regions. A supplementary AC sweeps all the ions out of the quadrupole region. A second quadrupole scan demonstrates that the quadrupole region is empty. Another AC signal applied to the toroidal region transfers ions from the toroidal to the quadrupole region. Finally, AC applied to the quadrupole region mass-selectively ejects ions out to the detector.

cooled within the quadrupole region, then resonantly ejected through the center hole in the substrate and onto the electron multiplier detector. The AC signal used for resonant ejection had an amplitude of 1 V_{p-p} and was applied to the innermost ring on one of the plates, while keeping the corresponding ring on the other plate grounded, analogous to dipole ejection in conventional ion traps. The frequency of the AC signal applied to the toroidal region was 1100 kHz, and the AC signal applied to the quadrupole region was scanned from 800 kHz to 50 kHz over a period of 100 ms, providing mass-selective ejection. The signal was amplified by a current sensitive amplifier (EG&G PARC, Model 181, Oak Ridge, TN) and then recorded by a digital oscilloscope (LeCroy, WaveRunner 6050A, Chestnut Ridge, NY). Figure 3.6 illustrates ion movement inside the trap at each scan step: creation of ions inside the trap, cleaning of ions inside the quadrupolar region, transfer of ions from the toroidal region to the quadrupolar region and mass selective ejection of ions from the quadrupolar region to the detector. This sequence is also represented in Figure 3.7(a). Any combination of quadrupole and toroidal scans is possible with this setup. For instance, Figure 3.7(b) shows an experiment in which three transfer steps were applied in sequence (using a single ionization event) with a quadrupole scan subsequent to each transfer. This multiple-transfer process was investigated to study the ion capacity of the toroidal trapping region.

3.3 Result and Discussion

3.3.1 Target Sample Analysis

Instrument performance was tested using several volatile organic compounds, including bromopentafluorobenzene, toluene, trichloroethylene, and tetrachloromethane with the above

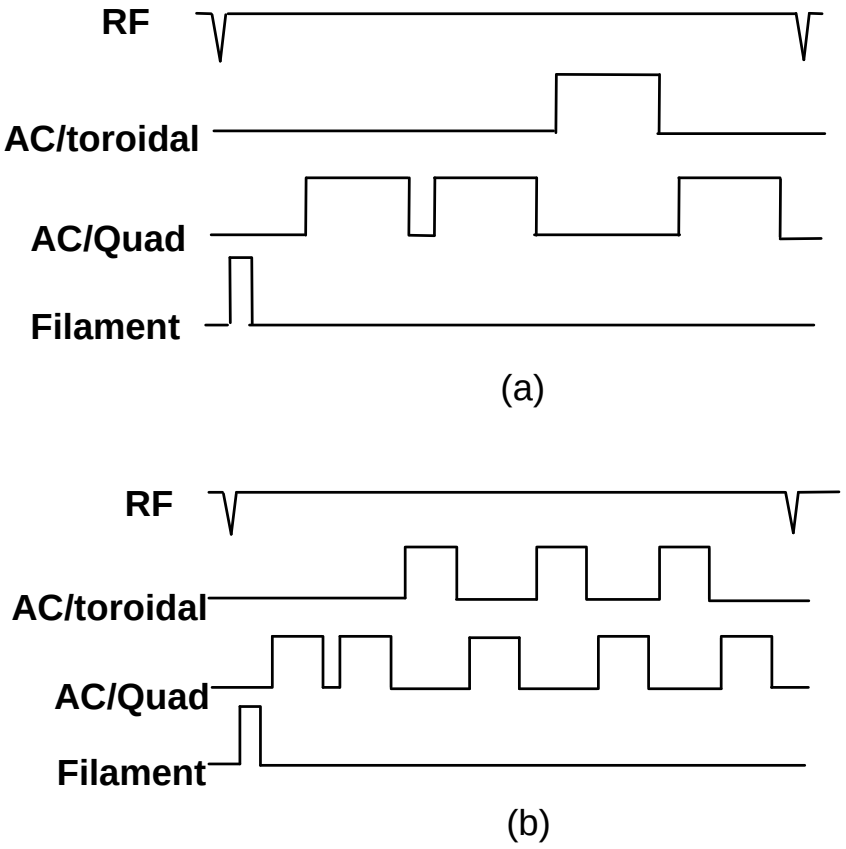

Figure 3.7. Experiment with (a) a single transfer scan of ions from the toroidal region to the quadrupole region corresponding to the scan function shown in figure 4, (b) scan pulse used for multiple transfer processes of ions from the toroidal to the quadrupolar region.

procedure. Figure 3.8(a) shows the resulting spectra of bromopentafluorobenzene at a pressure of 2×10^{-5} Torr (helium pressure 3.45×10^{-3} Torr). The spectra were obtained by sweeping the resonant ejection frequency from 800 to 50 kHz in 100 ms for the mass analysis in the central region and applying 1100 kHz AC signal in 100 ms for the transfer process from the toroidal region to the quadrupole region. Mass assignments are based on calculated secular frequencies for the quadrupolar trapping region. During the first quadrupole scan, peaks with mass-to-charge ratio (m/z) of 98, 117, 129, 136 and 168 were detected, as shown in Figure 3.8(b) and 6(c), matching well with the standard mass spectrum of bromopentafluorobenzene.[26] Because the applied AC for resonant ejection out of the quadrupole trap relied on a linear scan of frequency, the mass resolution drops at higher masses when plotted as a mass-domain spectrum. Mass resolution in this device is better than that previously demonstrated by radial ion ejection in the halo ion trap, which is similar to the toroidal trapping region in the present device acting alone. Mass spectra for other compounds are available in Figure 3.9, and show similar performance and the expected patterns for each compound.

As shown in Figure 3.8(a), no ions were ejected from the quadrupole region during the second quadrupole scan, indicating that the quadrupole region was empty prior to the first transfer step. After the first toroidal transfer step, ions were detected during the next quadrupole scan, demonstrating that these ions had been transferred from the toroidal trapping region to the quadrupole trapping region.

Following the first transfer step and subsequent mass analysis, additional toroidal transfer scans and quadrupole mass scans on the same population of ions showed additional ejected ions (Figure 3.8(a)). These ions presumably were trapped in the toroidal region, were not transferred

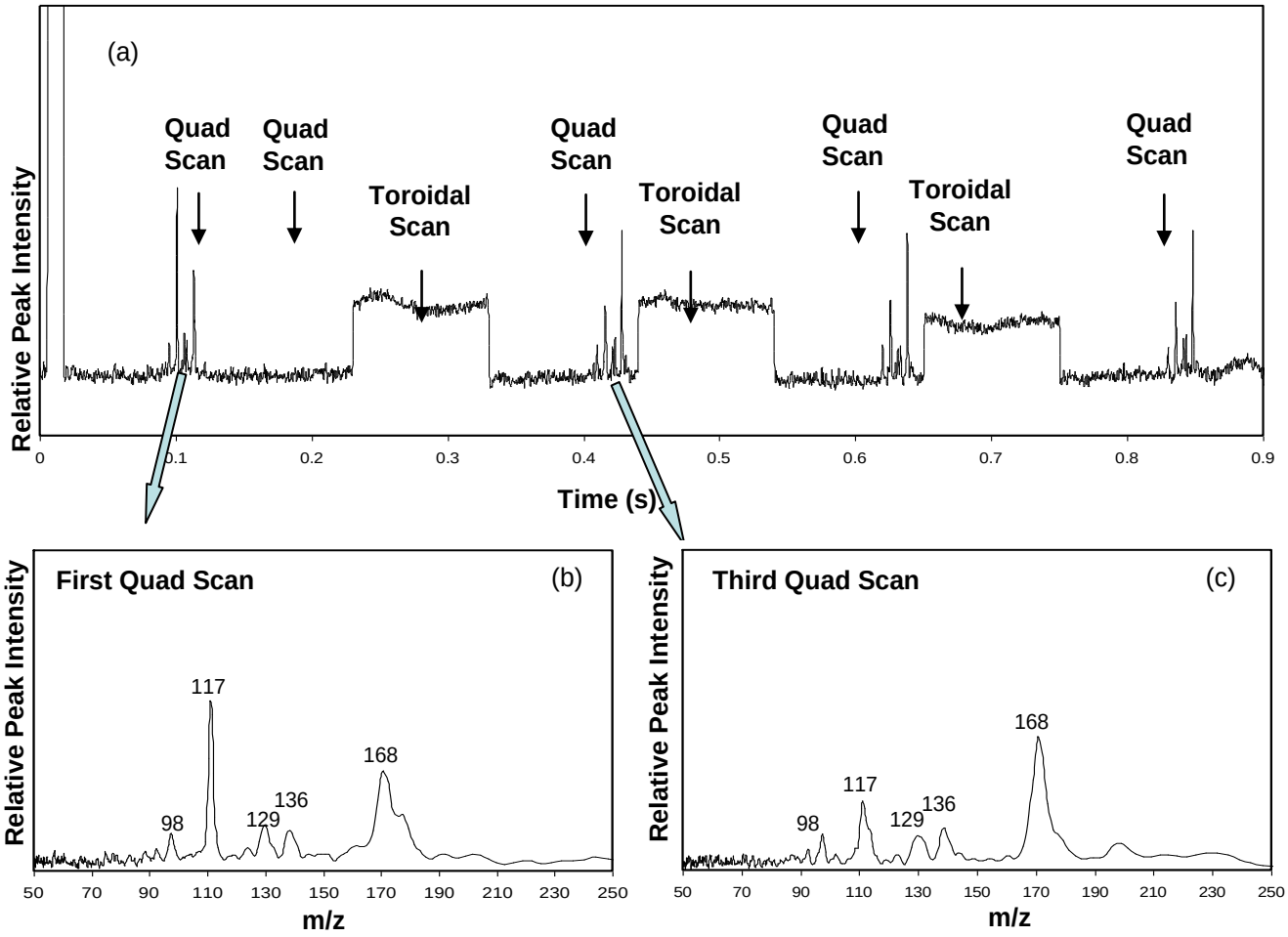

Figure 3.8. Coaxial ion trap mass spectrum of bromopentafluorobenzene: (a) data acquired during entire experiment (b) mass spectrum for the first quadrupole scan, (c) mass spectrum for the third quadrupole scan (after the first toroidal transfer).

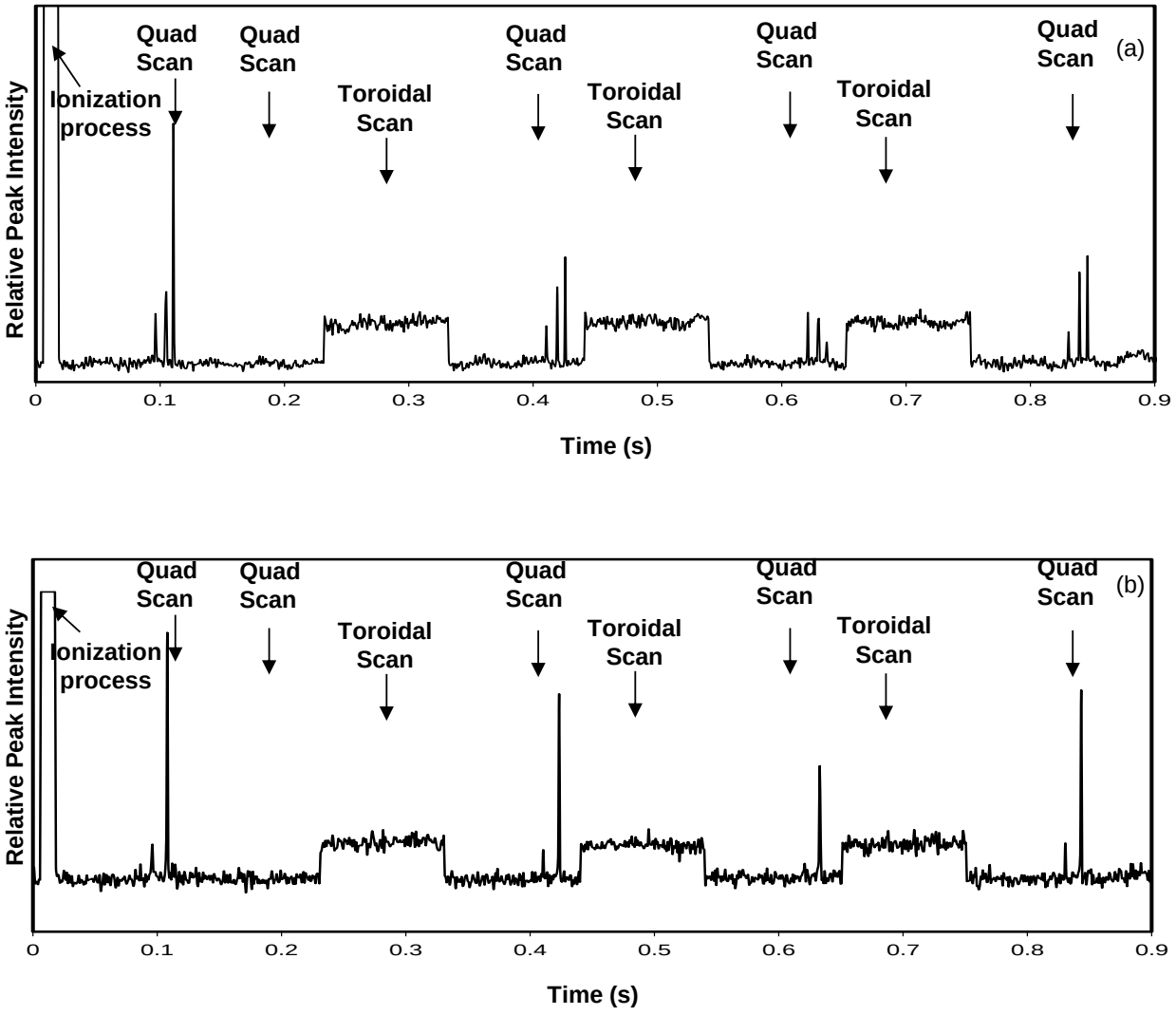

Figure 3.9. Coaxial ion trap spectrum of (a) trichloroethylene and (b) tetrachloromethane.

to the quadrupole region during the first transfer scan, and were subsequently transferred. Multiple sets of toroidal and quadrupole scans showed the same result, implying (1) that the toroidal region had trapped many more ions than the quadrupole region, as the populations of ions does not appear to be depleted after three transfer scans, and (2) that the transfer of ions from the toroidal region to the quadrupole region was either not very efficient or proceeded only until the quadrupole region had reached a certain population. Slight mass discrimination may be observed during the transfer process by comparing the mass spectra obtained from the first quadrupole scan and third quadrupole scan after a toroidal transfer process as shown in Figure 3.8(b) and (c).

In Figure 3.8 and 3.9, the baseline during the toroidal scans is elevated due to electrical noise. This elevated baseline is present whether ions are analyzed or not, and does not diminish after repeated scans from a single ionization event.

3.3.2 Transfer Mechanism Study

The originally intended mode of operation using this device was to employ resonant transfer of ions, i.e., the radial secular motion of ions in the toroidal region would be resonantly excited by the AC signal applied to the outside rings. Had this been the case, mass-selective transfer should have been observed. However, we observed that a wide range of masses was transferred, even if only one frequency of applied AC was used. In addition, applied AC with frequency higher than the secular frequencies of any trapped ion was also effective at transferring ions. From these results we conclude that resonant excitation was not responsible for the observed ion transfer.

In order to determine the mechanism of observed ion transfer, we next studied the relationship between the phase of the drive RF and the phase of the AC applied to the outer rings

during the toroidal transfer step. In general, and in the work described above, these frequencies are not exact multiples of each other, and the phase relationship between them is random. However, reports by Harden and Wagner[27], by Mastoris[28] and by Dawson and Lambert[29] describe the possible importance of synchronizing the ejection pulse to the ring electrode in quadrupole ion traps. They concluded that relative efficiencies of ejecting different masses would be dependent on the phase relationship between the drive RF and the AC signal applied for resonant ejection. Many experimental systems[30-32] have been employed to test this "pulse/RF synchronization circuit" on the performance of ion traps both as an ion source and as mass analyzers. In those experiments, an output trigger pulse gated to a specified phase angle of the drive potential was used. This triggered pulse activated the ejection pulse generator and the phase angle was swept over several complete cycles so that the ejected ion signal was recorded in respect to the phase differences between trigger pulse and RF signal.

To investigate the effect of phase-synchronized ion ejection on the ion transfer process in the coaxial ion trap, a periodic DC pulse was applied to the outmost ring to replace the original AC signal applied during the toroidal transfer scan. This DC pulse was synchronized with the drive RF. The RF phase at which this DC pulse was applied, the repetition rate of the DC pulse, and the length of the DC pulse were explored for their effect on ion transfer. A short DC pulse produced by the same BNC 575 pulse generator with 24 ns width and 12 V amplitude was applied to the toroidal region at different RF phases. DC pulses with different widths from 24 ns to several RF wavelengths including 1.5 λ, 2 λ and 3 λ were investigated, applied at different RF phases (Figure 3.10). The relationship of peak intensity with RF phase angles when short DC pulses were used for the transfer process is shown in Figure 3.11 (a). When DC pulses were applied at certain RF phases, ions could not be transferred from the toroidal to the quadrupolar

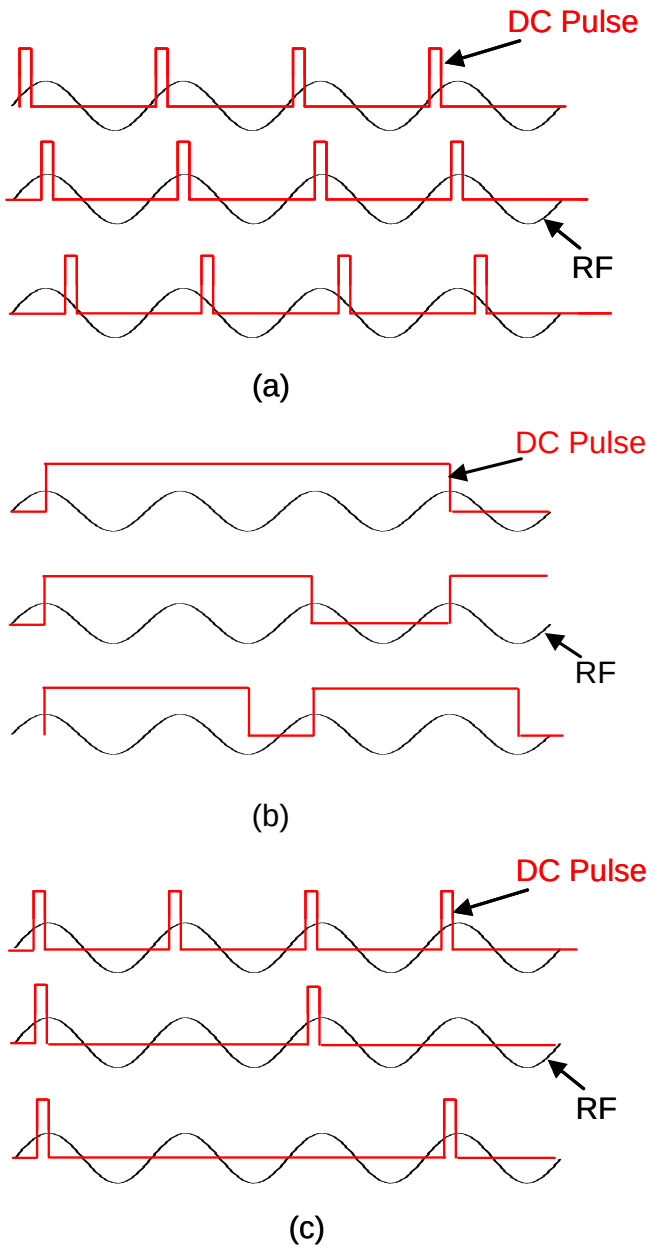

Figure 3.10. (a) Short DC pulses applied at different RF phases, (b) DC pulses with different widths relative to RF signal, (c) DC pulses of different frequencies compared with RF signal applied to the toroidal transfer process.

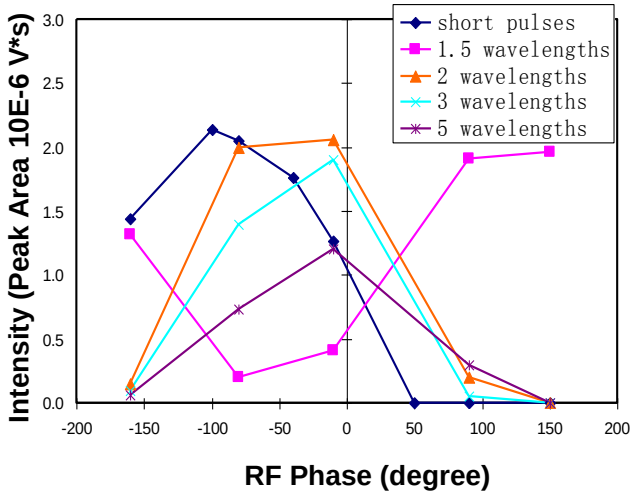

(a)

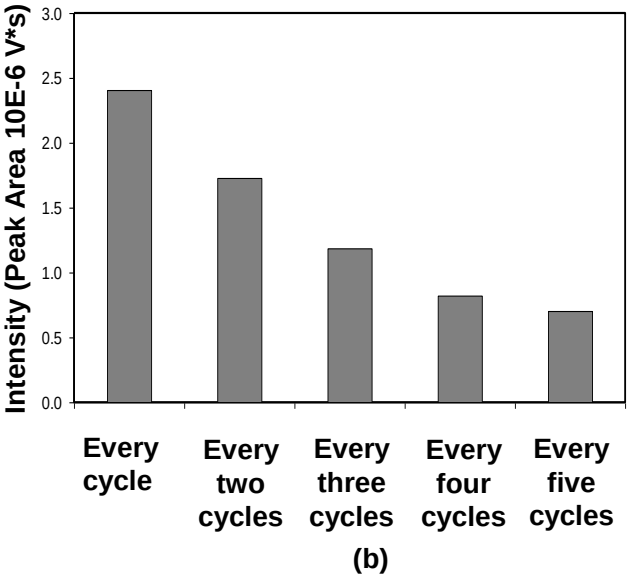

(b)

Figure 3.11. Detected signal intensity (a) as a function of RF phase and pulse duration when DC pulses are used to affect ion transfer, (b) as a function of rate of DC pulses.

trapping regions, whereas at other phases transfer occurred. In addition, when the repetition rate of the DC pulses was reduced, the number of ions transferred decreased proportional to the number of pulses applied as shown in Figure 3.11 (b), which indicates transfer time also has an effect on the transfer process. Similarly, when using sinusoidal signals to effect ion transfer, the number of ions detected increases in proportion to the duration of the applied supplementary AC signal, at least up to the point of saturation. Although these results are consistent with the phase-synchronized ion ejection observed by previous groups, the lack of dependence on AC frequency points to a transfer mechanism in which ions are pushed, out of resonance, into the quadrupole trapping region. The amplitudes needed to affect this transfer are larger than those typically used for dipole resonant ejection in conventional quadrupole ion traps, further supporting this conclusion.

The time-independent electric fields shown in Figure 3.3 assume that the RF driving the two trapping regions is exactly 180-degrees out of phase, with the same frequency. The center of the toroidal trapping region is of the opposite polarity as the center of the quadrupole region. Obviously this is the simplest experimental approach, as a single RF power supply can be used to operate the device. Alternatively, it may be possible to operate the two trapping regions with separate frequencies or other phase relationships. The consequences of a two-RF-frequency coaxial trap remain to be explored.

A possible application of the coaxial device takes advantage of the higher ion storage capacity of the toroidal trapping region. Ions in a quadrupole trap are confined to a small volume in the trap center, leading to onset of space-charge problems when the number of trapped ions becomes too large. In contrast, some trapping geometries, such as those used in linear, rectilinear, and toroidal ion traps, are extended in one dimension, allowing a greater number of

ions to be analyzed. The coaxial ion trap uses a toroidal trapping geometry for initial ion trapping, and might thus take advantage of this feature. In order to characterize the increased trapping capacity of the coaxial trap relative to the central quadrupolar trap acting alone, up to 30 sets of toroidal transfer scans and quadrupole analysis scans (demonstrated in Figure 3.12) were used on a single ion population (from a single ionization event). The ion signal did not diminish noticeably after 30 transfers. This is consistent with the larger trapping capacity of the toroidal region, which, based on geometrical arguments, can contain 100-200 times as many ions as the quadrupole region alone. This experiment could not be continued past 30 scans due to length limitations in the signal recording electronics. Ensemble averaging of these spectra demonstrated improvement in the signal-to-noise ratio, sensitivity, and dynamic range of the device. Trapping ions from a single ionization event, with multiple subsequent analyses, might enable sensitive mass analysis and characterization of dynamic or transient systems.

3.4 Conclusion

The coaxial ion trap, combining quadrupolar and toroidal trapping regions, has been constructed and demonstrated. Ions can be transferred from the toroidal to the quadrupolar region, although the mechanism of this transfer is not clear, and is not based on resonant excitation of the radial secular motion of the trapped ion. Because of the larger ion trapping capacity of the toroidal region, more ions from a given ionization event can be trapped and mass analyzed, leading to an improvement in sensitivity and dynamic range over the planar quadrupole ion trap acting alone. Similarly, mass analysis using quadrupolar fields instead of toroidal fields produces higher mass resolution than the halo ion trap. It is notable that the physical device of the coaxial ion trap is identical to that of the planar quadrupole ion trap, the

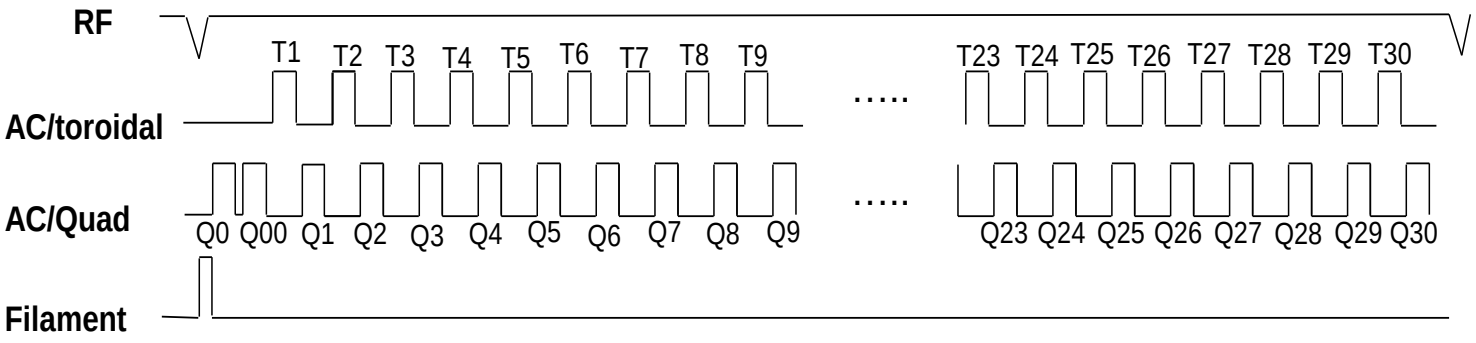

Figure 3.12. Schematic of scan pulse used for 30 sets of transfer processes of ions from the toroidal to the quadrupolar region in a single ionization event.

difference being only the RF amplitudes applied to each patterned electrode ring. This underscores the versatility of making electro-optic devices using this approach.

3.5 References

1. Le Blanc, J. C. Y.; Hager, J. W.; Ilisiu, A. M. P.; Hunter, C.; Zhong, F.; Chu, I., Unique scanning capabilities of a new hybrid linear ion trap mass spectrometer (Q TRAP) used for high sensitivity proteomics applications. *Proteomics* **2003,** *3* (6), 859-869.

2. Gabelica, V.; Tabarin, T.; Antoine, R.; Rosu, F.; Compagnon, I.; Broyer, M.; De Pauw, E.; Dugourd, P., Electron photodetachment dissociation of DNA polyanions in a quadrupole ion trap mass spectrometer. *Anal. Chem.* **2006,** *78*, 6564-6572.

3. Wilson, J.; Vachet, R. W., Multiplexed MS/MS in a quadrupole ion trap mass spectrometer. *Anal. Chem.* **2004,** *76*, 7346-7353.

4. Payne, A. H.; Chelf, J. H.; Glish, G. L., C-terminal peptide sequencing using acetylated peptides with MSn in a quadrupole ion trap. *Analyst* **2000,** *125*, 635-640.

5. March, R. E., Quadrupole ion trap mass spectrometry: a view at the turn of the century. *Int. J. Mass Spectrom.* **2000,** *200*, 285-312.

6. Fisk, P. T. H.; Lawn, M. A.; Coles, C., Laser Cooling of Yb-171(+) Ions in a Linear Paul Trap. *Appl. Phys. B-Photo* **1993,** *57*, 287-291.

7. Campbell, J. M.; Collings, B. A.; Douglas, D. J., A new linear ion trap time-of-flight system with tandem mass spectrometry capabilities. *Rapid Commun. Mass Spectrom.* **1998,** *12*, 1463-1474.

8. Schultz-Johanning, M.; Schnabel, R.; Kock, M., A linear Paul trap for radiative lifetime measurements on ions. *Eur. Phys. J. D* **1999,** *5*, 341-344.

9. Ouyang, Z.; Wu, G. X.; Song, Y. S.; Li, H. Y.; Plass, W. R.; Cooks, R. G., Rectilinear ion trap: Concepts, calculations, and analytical performance of a new mass analyzer. *Anal. Chem.* **2004,** *76*, 4595-4605.

10. Kothari, S.; Song, Q. Y.; Xia, Y.; Fico, M.; Taylor, D.; Amy, J. W.; Stafford, G.; Cooks, R. G., Multiplexed Four-Channel Rectilinear Ion Trap Mass Spectrometer. *Anal. Chem.* **2009,** *81*, 1570-1579.

11. Wells, J. M.; Badman, E. R.; Cooks, R. G., A quadrupole ion trap with cylindrical geometry operated in the mass selective instability mode. *Anal. Chem.* **1998,** *70*, 438-444.

12. Tabert, A. M.; Griep-Raming, J.; Guymon, A. J.; Cooks, R. G., High-throughput miniature cylindrical ion trap array mass spectrometer. *Anal. Chem.* **2003,** *75*, 5656-5664.

13. Lammert, S. A.; Plass, W. R.; Thompson, C. V.; Wise, M. B., Design, optimization and initial performance of a toroidal rf ion trap mass spectrometer. *Int. J. Mass Spectrom.* **2001,** *212*, 25-40.

14. Lammert, S. A.; Rockwood, A. A.; Wang, M.; Lee, M. L.; Lee, E. D.; Tolley, S. E.; Oliphant, J. R.; Jones, J. L.; Waite, R. W., Miniature toroidal radio frequency ion trap mass analyzer. *J. Am. Soc. Mass Spectrom.* **2006,** *17*, 916-922.

15. Contreras, J. A.; Murray, J. A.; Tolley, S. E.; Oliphant, J. L.; Tolley, H. D.; Lammert, S. A.; Lee, E. D.; Later, D. W.; Lee, M. L., Hand-Portable Gas Chromatograph-Toroidal Ion Trap Mass Spectrometer (GC-TMS) for Detection of Hazardous Compounds. *J. Am. Soc. Mass Spectrom.* **2008,** *19*, 1425-1434.

16. Austin, D. E.; Wang, M.; Tolley, S. E.; Maas, J. D.; Hawkins, A. R.; Rockwood, A. L.; Tolley, H. D.; Lee, E. D.; Lee, M. L., Halo ion trap mass spectrometer. *Anal. Chem.* **2007,** *79*, 2927-2932.

17. Wang, M. A.; Quist, H. E.; Hansen, B. J.; Peng, Y.; Zhang, Z. P.; Hawkins, A. R.; Rockwood, A. L.; Austin, D. E.; Lee, M. L., Performance of a Halo Ion Trap Mass Analyzer with Exit Slits for Axial Ejection. *J. Am. Soc. Mass Spectrom.* **2011,** *22*, 369-378.

18. Zhang, Z. P.; Peng, Y.; Hansen, B. J.; Miller, I. W.; Wang, M.; Lee, M. L.; Hawkins, A. R.; Austin, D. E., Paul Trap Mass Analyzer Consisting of Opposing Microfabricated Electrode Plates. *Anal. Chem.* **2009,** *81*, 5241-5248.

19. Austin, D. E.; Hansen, B. J.; Peng, Y.; Zhang, Z. P., Multipole expansion in quadrupolar devices comprised of planar electrode arrays. *Int. J. Mass Spectrom.* **2010,** *295*, 153-158.

20. Zhang, Z. P.; Quist, H.; Peng, Y.; Hansen, B. J.; Wang, J. T.; Hawkins, A. R.; Austin, D. E., Effects of higher-order multipoles on the performance of a two-plate quadrupole ion trap mass analyzer. *Int. J. Mass Spectrom.* **2011,** *299*, 151-157.

21. Austin, D. E.; Peng, Y.; Hansen, B. J.; Miller, I. W.; Rockwood, A. L.; Hawkins, A. R.; Tolley, S. E., Novel Ion Traps Using Planar Resistive Electrodes: Implications for Miniaturized Mass Analyzers. *J. Am. Soc. Mass Spectrom.* **2008,** *19*, 1435-1441.

22. Williams, J. D.; Cox, K. A.; Cooks, R. G.; Mcluckey, S. A.; Hart, K. J.; Goeringer, D. E., Resonance Ejection Ion-Trap Mass-Spectrometry and Nonlinear Field Contributions - the Effect of Scan Direction on Mass Resolution. *Anal. Chem.* **1994,** *66*, 725-729.

23. Wu, G. X.; Cooks, R. G.; Ouyang, Z.; Yu, M.; Chappell, W. J.; Plass, W. R., Ion trajectory simulation for electrode configurations with arbitrary geometries. *J. Am. Soc. Mass Spectrom.* **2006,** *17*, 1216-1228.

24. Quarmby, S. T.; Yost, R. A., Fundamental studies of ion injection and trapping of electrosprayed ions on a quadrupole ion trap. *Int. J. Mass Spectrom.* **1999,** *191*, 81-102.

25. Franzen, J.; Gabling, R.-H.; Schubert, M.; Wang, Y., Nonlinear Ion Traps. In *Practical Aspects of Ion Trap Mass Spectrometry*, , March, R. E.; Todd, J. F. J., Eds. CRS Press: Boca Raton, FL, 1995; Vol. 1.

26. Mallard, W. G.; J., L. P. NIST Chemsitry WebBook, NIST Standard Reference Database Number 69.

27. Harden, C. S.; Wagner, P. E. P. E. Edgewood Arsenal Special Report (EASP) 100-93 and Edgewood Arsenal Technical Report (EATR) 4545, Edgewood Arsenal, Maryland, Edgewood Arsenal, Maryland, 1971.

28. Mastoris, S. In *UTIAS Tech. Note 172*, Institute for Aerospace Studies, University of Toronto Institute for Aerospace Studies, University of Toronto 1971.

29. Dawson, P. H.; Lambert, C., Pulse-out synchronization in the quadrupole ion trap *Int. J. Mass Spectrom. Ion Phys.* **1974**, 339-347.

30. Todd, J. F. J.; Waldren, R. M., Quadrupole Ion Store (Quistor) .2. Phase-Synchronized Ion Ejection from a Quadrupole Ion Storage Mass-Spectrometer. *Int. J. Mass Spectrom.* **1979,** *29*, 301-314.

31. Waldren, R. M.; Todd, J. F. J., Quadrupole Ion Store (Quistor) .3. Studies on Phase-Synchronized Ion Ejection - Effects of Ejection Pulse Width and Detection Pulse Delay. *Int. J. Mass Spectrom.* **1979,** *29*, 315-335.

32. Waldren, R. M.; Todd, J. F. J., Quadrupole Ion Store (Quistor) .4. Total Pressure Mode-Operation with Phase-Synchronized Ion Ejection. *Int. J. Mass Spectrom.* **1979,** *29*, 337-344.

CHAPTER 4: SIMULATION STUDY OF ION TRANSFER BETWEEN CONCENTRIC TOROIDAL AND QUADRUPOLE TRAPPING REGIONS IN A COAXIAL ION TRAP

4.1 Introduction

In pure quadrupole ion traps, the radiofrequency (RF) trapping field increases linearly in both axial (z-) and radial (r-) directions. The truncation of electrodes to finite size as well as the holes in end-cap electrodes, introduce superimposed multipole terms in the electric fields.[1] Several studies have been reported showing the dependence of the performance of the quadrupole ion trap on the nonlinear high-order components of quadrupolar trapping field.[2-6] Since ions trapped in a 3D quadrupole ion trap are ejected out along the axial direction (z-direction), these studies focused on z- oscillations.[7-8] Although some coupling with the r-direction exists, this can be neglected in most cases. The effect of superposition of multipole fields on oscillations in the z-direction has been investigated by simulating the ion trajectories along the z- axis[7, 9-10] and by experimental results.[11-13]

The coaxial ion trap presented in Chapter 3 combines two concentric trapping regions. A quadrupole trapping region is formed by the inner ring electrodes, surrounded by a toroidal trapping region on the outside, as shown in Figure 4.1. Ions can be trapped and mass analyzed in either trapping region and transferred between these two regions. The field in the radial direction plays an important role since ions are transferred along this direction (r-direction).

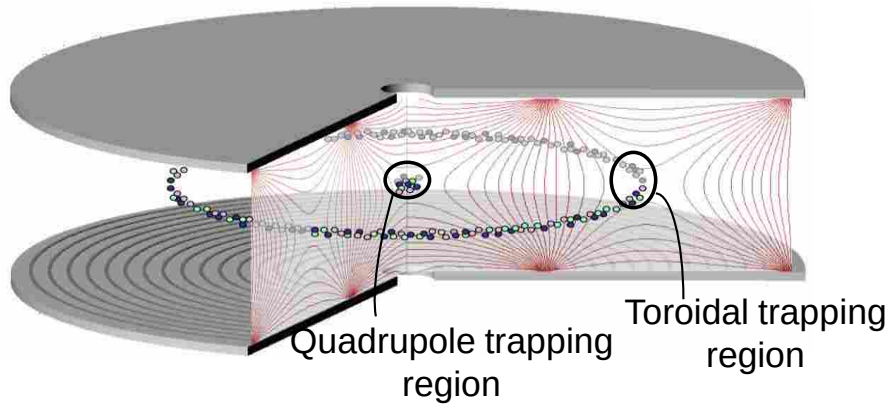

(a)

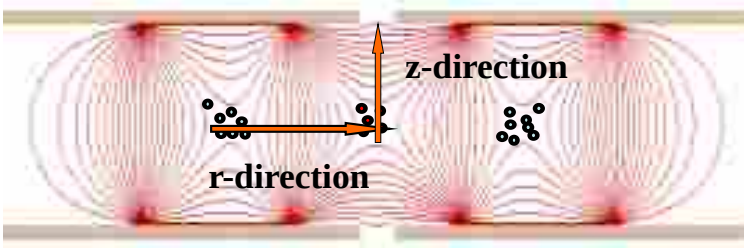

(b)

Figure 4.1. (a) Arrangement of fields in the coaxial ion trap with quadrupole trapping field formed in the center surrounded with toroidal trapping field, (b) cross section of the field and direction of ion motion in the coaxial trap.

4.1.1 Methods to Modify Nonlinear Components in Ion Traps

Nonlinear components of an electric field play a critical role in the performance of ion trap mass analyzers.[14] In conventional ion traps, electrode structure and geometry are adjusted and modified in order to obtain the best combination of field components and optimize the performance. One complete testing cycle including several steps: 1) electrode geometry including asymptote angles and the distance between electrodes is changed, 2) the resulting fields are calculated, 3) ion motion is simulated to identify the performance, and 4) later fabrication and optimization of the design of this ion trap are performed based on the result of the simulation. Usually several cycles need to be implemented to achieve optimal results. However, the relative strengths of multipoles contributing to the trapping field are not independently adjustable in this conventional method. In a newly-built planar ion trap reported by Austin et al.,[15] the mass analyzer is composed of two planar plates, the facing surfaces of which are imprinted with a series of concentric metal ring electrodes. In this design, when applying individually controllable potentials to each ring electrode patterned on the plate, the desired trapping field can be created. Because the potential on each ring is independently adjustable, some independent control of higher order multipoles is possible. Using simulations from SIMION, we explored modified potential functions, their resulting trapping fields, and the effects of these trapping fields on ion motion.

4.1.2 Why A One Dimensional Ion Simulation Method

In order to understand the behavior of ions in ion traps and to optimize the performance of ion traps, a number of investigations of multipole field components have been made on conventional quadrupole,[4, 6, 16] cylindrical,[13] linear,[17-18] rectilinear[19] and toroidal ion traps.[20] In the coaxial ion trap, ions are initially trapped and collisionally cooled to the centers of both

toroidal and quadrupolar trapping regions. Ions are expected to be transferred from the toroidal trapping region to quadrupolar trapping region in the radial direction. Therefore, the field in the radial direction in the coaxial ion trap plays a critical role on realizing ion transfer. To date, no detailed studies have been made on the field covering different trapping regions nor the effects of higher order components of the field on the ion motion between two trapping regions.

Simulation methods including SIMION, ISIS and ITSIM have been widely used in the study of ion motion in ion traps.[21-26] The movement of ions in the coaxial ion trap was simulated with SIMION (SIMION 8, Scientific Instrument Services, Ringoes, NJ, USA), an example of which is shown in Figure 4.2. This simulation uses time-varying fields in 3D geometry and is therefore time consuming to monitor the transfer process by adjusting multipole compositions of the radial field. Therefore, we used one-dimensional simulations in Microsoft Excel to study the motion of ions in such a complex system. In our study, the oscillation of each ion was calculated based on the force resulting from the electric field only along the r-axis. This permits us to study some distinct aspects of nonlinear effects and to investigate whether ions can be mass-selectively transferred in the r-direction from the toroidal region to the quadrupolar region.

4.2 Electric Field in the Coaxial Ion Trap

4.2.1 Field Design in Coaxial Ion Trap

The design and operation of the coaxial ion trap were already given in Chapter 3. Briefly, torodial and quadrupole trapping regions are created simultaneously and coaxially between a pair of patterned ceramic plates.

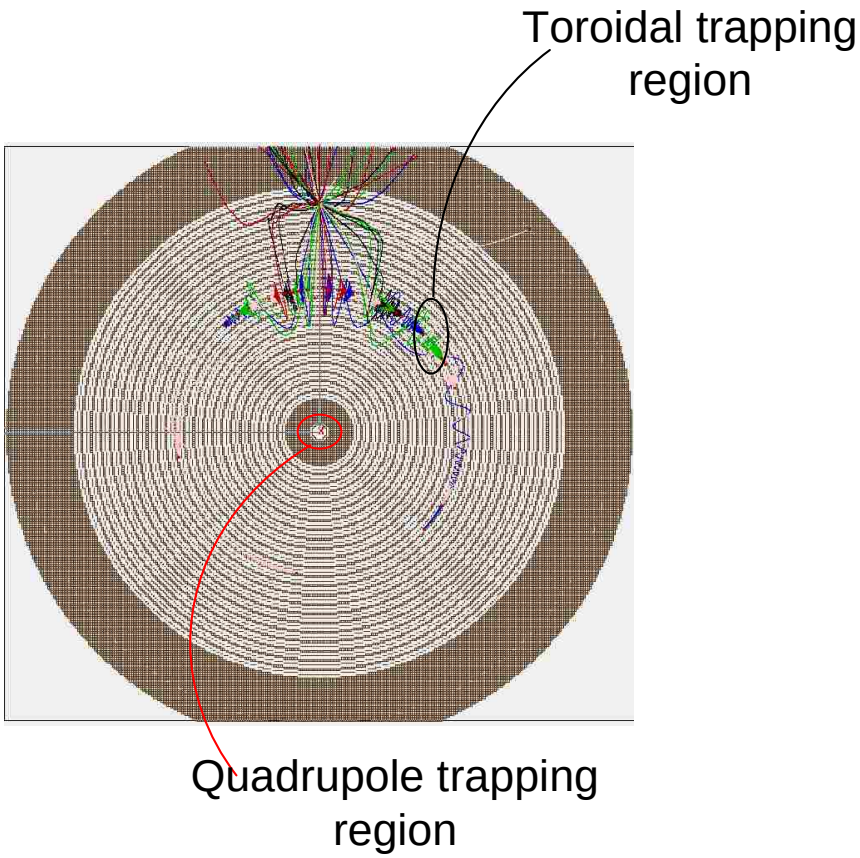

Figure 4.2. A top view of ions trapped in the coaxial ion trap, simulated using SIMION software. The outside region is the toroidal trapping region and the central region is the quadrupole trapping region.

Austin et al. reported how to independently adjust high-order components in planar ion traps.[10] The multipole expansion of each individual electrode can be explored using SIMION 8[27] and MATLAB R2008b. The needed potentials for each ring electrode can be determined by solving a set of linear equations for the multipole components produced by each electrode to get the desired overall trapping field in the z-direction as shown in the following expressions:

$$\Phi(z,\phi,t)_{r=0} = \Phi_0(t)\sum_{n=2}^{2n}[A_n(\frac{z}{z_0})^2] \quad (1)$$

$$A_2 = \sum_{m=1}^{24} A_{2.m}\Phi_{0m} \quad (2)$$

$$A_n = \sum_{m=1}^{24} A_{n,m}\Phi_{0m} \quad (3)$$

where $\Phi(z,\phi,t)_{r=0}$ is the RF potential along the z axis (r = 0); $\Phi_0(t)$ is the RF potential applied to the ring electrode of the ion trap; A_n is the magnitude of even odd poles in Equation (1). The second equation stands for the quadrupole term A_2 in the axial direction contributed from ring 1 to 24: Φ_{0m} is the applied RF amplitude (Φ_0) to ring m; A_2 is the magnitude of the quadrupole term and $A_{2,m}$ is the quadrupole (n=2) term created by ring m alone; A_n is the general expression for calculating any multipole.

Using this approach to optimize the trapping potentials, high-resolution spectra have been demonstrated in the planar quadrupole trap.[11] Using this approach combined with numerical simulation of ion motion potentials that should be applied to each electrode ring to create a coaxial ion trap and realize ion transfer from the toroidal trapping region to the central quadrupole trapping region was explored.

4.3 One Dimensional Simulation of Ion Transfer

A one dimensional simulation method was used to study the effects of nonlinear electric fields on the motion of ions in the coaxial ion trap. The oscillation of an ion moving from the center of the toroidal trapping region to the center of the quadrupole trapping region was simulated along the r-direction. This method does not consider any motion component in other directions, assuming no force on the ion in the z-direction. In this simple simulation model, the ion does not represent the trajectory of an ion in a real ion trap with all degrees of freedom. Yet we still can get useful information about the effect of superimposed fields on the behavior of ions by this simple method.

4.3.1 Calculation Method

In the coaxial ion trap, the oscillation of the ion in the radial direction can be observed, superimposed by an RF driving field and/or a supplementary AC field for resonant ejection. Initial parameters for an ion are restricted to the location and speed of this ion only in the r-direction. The ion is accelerated or decelerated by the force resulting from the electric field. After the field at every point along the radial direction was simulated and calculated, a very short time step (3 ns) was applied to calculate the instantaneous acceleration and the distance that ion travels during this period of time. A viscous dampening factor was used to approximate the effects of ion-neutral collisions in the simulation. Once the calculation of ion motion was obtained, the movement of the ion in the r-direction as a function of time was plotted.

4.3.2 Ion Motion along the Radial Direction in the Coaxial Ion Trap

This calculation is based on the assumption that an ion has been trapped in the toroidal region. The starting point of an ion is the center of the toroidal trapping region and its trajectory along the r-direction is plotted as a function of time as demonstrated in Figure 4.3, where the zero point in the y-axis is the center of the quadrupole trapping region. The force on the ion stably trapped in the torodial region is determined by the driving RF and a supplementary AC signal with a small amplitude:

$$\vec{F} = (\vec{E}_{RF} + \vec{E}_{AC}) * q = m * \vec{a} \quad (4)$$

where $\vec{F}$ is the force on the ion due to the electric field; $\vec{E}_{RF}$ and $\vec{E}_{AC}$ are the electric fields caused by the drive RF and AC signal respectively; *q* is the charge of the ion; *m* is the mass of the ion and $\vec{a}$ is the acceleration of the ion resulting from the coulombic force.

The electric field was calculated using SIMION 8 software by flying a neutral particle along the r- axis between the two plates after a designed potential function has been applied to each individual electrode on the plates. The multipole expansion of the electric field as a function of dimension r obtained by SIMION was solved by fitting the field along the r axis to a 20th order polynomial using the *polyfit* function in Matlab:

$$E_0 = f(r) = B_0 + B_1 * r + B_2 * r^2 + ... + B_{20} * r^{20} \quad (5)$$

where E_0 is the field along the r- axis; f is the *polyfit* function; B_n is a polynomial and r is the dimension along the r- axis (z = 0). A 20th order polynomial was chosen to provide sufficient level of accuracy for the field multipoles without excessive computation time. In this work, the multipole expansion of the whole device along the r- axis was

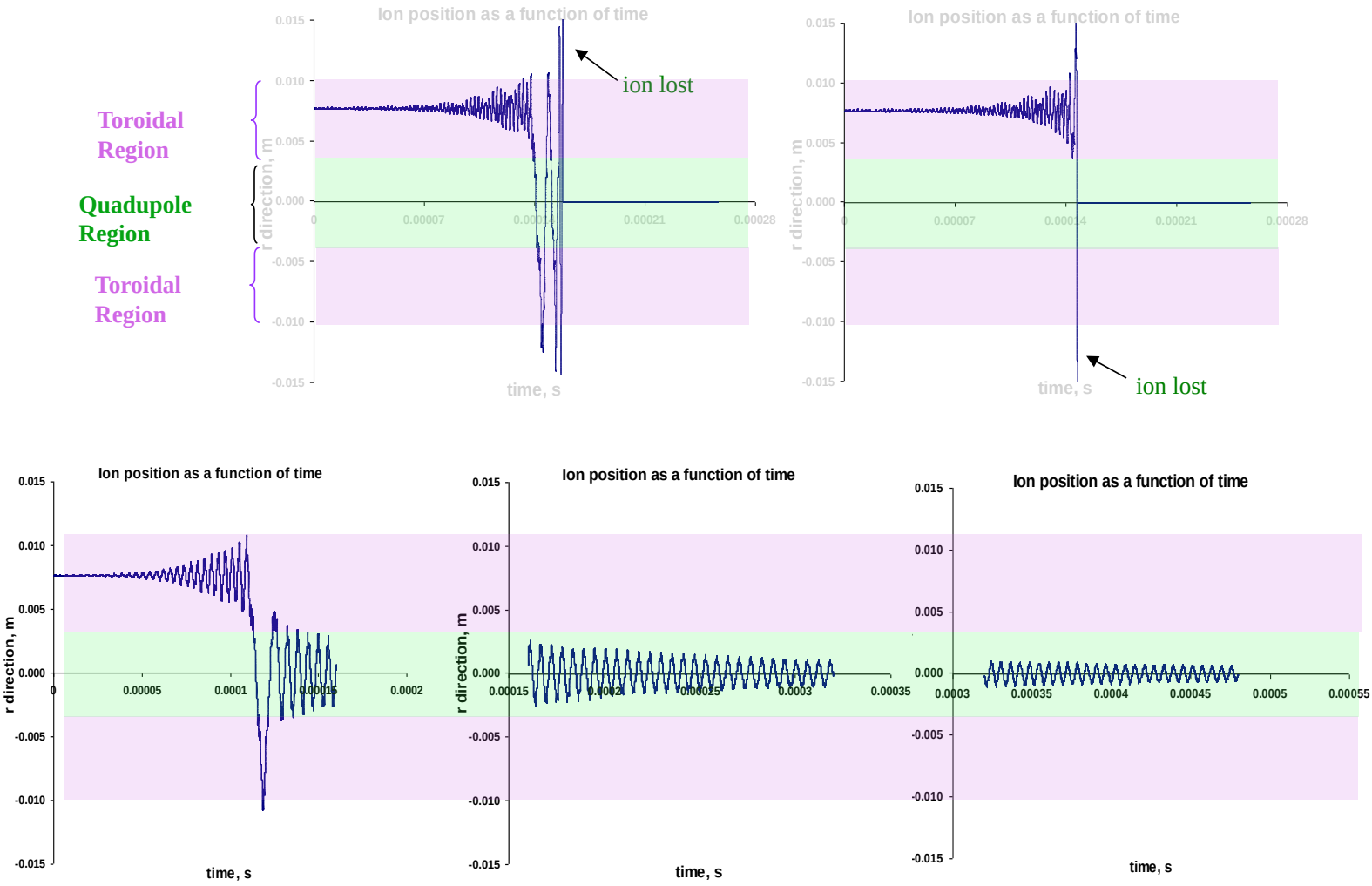

Figure 4.3. Motion of ions in the coaxial ion trap during resonant excitation from the toroidal trapping region to the central quadrupole trapping region in the radial direction. (a), (b) trajectory of ions lost between the two trapping regions, (c) trajectory of ions successfully transferred from the toroidal region to quadrupole trapping region and trapped in the quadrupole region.

expressed as a set of ratios of B_n to B_0, similar to our group's previous work on the planar Paul trap.[10] This procedure gives the time-independent field, corresponding to the applied RF.

In addition, the electric field in the coaxial ion trap changes not only with the position along the r- axis but also with time and phase angle of the applied potential function:

$$\Phi(r,t)_{z=0} = \Phi_0(r) * \cos(\Omega * t + \phi) \quad (6)$$

$$E(r,t)_{z=0} = E_0(r) * \cos(\Omega * t + \phi) \quad (7)$$

where $\Phi(r, t)_{z=0}$ and $E(r, t)_{z=0}$ are the potential and field along the r axis; $\Phi_0(t)$ and $E_0(t)$ are the initial potential and field along the r- axis when a potential function is applied to the plates; and Ω is the frequency of the primary RF or the supplementary AC signal, and ϕ is the starting phase angle of the primary RF or supplementary AC signal. When these variables were adjusted in the simulation process, significant differences of the trajectories of an ion were observed, as shown in Figure 4.3. As shown in Figure 4.3 (a) and (b) under some conditions an ion was lost between the two plates in either direction of the r- axis, while under some other conditions an ion was transferred from the toroidal trapping region to the central quadrupole region and was trapped in the central region (Figure 4.3 (c)). For each field considered, the fraction of ions successfully transferred was determined.

After the ion is transferred from the toroidal region to the central quadrupole region, it will be resonantly ejected out from the center region. Therefore the field in the z-direction (along r = 0) was also studied in this work. However, due to the continuity of the toroidal trapping field and the quadrupole trapping field which coexist in one mass

analyzer, the fields of both regions deviate from the ideal. It is difficult to achieve the desired field for quadrupole trapping region along the z- axis and the r- axis at the same time, which will affect mass resolution and transfer efficiency separately.

4.4 Discussion and Results

4.4.1 Field Design

The coaxial field was originally designed to closely approximate the field of the Halo ion trap[15] in the r-direction and the field of the planar QIT[28] in the z-direction. Figure 4.4 shows the first trial electric field and high-order multipole components of this field in both r- and z- directions when a potential function is applied to the 24 ring electrodes of the planar trap. In this design, 6.14% octopole (A_4/A_2, 8-pole) and 7.30% dodecapole (A_6/A_2, 12-pole) are present in the quadrupole trapping region along the z-axis (r = 0). Other high-order multipole components in z- axis of the coaxial ion trap are listed in Table 4.1 (trial field 1). The numbers in the first row of trial field 1 correspond to the parameters A_n in Equation (1), which were calculated in Matlab, and the numbers in the second row of trial field 2 correspond to their relative percentages to A_2 (quadrupole term). Because these higher order components have less effect on ions at the trapping center they will not be discussed in detail in this study.

Figure 4.4 (a), (b), and (c) also demonstrate multipole components along the r-axis (z = 0). Since the field in this direction covers both the toroidal trapping region and the quadrupole trapping region, the multipole fields of both regions are plotted in the figure. However, from Figure 4.4 (b) and (c) we notice that the radial fields of both

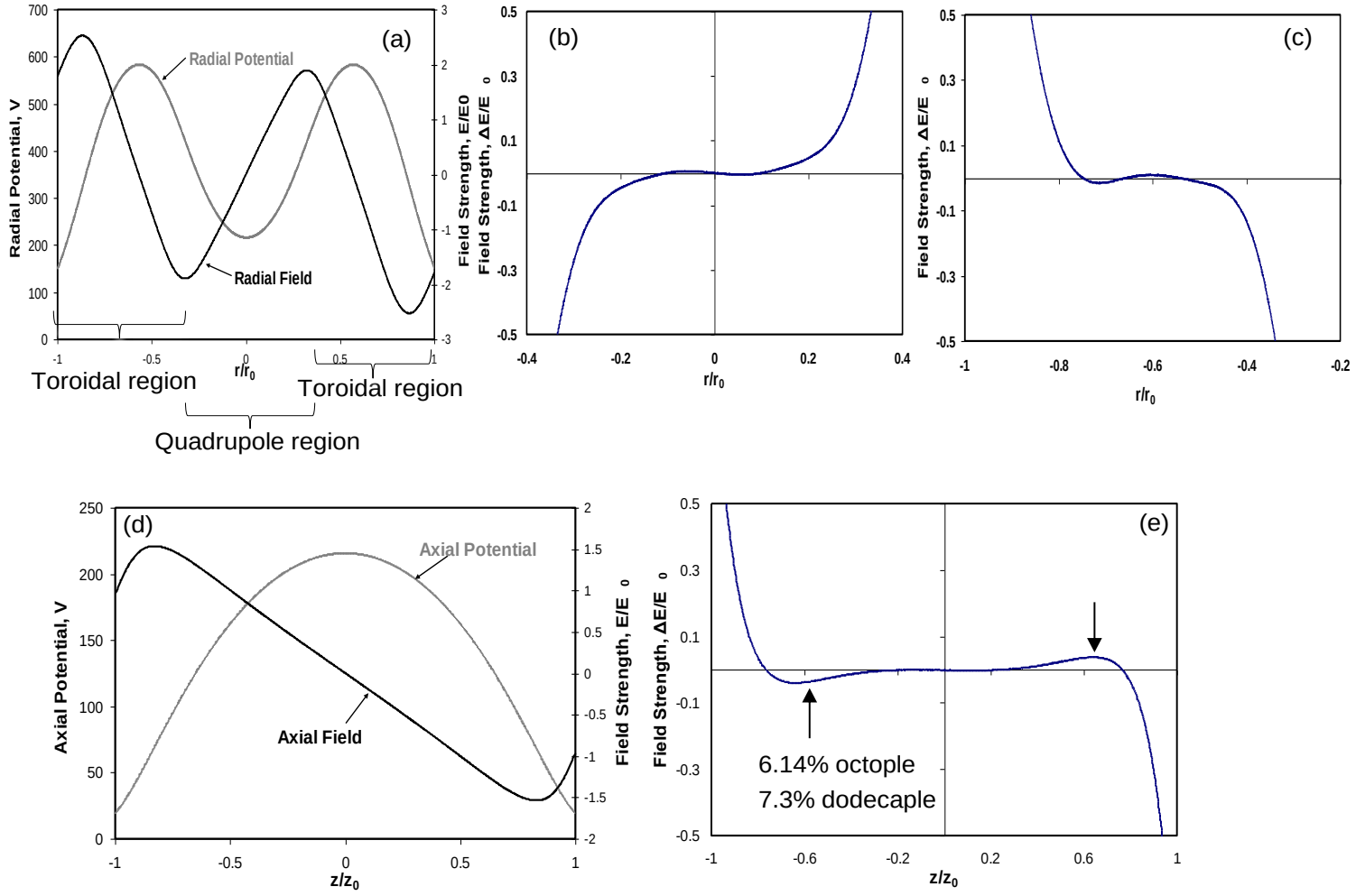

Figure 4.4. Schematic of (a) potential and field of trial field 1 in radial direction in coaxial ion trap, (b) nonlinear contribution to the central quadrupole field in radial direction, (c) nonlinear contribution to the toroidal trapping field in radial direction, (d) potential and field of trial field one in axial direction in coaxial ion trap, (e) nonlinear contribution to the central quadrupole field in the axial direction.

High-order components	Field one	(A_n/A_2) %	Field two	(A_n/A_2) %
A0	1		1	
A1	4.90E-16		-6.44E-16	
A2	-0.97		-1.01	
A3	-7.42E-15		3.00E-14	
A4	-0.06	**6.14**	0.05	**-4.54**
A5	8.62E-14	-8.9E-12	-4.19E-13	4.15E-11
A6	-0.07	**7.30**	-0.03	**3.23**
A7	5.27E-14	-5.4E-12	4.86E-12	-4.8E-10
A8	0.45	-46.60	0.37	-37.06

Table 4.1. High-order components of trial field 1 and 2 in the axial direction.

regions are not linear even in the central region. Nonlinear contributions to both trapping fields are illustrated in Figure 4.4 (b) and (c) by subtracting a linear extrapolation of a narrow region of the derived electric field around the center of the two trapping regions, where the contributions due to nonlinear fields approach zero. The potential function (trial 1) gives rise to a strongly sublinear radial field in the quadrupole trapping region and the linearity was even lost in the toroidal trapping region. In commercial quadrupole ion traps with "stretched geometry" a small superlinear contribution is incorporated to the field to achieve better performance of the traps. Lammer *et al*.[20] reported a performance improvement on a toroidal ion trap by reducing the sublinear multipole components in both r- and z- direction although the field in the r-direction was less important to mass analysis as ions were only resonantly ejected in the z-direction.

4.4.2 Trial field simulated to achieve high transfer efficiency

In our novel planar ion trap, the linearity of the radial fields in both trapping regions can be significantly improved by modifying the potential function on the ring electrodes. The resulting fields in both radial and axial directions resulting from this potential function (trial 2) are demonstrated in Figure 4.5. Figure 4.5 (b) and (c) show a small superlinear contribution in the radial fields of the toroidal and quadrupole regions. The performance of this trial field in terms of transfer efficiency is shown in Figure 4.6 and compared to trial field 1 along the r- axis. Ions with mass range from 77 Th to 138 Th in both trial fields were investigated after they were stably trapped in the toroidal trapping region. Their trajectories as a function of time were recorded as they were accelerated and resonantly excited by a tickle AC signal in both trial RF trapping fields.

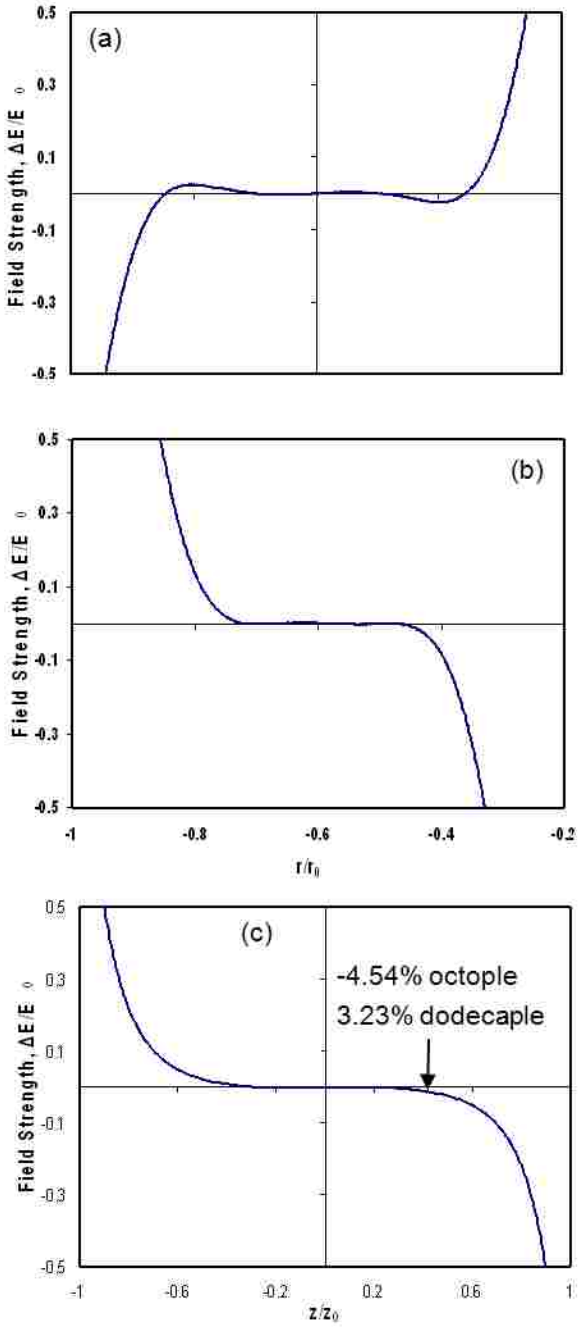

Figure 4.5. Schematic of (a) nonlinear contribution to the central quadrupole field in the radial direction, (b) nonlinear contribution to the toroidal trapping field in the radial direction, (c) nonlinear contribution to the central quadrupole field in the axial direction.

The nonlinear contribution in these two trial fields along the r- axis affects transfer efficiency greatly. Clearly, small superlinear contribution (positive higher-order components) as illustrated in Figure 4.5 (a) and (b) will provide higher transfer efficiency from the toroidal trapping region to the quadrupolar trapping region, which is around 65% for ions with *m/z* 120. In trial field 1 where sublinear fields are present, however, the transfer efficiency is much lower, around 35% for the ion with the same *m/z*. Since this is a one-dimension simulation, forces on other directions are not considered in the model. Effects resulting from coupled motions may produce ion excursion in other directions and reduce the transfer efficiency further. We also noticed that transfer efficiencies for both trial fields are relatively high around *m/z* 120, which corresponds to $\beta \sim 1/3$ (Figure 4.6). As a result, in these two field designs ions should be resonantly transferred from the toroidal region to the quadrupolar trapping region and collisionally cooled down in the center at $\beta \sim 1/3$. One thing to note is that ions can be resonantly excited from a wider range of β; however in these two fields, only ions resonant at $\beta \sim 1/3$ can be transferred between the two trapping regions. Other resonant ions were lost between the two plates as shown.

4.4.3 Condition for Ion Transfer and for High Mass Resolution

Even though field trial 2 provides higher transfer efficiency compared with field trial 1, some sublinear contributions (negative high-order components) can be observed in the z-direction of the central quadrupole region, where ions are mass-selectively ejected out to the detector (Figure 4.5 (c)). Different values of octopole (A_4/A_2, 8-pole, -4.54%) and dodecapole (A_6/A_2, 12-pole, 3.23%) present in trial field 2 and the comparison of the

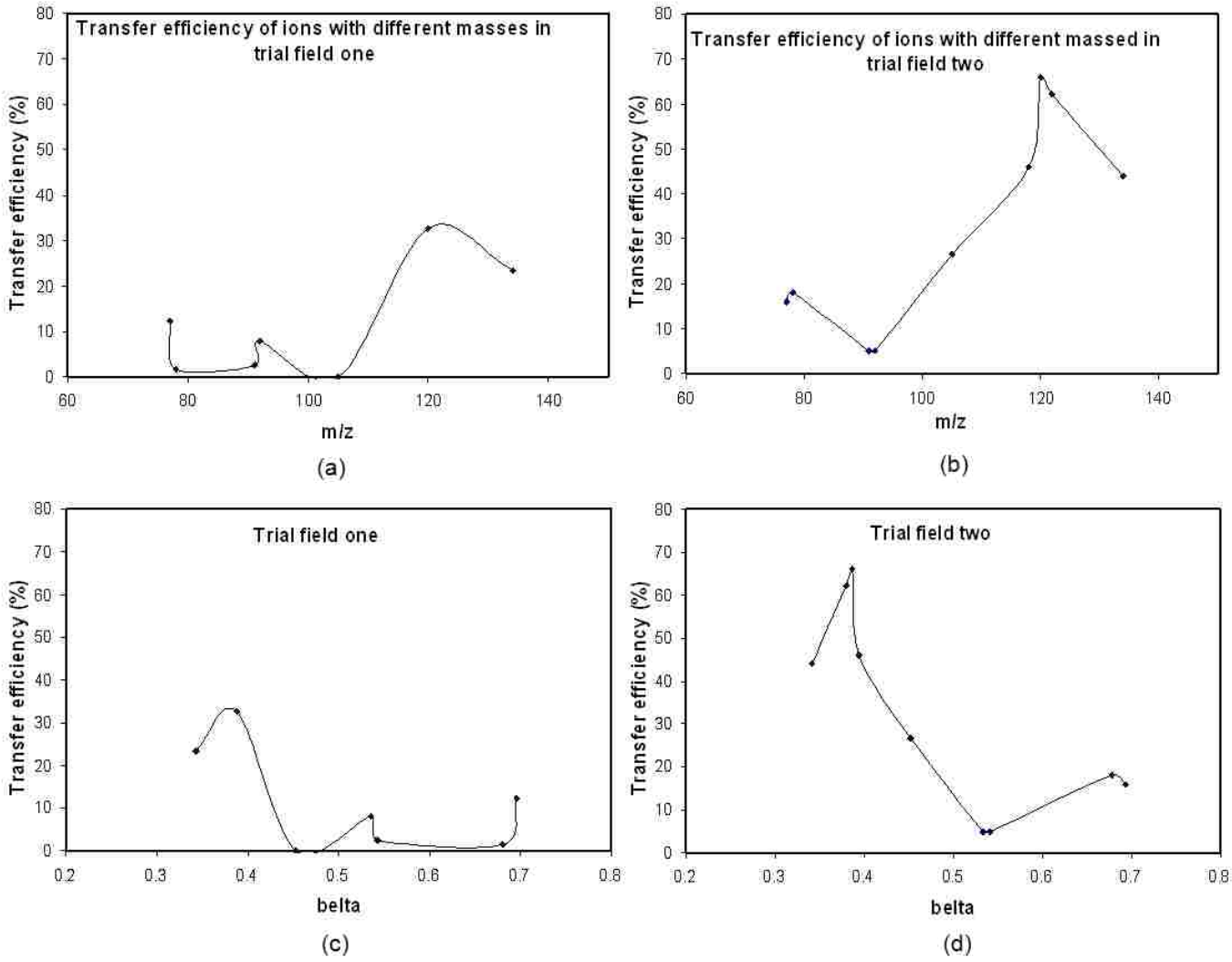

Figure 4.6. Relationship of transfer efficiency to *m/z* and β values in trial field 1 and 2.

multipole components of these two fields are made in Table 4.1. Zhang et al.[11] reported that 0% octopole and 6% dodecapole in the axial field in the planar QIT offered the best performance of this trap. In designing the coaxial trap field, the octopole and dodecapole were set to 0% and 6% in the axial field using the *solver* function in Excel after the multipole expansion of each independent electrode was calculated using SIMION 8 and MATLAB R2008b. Once the potential distribution was solved for an individual electrode, we adjusted these potentials on each ring and noticed that rings 1 to 5 have a significant effect on the components of multipole field in the z- axis while other rings have less effect. Therefore the potentials on the other rings are adjusted to achieve a superlinear contribution to the radial field in the toroidal trapping region and quadrupole trapping region. Table 4.2 and Figure 4.7 show the resulting potential functions (trial 3), fields and multipole contribution of the fields in both radial and axial directions. The components of the axial field in the coaxial ion trap are listed in Table 4.2, which matched well with the designed values for octopole and dodecapole. In addition, one-dimensional simulation (Figure 4.8) demonstrated that reasonable transfer efficiency between the two trapping regions along r- axis can be achieved in this trial field. The method to design the field by combining high transfer efficiency in the r-direction and high mass resolution in the z-direction provides a straightforward guide to further experiments.

It is important to note that no multipole expansion has been identified to completely satisfy the Laplace Equation of any toroidal trapping geometry. This one-dimensional simulation method is based on accurate calculation of the field along the r- axis using

High-order components	Field three	%
A0	1.000	
A1	-1.01E-16	
A2	-1.022	
A3	-4.02E-15	
A4	-5.83E-05	**5.71E-03**
A5	1.62E-13	-1.58E-11
A6	-0.061	**5.944**
A7	-5.78E-13	5.66E-11
A8	0.422	-41.256

Table 4.2. High-order components of trial field three in axial direction.

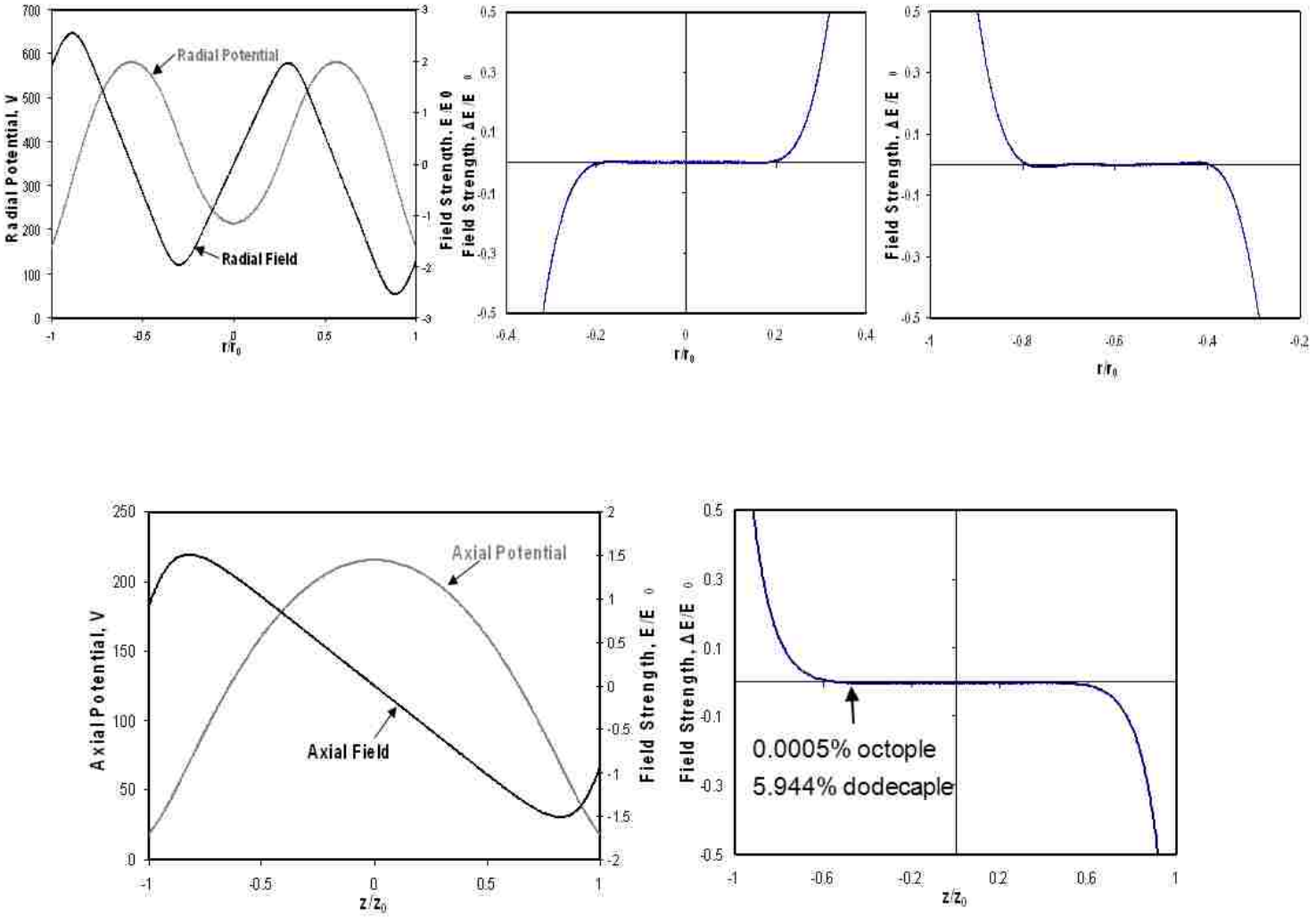

Figure 4.7. Schematic of (a) potential and field of trial field 3 in radial direction in coaxial ion trap, (b) nonlinear contribution to the central quadrupole field in radial direction, (c) nonlinear contribution to the toroidal trapping field in radial direction, (d) potential and field of trial field 1 in axial direction in coaxial ion trap, (e) nonlinear contribution to the central quadrupole field in axial direction.

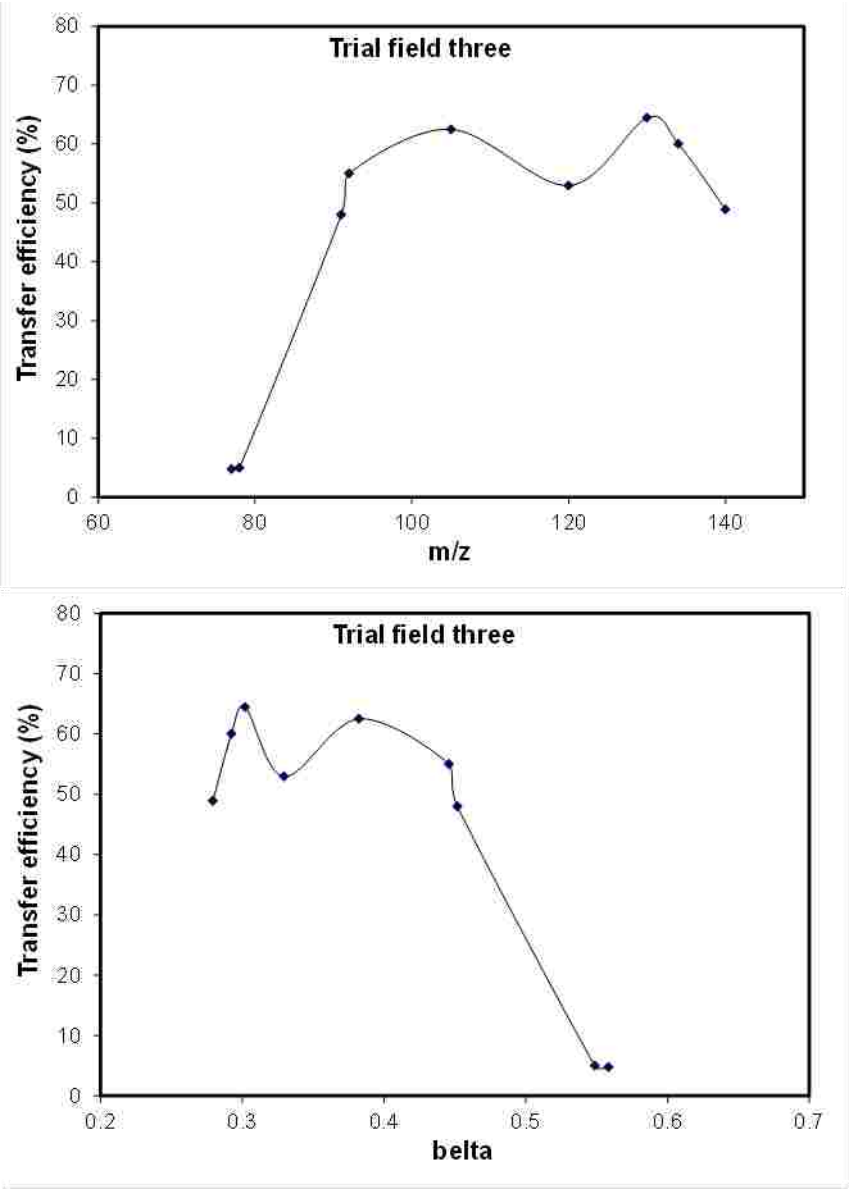

Figure 4.8. Relationships of transfer efficiency of trial field 3 to *m/z* and β values.

the *polyfit* function of MATLAB and can be applied to calculation of fields in all kinds of ion traps. The advantages of this simulation are that it offers a direct view of ions in one dimension and the multipole expansion of the electric field can be modified by changing the potential on each individual ring.

4.5 Conclusion

A coaxial ion trap combining more than one trapping region is designed using two lithographically-patterned plates. The coaxial field is designed to realize mass analysis of ions in both regions and transfer of ions between these two regions. One-dimensional calculation and simulation on the motion of an ion along the r- axis was studied in this chapter. It has been shown that the superimposed multipole fields along the r-axis have a great effect on the transfer efficiency of ions from the toroidal trapping region to the quadrupole trapping region. However, this work was limited to ion oscillation along the r- direcction only. The result would be modified if oscillation in the z-direction is coupled to the r-direction. Nevertheless, this simulation method represents a useful tool to study the effects of higher-order fields on ion transfer in the r-direction and combines the consideration of higher-order fields in the z-direction at the same time.

4.6 References

1. March, R. E., An introduction to quadrupole ion trap mass spectrometry. *J. Mass Spectrom.* **1997,** *32*, 351-369.

2. Sudakov, M., Effective potential and the ion axial beat motion near the boundary of the first stable region in a nonlinear ion trap. *Int. J. Mass Spectrom.* **2001,** *206*, 27-43.

3. Plass, W. R.; Li, H. Y.; Cooks, R. G., Theory, simulation and measurement of chemical mass shifts in RF quadrupole ion traps. *Int. J. Mass Spectrom.* **2003,** *228*, 237-267.

4. Chattopadhyay, M.; Verma, N. K.; Mohanty, A. K., Composite field approximations for ion traps with apertures on electrodes. *Int. J. Mass Spectrom.* **2009,** *282*, 112-122.

5. Krishnaveni, A.; Verma, N. K.; Menon, A. G.; Mohanty, A. K., Numerical observation of preferred directionality in ion ejection from stretched rectilinear ion traps. *Int. J. Mass Spectrom.* **2008,** *275*, 11-20.

6. Franzen, J., The nonlinear ion-trap .4. mass-selective instability scan with multipole superposition. *Int. J. Mass Spectrom.* **1993,** *125*, 165-170.

7. Franzen, J., Simulation study of an in cage with superimposed multipole fields. *Int. J. Mass Spectrom.* **1991,** *106*, 63-78.

8. Splendore, M.; Londry, F. A.; March, R. E.; Morrison, R. J. S.; Perrier, P.; Andre, J., A simulation study of ion kinetic energies during resonant excitation in a stretched ion trap. *Int. J. Mass Spectrom.* **1996,** *156*, 11-29.

9. Londry, F. A.; Hager, J. W., Mass selective axial ion ejection from a linear quadrupole ion trap. *J. Am. Soc. Mass Spectrom.* **2003,** *14*, 1130-1147.

10. Austin, D. E.; Hansen, B. J.; Peng, Y.; Zhang, Z. P., Multipole expansion in quadrupolar devices comprised of planar electrode arrays. *Int. J. Mass Spectrom.* **2010,** *295*, 153-158.

11. Zhang, Z. P.; Quist, H.; Peng, Y.; Hansen, B. J.; Wang, J. T.; Hawkins, A. R.; Austin, D. E., Effects of higher-order multipoles on the performance of a two-plate quadrupole ion trap mass analyzer. *Int. J. Mass Spectrom.* **2011,** *299*, 151-157.

12. Hager, J. W., A new linear ion trap mass spectrometer. *Rapid Commun. Mass Spectrom.* **2002,** *16*, 512-526.

13. Wu, G. X.; Cooks, R. G.; Ouyang, Z., Geometry optimization for the cylindrical ion trap: field calculations, simulations and experiments. *Int. J. Mass Spectrom.* **2005,** *241*, 119-132.

14. Austin, D. E.; Peng, Y.; Hansen, B. J.; Miller, I. W.; Rockwood, A. L.; Hawkins, A. R.; Tolley, S. E., Novel Ion Traps Using Planar Resistive Electrodes: Implications for Miniaturized Mass Analyzers. *J. Am. Soc. Mass Spectrom.* **2008,** *19*, 1435-1441.

15. Austin, D. E.; Wang, M.; Tolley, S. E.; Maas, J. D.; Hawkins, A. R.; Rockwood, A. L.; Tolley, H. D.; Lee, E. D.; Lee, M. L., Halo ion trap mass spectrometer. *Anal. Chem.* **2007,** *79*, 2927-2932.

16. Gupta, A.; Rao, P. M., Numerical calculations of potential distribution in non-ideal quadrupole trap and simulations of anharmonic oscillations. *Pramana-J. Phys.* **2008,** *70*, 457-470.

17. Douglas, D. J.; Frank, A. J.; Mao, D. M., Linear ion traps in mass spectrometry. *Mass Spectrom. Rev.* **2005,** *24*, 1-29.

18. Zhao, X. Z.; Douglas, D. J., Dipole excitation of ions in linear radio frequency quadrupole ion traps with added multipole fields. *Int. J. Mass Spectrom.* **2008,** *275*, 91-103.

19. Ouyang, Z.; Wu, G. X.; Song, Y. S.; Li, H. Y.; Plass, W. R.; Cooks, R. G., Rectilinear ion trap: Concepts, calculations, and analytical performance of a new mass analyzer. *Anal. Chem.* **2004,** *76*, 4595-4605.

20. Lammert, S. A.; Plass, W. R.; Thompson, C. V.; Wise, M. B., Design, optimization and initial performance of a toroidal rf ion trap mass spectrometer. *Int. J. Mass Spectrom.* **2001,** *212*, 25-40.

21. Hashimoto, Y.; Matsuoka, L.; Osaki, H.; Fukushima, Y.; Hasegawa, S., Trapping laser ablated Ca^+ ions in linear Paul trap. *Jpn. J. Appl. Phys. Part 1 - Regul. Pap. Brief Commun. Rev. Pap.* **2006,** *45*, 7108-7113.

22. Albrieux, F.; Antoine, R.; Chirot, F.; Lemoine, J.; Dugourd, P., Ion trajectory simulations in a high-pressure cylindrical ion trap. *Eur. J. Mass Spectrom.* **2010,** *16*, 557-565.

23. Salazar, G. A.; Masujima, T., Computer simulation of the gap-tripole ion trap with linear injection, 3D ion accumulation, and versatile packet ejection. *J. Am. Soc. Mass Spectomr.* **2008,** *19*, 1367-1374.

24. Forbes, M. W.; Sharifi, M.; Croley, T.; Lausevic, Z.; March, R. E., Simulation of ion trajectories in a quadrupole ion trap: a comparison of three simulation programs. *J. Mass Spectrom.* **1999,** *34*, 1219-1239.

25. Ouyang, Z.; Gao, L.; Fico, M.; Chappell, W. J.; Noll, R. J.; Cooks, R. G., Quadrupole ion traps and trap arrays: geometry, material, scale, performance. *Eur. J. Mass Spectrom.* **2007,** *13,* 13-18.

26. Wu, G. X.; Cooks, R. G.; Ouyang, Z.; Yu, M.; Chappell, W. J.; Plass, W. R., Ion trajectory simulation for electrode configurations with arbitrary geometries. *J. Am. Soc. Mass Spectrom.* **2006,** *17*, 1216-1228.

27. Manura, D.; Dahl, D. A. *SIMION Version 8.04*, Scientific Instrument Services, Inc.: Ringoes, NJ, 2006.

28. Zhang, Z. P.; Peng, Y.; Hansen, B. J.; Miller, I. W.; Wang, M.; Lee, M. L.; Hawkins, A. R.; Austin, D. E., Paul Trap Mass Analyzer Consisting of Opposing Microfabricated Electrode Plates. *Anal. Chem.* **2009,** *81,* 5241-5248.

Chapter 5: PERSPECTIVE AND FUTURE WORK

5.1 Summary

A new approach to making ion traps was presented in this dissertation. The electrodes of the trap consist of two ceramic discs, the facing surfaces of which are lithographically imprinted with sets of concentric metal rings and overlaid with a thin layer of germanium. A radial potential function can be applied to the resistive material such that the potential between the plates is quadrupolar, and ions are trapped in the quadratic field between the plates. Since the potential on each ring electrode is adjusted independently, the electric field is independent of geometry and can be optimized electronically. The trap can produce various field geometries, including a toroidal trapping geometry,[1] the traditional Paul-trap field[2] and a linear trapping field.[3]

It is important to note that changing the separation of the two ceramic plates does not directly change the trapping field as in conventional ion traps. In conventional traps "stretching" or modifying the geometries of the electrodes will change mutlipole components of the trapping field, thus affect the ion ejection and mass resolution. In planar resistive electrode traps, these higher order multipoles are added in by modifying the potential function on the resistive material. Since high-order multipoles can be modified electronically, and are not constrained by physical geometry, new opportunities exist for producing and experimenting with modified fields. For instance, resonant ejection can be applied to the planar traps using fields that closely approximate a pure dipole. In addition, the distance between the two plates can be modified to realize miniaturization of the planar ion traps without changing the components of the field.

At the same time, the simple electrode geometry (planar) addresses many issues related to existing technologies such as surface roughness, maintaining the accuracy of electrode geometry, and alignment of electrodes during miniaturization. Furthermore, the structure of the planar traps offers open access for ion injection and simpler assembly because of fewer degrees of freedom in the alignment. All these characteristics make planar ion traps a strong candidate for a portable mass spectrometer system.

5.1.1 Advantages of Miniaturizing Planar Ion Traps

According to Equation (4) in Chapter 1, reducing the size of ion traps (r_0 and z_0) requires either increasing the trap frequency, reducing the RF amplitude, or both to keep the same mass range. Reducing the RF amplitude also reduces the pseudopotential well depth. As the well depth decreases, ion trapping and storage capacity decrease, so the RF amplitude cannot be arbitrarily small. On the other hand, as electrodes are placed closer together, the maximum voltage that can be sustained between them without electrical discharge goes down, again constraining the RF amplitude. The well depth and electrical discharge limit the range of voltages that can be used in voltage-ramp mass analysis. Some miniaturized traps get around this problem by using frequency scanning at constant RF amplitude.

The current paradigm of ion trap miniaturization is to make traps smaller. While this may seem obvious, it is not necessarily the only option. Any method that produces a higher trapping field and a higher trapping frequency will produce the same result as physical miniaturization of the trap electrodes. In the case of planar resistive electrodes, in which quadratic potential functions are imposed on the resistive material, as the plates are moved closer together, the trapping potentials remain quadrupolar as illustrated in

Figure 5.1 (a), which shows isopotential contours in the halo ion trap with plate spacing, d, of 4, 2, and 1 mm. The potential function on the plates in Figure 5.1 (a) is identical for each set, and the resulting field shapes and magnitudes are identical (ignoring edge effects). At the same time by increasing the potential gradient along the resistive material and simultaneously increasing the trapping frequency, the trapping field increases, reducing the amplitude of ion motion. Figure 5.1 (b) shows SIMION 7 simulations of ion trajectories in traps under these conditions. The frequency in each case was chosen to provide a similar q_z value for each set. Ions have m/z = 100 Th, and the ion trap is operated with RF amplitude of 600 V_{p-p}. To facilitate an accurate comparison, ions originated at the same point in the RF phase, with 0.025 eV kinetic energy. Ions experienced hard-sphere collisions with helium in which the collision frequency was constrained to 0.05 times the frequency of the driving RF. For plates separated by 4 mm, the trapping frequency is 1.27 MHz, and the helium pressure is 0.8 mTorr. For each successively closer set of plates, the trapping frequency increases by a factor of 2, and the helium pressure increases by roughly a factor of 2. Ion excursion is reduced in each smaller scenario. When higher fields are created using the same plates, ion excursion and mean free path decrease, as they would in a miniaturized ion trap. In addition, the allowable pressure for trapping increases.[4] Because fewer rings are used to create the field, the applied voltage on each plate is the same regardless of plate spacing. The distance over which this voltage is extended is reduced, resulting in an increased electric field at the trapping region. Although this is a simplified model, it illustrates the promise of using planar ion traps for miniaturized mass spectrometry.

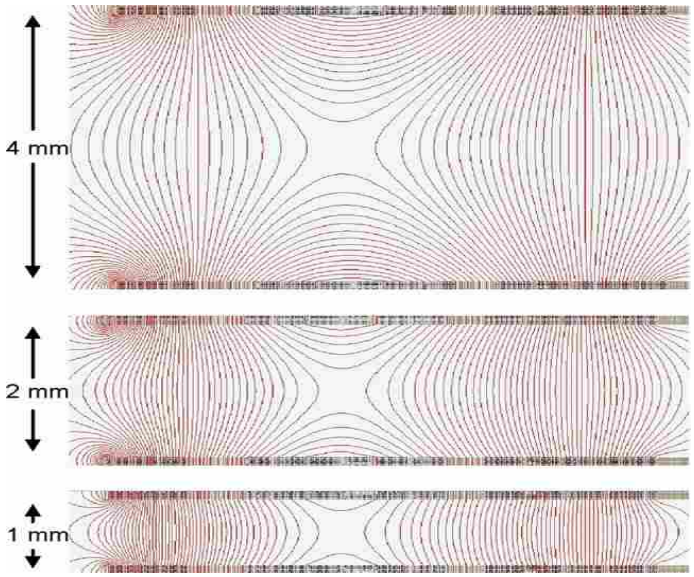

(a)

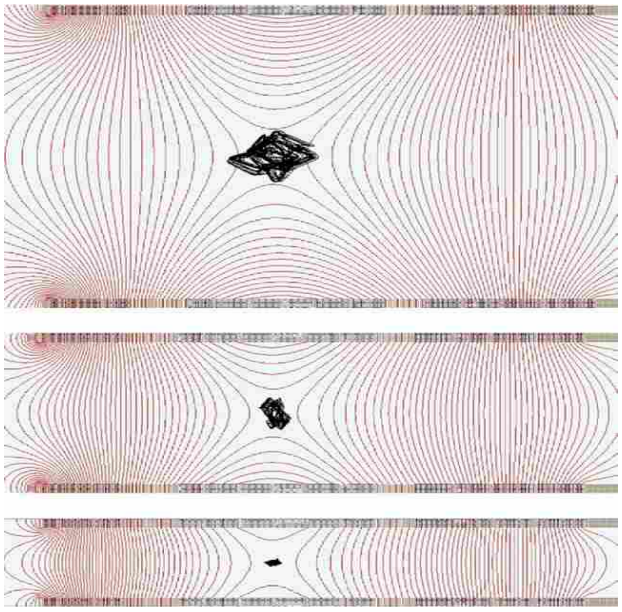

(b)

Figure 5.1. (a) As plates are moved closer together, the trapping potential remains quadrupolar. The same potential function is used in each set of plates, (b) simulations of ion motion as trapping plates are moved together. Plate separation is 4, 2, and 1 mm.

5.1.2 Miniaturizing Planar Ion Traps

As the plates are moved together, the radial pseudopotential well remains constant for a given voltage applied to each plate. Under these conditions, the pseudopotential well depth perpendicular to the plates is reduced. However, when the field is increased on the plates (by using fewer rings and the same applied voltage) the pseudopotential well depth perpendicular to the plates remains constant. Whereas the field in metal-electrode ion traps is limited by field emission between closely-spaced electrode surfaces, the field in planar electrode ion traps is limited by the voltage difference between the closely-spaced ring electrodes. However, because of the large number of electrode rings, the voltage difference between adjacent electrodes is much smaller than the voltage difference between electrodes in conventional ion traps.

5.2 Realizing Resonant Ejection from the Toroidal Region to the Quadrupole Region

As mentioned in Chapter 3, ions in the coaxial ion trap have been successfully transferred between two trapping regions. The intended mode of operation using this device was to employ resonant ejection of ions from the toroidal trapping region to the central quadrupolar trapping region. This would allow mass selectivity in transferred ions. Once mass selective ejection is realized, ions with the same mass to charge ratio can be transferred at one time, which provides an opportunity for tandem-in-space experiment with a single mass analyzer. Ions can be first accumulated in the trapping region with large ion capacity (toroidal trapping region) and then transferred to the trapping region with high mass resolution (quadrpole trapping region) for mass analysis.

If ions can be mass selectively transferred into the quadrupole region, ion isolation in the tandem experiment can be simplified, and because of the large storage capacity of the toroidal trapping region, the sensitivity of this mass analyzer can be greatly improved.

However, it appears that the mechanism of this transfer does not involve resonance with the ion secular frequency, and the process is not mass selective, at least not yet. In experiments, a periodic DC pulse was applied to the outmost ring to replace the original AC signal applied during the toroidal transfer scan. Experimental results demonstrated that when DC pulses were applied at certain RF phases, ions could not be transferred from the toroidal to the quadrupolar trapping regions, whereas at other phases transfer occurred. Ions are initially trapped in both trapping regions of the coaxial ion trap; however, they need to gain enough energy to transfer from one trapping potential well to another trapping potential well. This phenomenon offers us suggestions to modify the electric field in the coaxial trap in order to resonantly transfer ions.

5.2.1 Influence of the Hexapole Field on Ion Motion

As mentioned in Chapter 4, in practice it is impossible to create an ion trap with a pure quadrupole electric field. The influence of superimposed weak multipole components to the quadrupole field on mass resolution, scan speed, and ion storage stability has been widely studied.[5-6] Ion motions are mainly controlled by nonlinear resonances resulting from higher-order fields such as hexapole and octopole. The effects of hexapole and octopole components adding to quadrupole field are illustrated in Figure 5.2. When ions are resonantly excited from the trapping potential well they will be

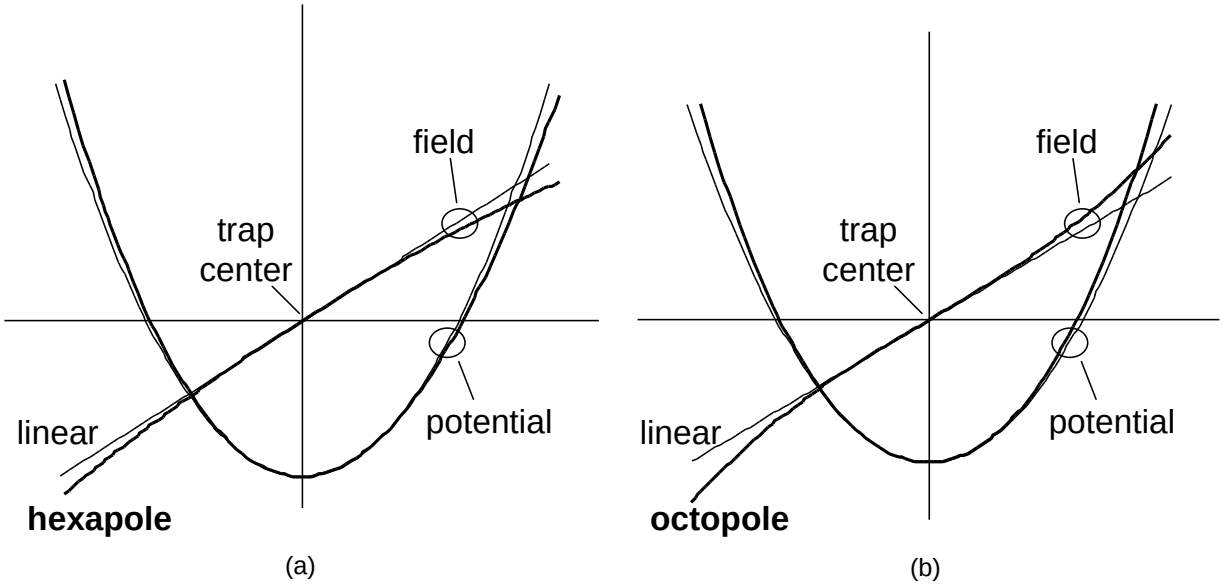

Figure 5.2. The field increases linearly in a pure quadrupole ion trap. Schematic of (a) linear field added by a weak hexapole field, (b) linear field added by a weak octopole field. Those fields generated are called nonlinear fields.

slowed down in one side of the well and were faster in the other side of the well in the field with the added hexapole field, while they will be faster in both sides of the octopole field. Thus the hexpole component in the field will not change the secular frequency of ions: it will stop ions in the outside part of the torodial region and help resonantly eject ions to the central quadrupole region. While in the field superimposed with an octopole component, ions will be out of resonance because their secular frequencies change with the increase of amplitude from the center of the trapping region.

5.2.2 Adding a Hexapole Component to the Field of the Coaxial Trap

In designing the trapping field of the coaxial ion trap, much attention was focused on the octopole and dotacopole components of the field to improve mass resolution of the central quadrupole field. In order to obtain resonant ejection of ions from the toroidal trapping region to the quadrupole trapping region in the coaxial ion trap, the field in the toroidal trapping region needs to be considered because ions are initially trapped and stored in the toroidal trapping field. According to the effect of hexapole field on the motion of ions, some hexapole component can be added to the field of the toroidal trapping region in the radial direction to improve resonant ejection of ions from the toroidal region to the quadrupole region. Since the components of the field can be independently controlled in the planar ion trap,[7] different percentages of hexapole can be investigated either in the simulation of ion motion with SIMION or in real experiments.

5.3 Tandem Mass Spectrometry

As mentioned, once ions can be mass selectively transferred from the toroidal region to the quadrupole region, tandem experiments can be performed in the coaxial ion

trap. An example of a possible scan function for tandem analysis performed in the coaxial ion trap is illustrated in Figure 5.3. After ions are created and trapped in both trapping regions of the coaxial ion trap, a supplementary AC (Paul AC) signal will be applied on the quadrupole trapping region to remove all the ions from the central region. Then another supplementary AC (toroidal AC) with the frequency matching the secular frequency of ions trapped in the toroidal region will mass selectively eject the ions to the central region in the radial direction. A dissociation AC signal with a small amplitude and designed frequency will be applied. When this dissociation AC excites the secular motion of the precursor ions which have been transferred from the toroidal region and trapped in the quadrupolar region, the kinetic energy of these ions will increase and they will collide with the helium buffer gas, which will cause dissociation of the parent ions through CID (collision-induced dissociation). Finally these fragments ions will be mass analyzed in the central quadrupole region using the resonant AC signal.

There are several advantages to using the coaxial ion trap to perform tandem analysis. First, no complicated operation is needed to isolate parent ions from other ions as in normal tandem-in-time experiments. In the conventional quadrupole ion trap, all the ions are crowded in the central region and then parent ions are isolated whereas in the coaxial ion trap only parent ions will be selectively transferred to the central quadrupole trapping region. Therefore fewer space- charge problems exist in the coaxial trap, and sensitivity will improve because only ions with the same mass to charge ratio will be trapped at one time in the quadrupole region. In one ionization process, all the target parent ions can be mass analyzed by scanning the toroidal AC frequencies to transfer them to the central quadrupolar trapping region each at one time. This process will

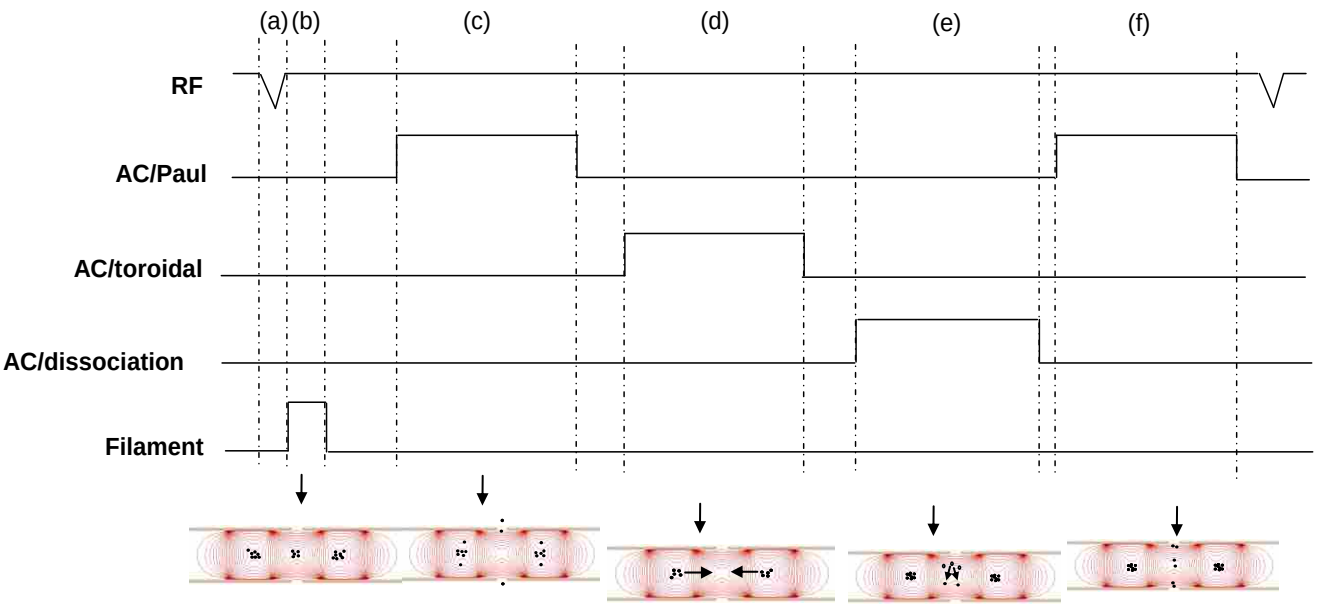

Figure 5.3. Scan function for possible tandem experiment performed in the coaxial ion trap. (a) All the ions cleaned out of the trap, (b) ions created and trapped in both trapping regions of the coaxial ion trap, (c) ions cleaned out from the central quadrupole trapping region, (d) parent ions transferred from the toroidal trapping region to the quadrupole trapping region, (e) parent ions dissociated in the central quadrupole region, (e) fragment ions mass-analyzed in the quadrupole region.

greatly reduce the sample consumption compared to normal tandem experiments, where usually one kind of targeted parent ion will be selected and mass analyzed at one ionization step. In addition, the coaxial ion trap combines two mass analyzers in one device, which significantly decreases the size and weight of mass analyzers required to perform tandem-in-space experiments.

Later, more than one compound will be investigated in this coaxial ion trap at one time. The sample mixture will be ionized and all the ions can be stored in the toroidal trapping region first. After scanning the toroidal AC frequency precursor ions with one mass will be transferred and mass analyzed in the quadrupole trapping region. After mass analysis of this kind of precursor ion, the same process can be applied to another kind of precursor ion by scanning another toroidal AC frequency. As illustrated in Figure 5.3, the scan function demonstrates a complete mass analysis for one precursor ion; in the same ionization process another precursor ion analysis can be repeated using another toroidal transfer AC frequency. If these samples have precursor ions with different m/z, they can be analyzed directly in the coaxial ion trap without a separation step such as GC or LC.

5.4 References

1. Austin, D. E.; Wang, M.; Tolley, S. E.; Maas, J. D.; Hawkins, A. R.; Rockwood, A. L.; Tolley, H. D.; Lee, E. D.; Lee, M. L., Halo ion trap mass spectrometer. *Anal. Chem.* **2007,** *79*, 2927-2932.

2. Zhang, Z. P.; Peng, Y.; Hansen, B. J.; Miller, I. W.; Wang, M.; Lee, M. L.; Hawkins, A. R.; Austin, D. E., Paul Trap Mass Analyzer Consisting of Opposing Microfabricated Electrode Plates. *Anal. Chem.* **2009,** *81*, 5241-5248.

3. Hansen, B. J.; Quist, H.; Barley, B.; Hawkins, A. R.; Austin, D. E. In *A Linear-type Ion Trap Realized with Two Lithographically Patterned Substrates*, 58th ASMS conferrence Salt Lake City, UT, Salt Lake City, UT, May, 2010.

4. Badman, E. R.; Cooks, R. G., Special feature: Perspective - Miniature mass analyzers. *J. Mass Spectrom.* **2000,** *35*, 659-671.

5. Franzen, J., Simulation study of an ion cage with superimposed multipole fields. *Int. J. Mass Spectrom.* **1991,** *106*, 63-78.

6. Zhang, Z. P.; Quist, H.; Peng, Y.; Hansen, B. J.; Wang, J. T.; Hawkins, A. R.; Austin, D. E., Effects of higher-order multipoles on the performance of a two-plate quadrupole ion trap mass analyzer. *Int. J. Mass Spectrom.* **2011,** *299*, 151-157.

7. Austin, D. E.; Hansen, B. J.; Peng, Y.; Zhang, Z. P., Multipole expansion in quadrupolar devices comprised of planar electrode arrays. *Int. J. Mass Spectrom.* **2010,** *295*, 153-158.